Random distributed feedback fibre lasers

Sergei K. Turitsyn [a,b,*], Sergey A. Babin [b,c], Dmitry V. Churkin [a,b,c],
Ilya D. Vatnik [c], Maxim Nikulin [c], Evgenii V. Podivilov [b,c]

[a] *Aston Institute of Photonic Technologies, Aston University, Birmingham B4 7ET, United Kingdom*
[b] *Novosibirsk State University, 2 Pirogova str., 630090, Novosibirsk, Russia*
[c] *Institute of Automation and Electrometry SB RAS, 1 Ac. Koptug. ave., 630090, Novosibirsk, Russia*

ARTICLE INFO

ABSTRACT

The concept of random lasers exploiting multiple scattering of photons in an amplifying disordered medium in order to generate coherent light without a traditional laser resonator has attracted a great deal of attention in recent years. This research area lies at the interface of the fundamental theory of disordered systems and laser science. The idea was originally proposed in the context of astrophysics in the 1960s by V.S. Letokhov, who studied scattering with "negative absorption" of the interstellar molecular clouds. Research on random lasers has since developed into a mature experimental and theoretical field. A simple design of such lasers would be promising for potential applications. However, in traditional random lasers the properties of the output radiation are typically characterized by complex features in the spatial, spectral and time domains, making them less attractive than standard laser systems in terms of practical applications. Recently, an interesting and novel type of one-dimensional random laser that operates in a conventional telecommunication fibre without any pre-designed resonator mirrors – random distributed feedback fibre laser – was demonstrated. The positive feedback required for laser generation in random fibre lasers is provided by the Rayleigh scattering from the inhomogeneities of the refractive index that are naturally present in silica glass. In the proposed laser concept, the randomly backscattered light is amplified through the Raman effect, providing distributed gain over distances up to 100 km. Although an effective reflection due to the Rayleigh scattering is extremely small (∼0.1%), the lasing threshold may be exceeded when a sufficiently large distributed Raman gain is provided. Such a random distributed feedback fibre laser has a number of interesting and attractive features. The fibre waveguide geometry provides transverse confinement, and effectively one-dimensional random distributed feedback leads to the generation of a stationary near-Gaussian beam with a narrow spectrum. A random distributed feedback fibre laser has efficiency and performance that are comparable to and even exceed those of similar conventional fibre lasers. The key features of the generated radiation of random distributed feedback fibre lasers include: a stationary narrow-band continuous modeless spectrum that is free of mode competition, nonlinear power broadening, and an output beam with a Gaussian profile in the fundamental transverse mode (generated both in single mode and multi-mode fibres).

This review presents the current status of research in the field of random fibre lasers and shows their potential and perspectives. We start with an introductory overview of conventional distributed feedback lasers and traditional random lasers to set the stage for

---

* Corresponding author at: Aston Institute of Photonic Technologies, Aston University, Birmingham B4 7ET, United Kingdom.
 E-mail addresses: s.k.turitsyn@aston.ac.uk, skturitsyn@gmail.com (S.K. Turitsyn).

discussion of random fibre lasers. We then present a theoretical analysis and experimental studies of various random fibre laser configurations, including widely tunable, multi-wavelength, narrow-band generation, and random fibre lasers operating in different spectral bands in the 1–1.6 μm range. Then we discuss existing and future applications of random fibre lasers, including telecommunication and distributed long reach sensor systems. A theoretical description of random lasers is very challenging and is strongly linked with the theory of disordered systems and kinetic theory. We outline two key models governing the generation of random fibre lasers: the average power balance model and the nonlinear Schrödinger equation based model. Recently invented random distributed feedback fibre lasers represent a new and exciting field of research that brings together such diverse areas of science as laser physics, the theory of disordered systems, fibre optics and nonlinear science. Stable random generation in optical fibre opens up new possibilities for research on wave transport and localization in disordered media. We hope that this review will provide background information for research in various fields and will stimulate cross-disciplinary collaborations on random fibre lasers.

Contents

1. Introduction to laser science and applications

The invention of the laser in the late fifties of the 20-th century has initiated a continuous development of new generations of photonic devices and advanced optical engineering techniques. Photonics is established now as an enabling technology, having wide impact across many traditional and emerging sectors of the economy. The progress in photonics continues at a rapid pace world wide, with lasers playing a major role in this fast development. Lasers are typically an integrated product of several research fields and technologies, making them an inherent frontier of interdisciplinary research and development. A great variety of lasers have been demonstrated that cater to a range of applications in very diverse inter-related areas of science and industry. Laser systems are produced on very different spatial scales from nano-lasers to huge laser systems such as the National Ignition Facility in Livermore. Temporal and spectral characteristics of laser radiation also vary greatly from continuous waves with a narrow spectrum to ultra-short pulses with very broad bandwidth. There has been incessant progress in laser technology thanks to advances in: (i) material science, (ii) optical engineering, and (iii) an understanding of the fundamental physical effects underlying the operation and performance of new types of lasers.

Conventional lasers consist of an amplifying medium placed inside a resonant cavity that provides a positive feedback. The material of the medium determines the scale of photon amplification and wavelengths at which lasing is possible, whereas cavity modes define exact values for generated frequencies and provide a spatial structure to the output beam. Nonlinear properties of laser system materials are utilized for the transition from continuous wave (CW) to pulsed regime, for example via mode-locking, and laser frequency conversion via harmonics generation, four-wave mixing, super-continuum generation and other nonlinear processes. Optical engineering is pushing the frontiers of laser performance, for instance, it is critical for the up-scaling of laser systems to high power/pulse energy levels. Optical engineering on the one hand transforms laboratory laser demonstrations into real world applications through advancing architecture and design, integration of all system elements, testing and evaluation of exploitation and so on. On the other hand, optical engineering includes frontier research such as the development of special media with wave-guiding properties (for example, large mode area and photonic crystal fibres), special dispersion elements and nonlinear crystals, advanced cavity design etc. Furthermore, optical laser engineering also deals with resolving numerous technical issues, for instance, with heating, the efficiency of power conversion from pumping sources, stability of operation and various technical issues relevant to laser operation in a non-laboratory environment. It is practically impossible to overview all important aspects of laser science and technology even for a specific type of lasers. In this review, we will focus on the new laser concepts and underlying physical science, rather than on the technological and engineering problems.

It is quite remarkable, that despite the variety of system configurations, material bases and applications, the underlying operational and design principles appear to be very similar from one device to another, and, thus, similar basic mathematical models can be applied to rather different families of lasers [1,2]. Generic laser models are helpful for knowledge transfer from one area of laser science to another and also they attract interest of the mathematical community providing a basis for useful interdisciplinary collaborations. Arguably, the most important laser master model is the semiclassical laser theory based on the Maxwell–Bloch equations. This model is successfully used in a range of modern lasers to describe properties of generated radiation. The Maxwell–Bloch master model accounts for the coupling the electromagnetic field (governed by Maxwell's equations) to the nonlinear polarization of the gain material (described by the Bloch quantum equations for a laser medium). This model covers most of the key physical phenomena in lasers, including mode competition and selection, frequency and phase locking, self-pulsations, frequency pulling/pushing, mode synchronization, pulse stretching/compression and many others.

Even more complex behaviour takes place in the laser systems where the growth and shaping of radiation is affected by nonlinearity and the dispersion of the cavity medium. In this case conservative (not changing energy) effects compete with gain and loss making light dynamics very complex. The propagation of the optical field in the laser cavity in general is governed by the Maxwell's equations. However, in the majority of practical situations a slowly varying envelope approximation [3] can be applied to derive a simpler light evolution model, that accounts for all important physical effects accounting for light propagation in the cavity. A slowly varying envelope approximation is valid when the spectral width of the radiation $\Delta\omega$ is much smaller than the central operational frequency ω_0: $\Delta\omega/\omega_0 \ll 1$. The important step here was the introduction of the master mode-locking equation by H. Haus [4–8]. This model is a variation of the more general physical approach used in various areas of physics — the so-called Ginzburg–Landau equation [9]. In this approach the effect of discrete laser system elements is averaged over the cavity round trips and is effectively presented by a truncated Taylor expansion of corresponding physical effects occurring in a laser cavity, such as, for example, group velocity dispersion, nonlinearity, spectral filtering, linear and nonlinear gain/loss [4–8,10,11]. More advanced models characterize the intra-cavity radiation evolutions [11–13]. Critical in driving the intra-cavity dynamics are the amplitude and phase modulations generated by the discrete elements in the laser. Such theoretical approaches also have a very clear and simple geometrical

description of the intra-cavity dynamics making interesting links to the Poincaré mapping technique [11,14–16]. In a stable lasing regime, periodic round trips of light generate a cyclic reproduction of the optical field parameters (closed periodic loop), or Poincaré map in some phase space. Indeed, it is this phase–space representation that highlights the light dynamics or lack of changes per cavity round trip. This geometrical representation can be used for simplified and efficient modelling of lasers giving physical insight into the changes of key parameters from one cavity round trip to another.

The performance and operation of most advanced modern laser systems are determined by a rather complex interplay between the dissipative and conservative linear and nonlinear physical effects. For instance, ultra-short pulse lasers exploit the nonlinear (intensity dependent) optical response of the cavity medium for the generation and shaping of the pulses. The nonlinear science governs the complex behaviour of such systems providing the adequate language to describe coherent structures generation, their nonlinear interactions and the onset of their instabilities. Effects of gain and loss saturation, the spectral dependence of gain and loss, and the nonlinear dynamics of radiation in laser cavity make such lasers even more complex physical systems. Therefore, design optimization and the modelling of lasers often presents a complex multi-parametric nonlinear problem. Theoretical and numerical studies based on the nonlinear physics of lasers have yielded a wealth of important knowledge pertinent to the design of laser systems and for the discovery of new operational regimes.

In this review our main focus is on random fibre lasers. Apart from the practical importance in numerous applications, fibre lasers represent a class of very interesting physical systems. Light propagating down the optical fibre is trapped (in the directions perpendicular to the propagation) in a very small core of the fibre-optic waveguide. Propagation length can be very large due to low loss, making possible accumulation of the nonlinear effects characteristic of densely localized light. The combination of such inherent nonlinear properties of an optical fibre with the light amplification provided by excited atoms/ions in an active fibre or through the Raman effect in a passive fibre makes a fibre laser specially suited for studies of nonlinear processes. In the classical laser science, a resonant cavity (or resonator) is one of the fundamental elements of a laser system that defines the properties of the emitted radiation. For instance, resonator length determines the spectral spacing between longitudinal modes in a mode-locked laser and thus, the characteristics of the output frequency comb. The scale of the laser cavity can vary greatly. The shortest lasers have a sub-wavelength (sub-micron) cavity length, for example, a semiconductor nano-wire laser [17] and a spaser-based nano-laser [18]. The cavity of fibre lasers is usually formed by in-fibre end reflectors such as fibre Bragg gratings providing uniquely stable hands-free operation. Thanks to excellent optical-guiding characteristics with low loss, fibre lasers can have cavity lengths from a few centimetres to several hundred kilometres in ultra-long fibre lasers [19]. Interestingly, such ultra-long lasers can be used both as a light source, and, as a new and unique type of transmission medium [20]. The large cavity lengths of the fibre laser along with the broad gain bandwidth of doped fibres and/or Raman gain, ensures that a large number of longitudinal modes experience amplification and coexist inside the resonator, coupled through the shared gain. Hence, typical fibre lasers operate in a highly multi-mode regime having rich nonlinear dynamics. As a result of a broad gain bandwidth, longitudinal multi-mode interactions can produce temporal fluctuations much shorter than the laser cavity round-trip time. Such interactions can lead to mode locking and more complex temporal dynamics, for instance, period doubling and transition to chaos following the Feigenbaum scenario [21].

Fibre lasers feature interesting deviations from a typical mode-locking behaviour manifested as a sharp transition to coherent pulses from initial irregular mode dynamics during radiation growth from noise. In [22] the coexistence and interactions of the dispersive waves and many solitons were shown. The so-called "rain of solitons" regime results from the complex self-organization processes involving large numbers of solitons and dispersive waves. Another intriguing feature is the generation of double-scale noisy pulses in fibre lasers [23]. This is rather typical behaviour for long cavity pulsed fibre lasers [24], which is related to loss of coherence of radiation in the extended cavity. Coherence of fibre lasers is a fascinating area of research. In [25] an interesting analogy has been examined between the loss of coherence in a fibre laser with an increased power or cavity length and the transition to turbulence from a laminar state in a pipe flow.

The transition to stochastic turbulence-like behaviour of light waves (modes) generated in fibre laser cavities that becomes apparent at increasing power and length provides similarities to another class of lasing devices with irregular dynamics, namely, to random lasers. The concept of random lasers (see review papers [26,27] and references therein) has attracted recently a great deal of attention, because such lasers are able to generate coherent light without a well-defined cavity by exploiting multiple scattering in an amplifying disordered medium, for example, powders of "active" crystals or semiconductor particles. Multiple scattering increases the effective amplification path and provides random feedback resulting in lasing. The spectral, temporal and spatial properties of the random laser output beam are determined by a build-up of the radiation in such extended non-localized or local spatial modes randomly embedded in the bulk disordered material. Random lasers have some attractive features, such as, simple technology for providing compact design without the need to form a precise micro-cavity, e.g. as used in semiconductor lasers. However, for many applications their current performance characterized by pulsed operation with complex features in their emission spectra and angular dependence of the output beam, has to be modified to be able to challenge conventional lasers.

One of the ways to overcome these problems of random lasing is to use low-dimensional random systems. Directional pulsed random lasing has been demonstrated in few millimetre photonic crystal fibre with the hollow core filled by a random material consisting of R6G dye solution with TiO_2 particles [28]. An alternative approach is to use the intrinsic disorder in conventional silica fibres, as schematically shown in Fig. 1. Indeed, the refractive index of the telecommunication fibre has sub-micron-scale inhomogeneities, which are randomly distributed along the fibre. Rayleigh scattering (RS) on the inhomogeneities is responsible for setting a loss limit ∼0.2 dB/km at wavelengths around 1.55 μm, corresponding to the
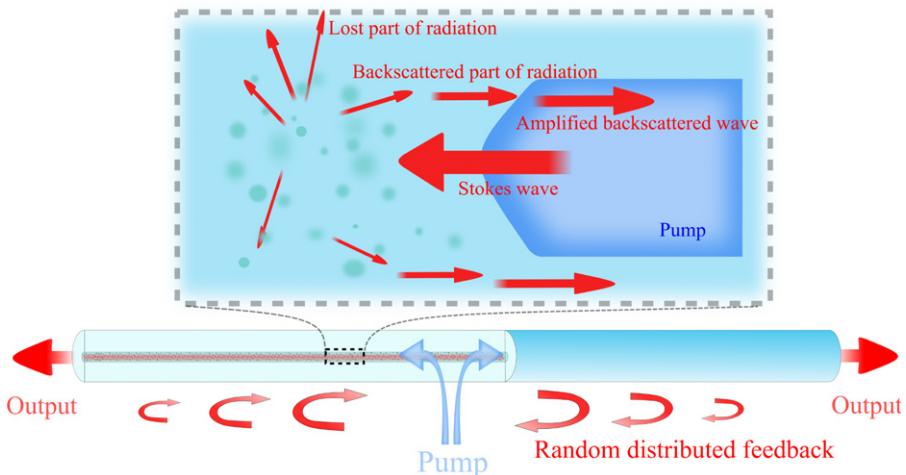
Fig. 1. A concept of the random distributed feedback fibre laser. Photons propagating in an optical fibre are elastically scattered by random refractive index inhomogeneities complying with Rayleigh's law. Most of the scattered photons leak out of the fibre core. Only 10^{-3} of them are backscattered and guided by the fibre. The Raman gain is used to amplify the backscattered guided photons that results in random lasing from both fibre ends.

transparency window of silica glasses used as a basic material in telecommunication fibres [29]. The fraction of the total Rayleigh scattered radiation which is reflected back into the fibre waveguide can be utilized for the feedback. Although the fraction of the backscattered radiation is extremely small, being only $\varepsilon = \alpha_s \cdot Q \sim 5 \cdot 10^{-5}$ km^{-1}, where the geometrical factor $Q \sim 0.001$ is defined by the numerical aperture and geometrical dimension of the fibre [30]. Therefore, the total backscattered radiation within the fibre is negligibly small ($R \sim Q \sim 0.1\%$) even in a ~100-km-long passive fibre. However, the situation is dramatically changed when the scattered radiation is amplified via Raman gain. Indeed, even extremely small random feedback initiates the generation under the condition of the high round-trip gain, $\sim 1/R^2$. This feature makes this system rather different from many other random lasers exploiting a strong scattering effect. It is also different from conventional Raman fibre lasers with regular reflectors, although in ultra-long fibre cavities with length above 270 km [19], the effect of distributed random backscattering becomes comparable to the regular feedback in the cavity formed by the point action reflectors placed at the ends of the fibre.

The first endeavour to get Rayleigh scattering based lasing in a long fibre without any regular reflector was resulted in very good output characteristics of this specific random laser called a random distributed feedback (DFB) fibre laser [31]. Low-threshold (~1 W), efficient (up to 30%), narrowband (~1 nm), and stable CW lasing of the near-Gaussian beam at 1.55 μm has been demonstrated just in a conventional telecom fibre with Raman gain homogeneously distributed along the 83-km long span. Since the laser is based on distributed gain and distributed feedback, it has some similarity with the conventional distributed feedback fibre laser that usually utilizes regular fibre Bragg gratings permanently inscribed in several cm-long highly-doped active fibre with π-shift in the middle. The random inhomogeneities of the refractive index in the fibre core are also "frozen". They represent a fingerprint of a particular fibre span defined by material and fabrication imperfections. Therefore, the partial reflections are random in space, but fully deterministic in time (both for amplitude and phase), interfering coherently with each other. Any random spatial sequence of distributed reflectors in terms of the Fourier presentation can be thought of as a sum of a large number of very weak regular gratings with fixed periods. A single periodic grating inscribed in an amplifying fibre is nothing more than a conventional DFB laser generating a single longitudinal mode. In this sense the random fibre laser based on RS may be thought of as the sum of a multitude of monochromatic regular DFB lasers with arbitrary phase and amplitude, which sum up into the resulting multi-frequency output. The main difference between these lasers is that the conventional DFB fibre laser exploits a regular *strongly* reflecting grating, whereas the random fibre laser has extremely *weak and long* random gratings. Therefore, the mode structure of the conventional DFB fibre laser is defined by the grating whereas the spatial power distribution in the RS-based long random fibre laser is mainly defined by the gain. Analysis based on conventional DFB fibre lasers used as building blocks has been applied previously for modelling of one dimensional random lasing with equal scattering centres randomly distributed in amplifying media, assuming that semi-periodic configurations with Bragg-like reflection are responsible for lasing [32]. So, the new concept of random fibre laser is closely related and even based on the earlier concepts of DFB fibre lasers, on the one hand, and random lasers, on the other hand.

In this review we would like to stress similarities between standard distributed feedback fibre lasers and random fibre lasers. In the DFB laser the amplification region is periodically structured, thus, providing through one-dimensional Bragg grating scattering of light propagating back into the cavity and an optical feedback for the laser. Random DFB fibre laser also features scattering of radiation back into the resonator, in this case by random scattering events. This is one of the lines of our review — we will consider random DFB fibre lasers in parallel and in comparison with DFB fibre lasers and will build an analysis on this analogy. We believe that parallel consideration of DFB lasers and random DFB fibre lasers may provide

new useful insights into random laser research. On the other hand, the feedback in random fibre lasers is based on random scattering in amplifying media, just like in traditional random lasers. The main difference with them is that the Rayleigh scattering in fibres is extremely weak and, therefore, the operating principle is different. The mean free path length in this case is much larger than the characteristic gain length, in contrast to the condition for conventional random lasers, which makes the properties of the new lasing scheme considered here rather unique. Thus, we will also present a current status of research in the field of random lasers.

We start with an introductory overview of traditional random lasers and conventional distributed feedback fibre lasers. Next we present experimental studies of various random fibre laser configurations including widely tunable, multi-wavelength, narrow-band generation, and random fibre lasers operating in different spectral bands with different pump lasers, including direct laser diode pumping as well as cascaded operation. Existing and future applications of random fibre lasers are discussed including telecommunication and sensor systems. A theoretical description of random lasers is very challenging and is strongly linked with the theory of disordered systems and kinetic theory. We describe in detail various models governing generation of random DFB fibre lasers, including balance average power models and the nonlinear Schrödinger equation based model. Finally, perspectives of the random fibre lasers are discussed.

The demonstrated random distributed feedback fibre lasers represent a new exciting field of research that brings together such diverse areas of science as laser physics, the theory of disordered systems, fibre optics and nonlinear science. Stable random generation in optical fibre opens a new direction for research of wave transport and localization in disordered media.

2. Random lasers

2.1. Introduction to random lasers and the main concepts

The concept of laser light generation in cavityless random active media was introduced by Letokhov in 1966–1968 [33,34], initially in the context of studies of interstellar radiation. Since then the field of random lasing has developed into a sophisticated and exciting area of laser research. The random laser has attracted a lot of interest, both as a rich complex physical system, and as a relatively simple laser device with a potential for cost-efficient mass manufacturing. The broad interest in random lasers arises also due to a number of inter-disciplinary links to other research fields, such as the theory of disordered systems, material science, applied mathematics and theoretical physics, transport theory, spectroscopy, laser physics, medical photonics and others.

In conventional lasers, the cavity (resonator) determines the key properties of laser radiation, such as spectral and spatial mode structure, directionality/divergence, polarization and other parameters of the output beam. In random lasers, there is no traditional cavity, and properties of the generated light are defined by random multiple scattering of photons in the gain medium. Therefore, material properties are especially important for random lasers. There are many examples of materials and media with a disordered structure, for example, powders, granular materials, plastics or polymers, dye materials, porous glasses in which random lasing was demonstrated. The use of disorder for controlling of a laser output performance is challenging, due to a number of technical and fundamental issues originating from the randomness, for instance, low signal-to-noise ratio of the lasing peak, sporadic laser oscillations at multiple wavelengths, high value of the generation threshold, lack of directionality and others. On the other hand, due to randomness, properties of generated light might be dramatically different from that produced by conventional lasers giving promise of new applications. We anticipate, that random optical structures with an intrinsic disorder may be used in photonic devices similar to well established technologies based on periodic optical structures. Note that the application of periodic structures in photonics has a long history, and the periodicity is nowadays an inherent ingredient in a variety of optical methods, techniques, devices and technologies. The use of random structures in photonics is still at the initial stage of research on the underlying physics level. Therefore a lot of new ideas are still continuously generated in the field and it may take some time before they will be implemented into practice. We believe that the impact of the emerging studies of random optical structures on future photonic technologies will be comparable with the leverage of periodic patterns and compositions.

In this review paper we combine a discussion of the distributed feedback fibre lasers and random fibre lasers to demonstrate similarities and differences between lasers based on periodic structures and random ones. Physics and applications of random lasers have already been well featured in a number of comprehensive review papers and books [26,27,35–38], and we do not intend to make a new overview here of the well known properties and types of random lasers. Instead, we would rather focus on fibre random lasers that became the subject of extensive studies only recently. However, to set a stage for discussion we have to highlight briefly the basic facts about "traditional" random lasers relevant to the main topic of the paper.

Before going into details, we would like to mention several important, relatively recently introduced concepts in a random laser science. An interesting configuration of random lasing in a dye-circulated structured polymeric micro-fluidic channel was proposed and demonstrated in [39]. In this instance, the disorder appears due to the limited accuracy of the photolithographic process. Lasing thresholds comparable to those of conventional micro-fluidic lasers were demonstrated while keeping a relatively simple random laser design compared to the challenges of the micro-fluidic laser cavity fabrication. The application of low cost random lasers in the area of opto-fluidics might be an attractive alternative to on-chip laser integration with light and fluidic functionalities [39]. In a more general sense, a combination of lasers and micro-fluidics has a great promise for a new breakthrough in laser science and technology. One of the promising directions here is to apply opto-fluidics for the improvement of a control over the generated emission, namely its angular and spectral stability, that
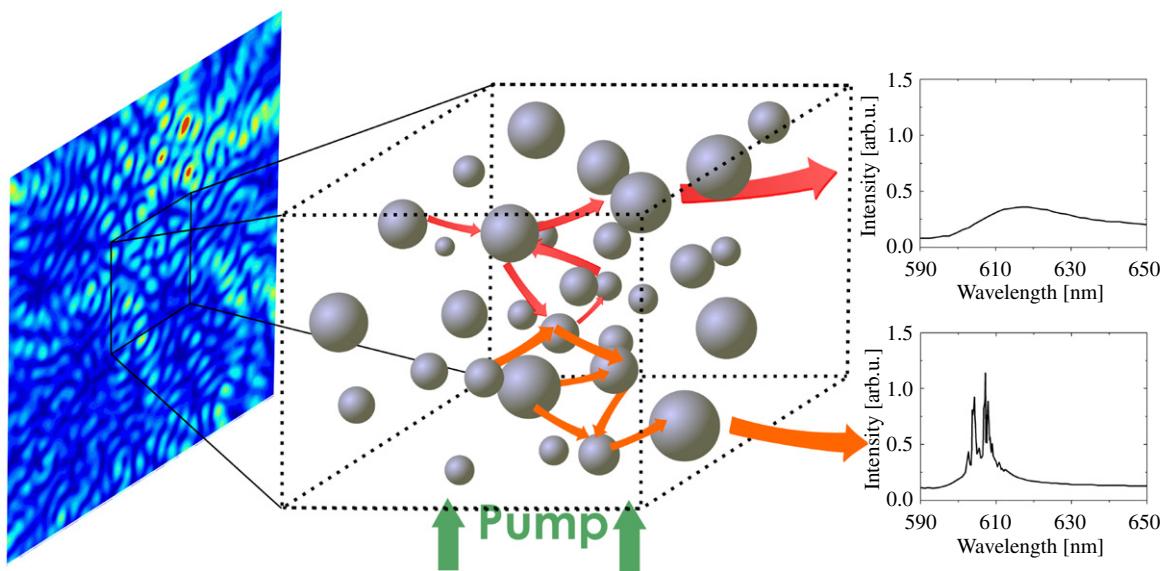
Fig. 2. Random lasing. In the random media light can propagate on different paths that results in different generation spectra emitted in different directions; the laser has poor directionality. The power distribution is highly non-uniform in the gain media (left, after Ref. [38]).
Source: Optical spectra are reprinted with permission from Ref. [41].

is one of the major challenges in random laser technology. In the recent work [40], a novel approach is proposed to control output radiation of random lasers, based on spatial shaping methods employed for coherent light control in complex media. The spatial pumping profile control was implemented in an opto-fluidic random laser where modes are spatially extended and strongly overlapping [40].

The nature of lasing modes in random scattering active media is a fascinating research problem that is still under extensive studies and discussions. Randomly scattered light travels in the amplifying medium along very complicated paths, as illustrated by Fig. 2. It is broadly accepted now (see [37,38] for details) that the output characteristics of random lasers are defined by the randomly embedded localized spatial modes that can coexist with non-localized extended modes. The spatial distribution of modes is a fingerprint of randomness that is one of the key features distinguishing random lasers from conventional ones. The complexity of a spatial mode distribution in random lasers makes its description a challenging scientific problem and also offers new possibilities for applications that cannot be achieved in conventional lasers.

Other interesting studies were recently undertaken on lasing in granular media. The granular materials are very important for a range of industrial applications from pharmaceutical to agriculture. In [42,43] random lasing was applied to produce the first phase-diagram of a granular. This was implemented through "a shaking random laser" — the generation of light in a vertically-oscillated granular material put in a liquid solution in a container. The properties of the laser emission from such a system depend on the characteristics of the mechanical motion of the granular medium. This makes it possible to link the different phases of granular medium through disparity in the corresponding laser radiation. This is, certainly, somewhat radically different from standard laser applications.

Though lasers are normally thought of as a source of coherent light, they can also emit radiation in the regimes of temporally or spatially incoherent laser emission. The high power sources with spatially incoherent radiation might be useful in illumination and projection systems. One of the important applications of random lasers may be in imaging. Highly coherent sources such as conventional lasers suffer in some imaging applications from shifting patterns of bright and dark zones that appear when a laser beam passes through a scattering medium — speckles. Such speckles result in the degradation of images recorded using laser radiation. Random lasers with low spatial coherence are very attractive for speckle-free imaging offering solutions alternative to low-brightness light emitting diodes or incoherent lamps [44]. A range of other potential applications of random lasers include medical applications, compact light sources, spectroscopic monitoring devices, illumination materials and others.

2.2. Resonant and non-resonant feedback in random lasers

Random lasers can be divided into two major classes depending on the nature of the laser feedback, namely resonant feedback (field feedback) and non-resonant feedback (intensity feedback). The main features of random lasers with resonant and non-resonant feedback will be examined in this section.

A conventional laser scheme normally requires two key elements: a gain material that provides amplification and an optical cavity that traps the light creating a positive feedback. The generation can be achieved (consider without loss of generality a Fabry–Pérot resonator) if the total losses are equal to the total gain, $R_1 R_2 \exp(2gL) = 1$. Here L is the cavity

length, R_1 and R_2 are reflection coefficients of the cavity mirrors, g is the gain. The light makes a round-trip in the Fabry–Pérot cavity, so only longitudinal modes with frequency ν_n satisfying the relation $\nu_N = Nc/(2Ln)$ are generated in the cavity (for the sake of simplicity, we do not take into account here phase delays on laser mirrors and assume a linear laser cavity). Here n is the refractive index of gain media, c is the speed of light, N is an integer number. The modes are spaced equally in the spectral domain with a separation $\Delta\nu = c/(2Ln)$. Radio-frequency inter-mode beatings could be directly measured by an electrical spectrum analyser. The laser mirrors imply specific phase relations on different modes generated in the cavity leading, in general, to the resonant feedback.

In 1966 Ambartsumyan et al. suggested a different type of a feedback — a non-resonant feedback [45,46]. They used the conventional laser design, but one of the cavity mirrors were replaced by a highly scattering bulk medium. The generated light does not accomplish exact round-trips in such a cavity, as the light changes the direction of the propagation being scattered each time from the different parts of the bulk scatterer. As a result, the laser generation consists of a large number of broad and overlapping low-Q modes contrary to high-Q narrow longitudinal modes in a conventional Fabry–Pérot cavity. These broad low-Q modes could overlap sufficiently, so the laser radiation can be thought of as radiation without spatial modes. As there is no any spectral selectivity imposed by the cavity, the feedback in this case is frequency independent and non-resonant, being just and energy/intensity feedback without phase relations implied on each cavity round-trip. The generation spectrum is continuous within gain bandwidth being centred on the frequency where the gain is maximum.

As we have mentioned above, the self-generation of light in an active scattering medium without any laser mirror was proposed by Letokhov in [33,34]. Under the assumption that the photon mean free path l is much smaller than the average dimension of the system L, and much longer than the generation wavelength λ, i.e. $\lambda \ll l \ll L$, the light propagation can be treated using the diffusion equation. It was assumed that any phase information is lost during numerous scattering events. Despite the non-resonant nature of a feedback the laser generation can be achieved in this regime. Indeed, Letokhov shown that the integral gain is proportional to the volume of the scattering system. At the same time, the integral losses are proportional to the surface area of the scattering system. Therefore, at some critical volume the gain can overcome the losses and the generation threshold can be reached. The feedback in this laser is treated to be non-resonant due to a lack of phase sensitive feedback. Letokhov also described [34] the other key feature of lasing — spectrum narrowing, and demonstrated existence of the relaxation oscillations in this system. The next important step in the field was the experimental demonstration of the features predicted by Letokhov. It was done by Markushev et al. [47] in scattering systems containing laser crystals processed into the powder (see also other early works [48,49]). The narrowing of the emission spectrum as well as the threshold behaviour of the output power under optical excitation were observed.

Further progress has been achieved in a seminal paper by Lawandy et al. [50] who used a suspension of TiO_2 micropartiocles in rhodamine 640 perchlorate laser dye. Again, the manifestation of the generation threshold and the narrowing of the emission line suggested a laser behaviour and, therefore, the existence of the feedback being non-resonant in this case. As the generation depends strongly on the density of scattering particles, it was assumed that the feedback is directly related to the scattering. The system was called by the authors of [50] a laser paint, as it could be painted on surfaces and be lasing under appropriate excitation. In 1995 the term *random laser* was used for the first time [35,51] igniting re-emerged interest in this fascinating research field.

An important next step was made in 1998 by H. Cao. A completely different type of random lasing was demonstrated in [52,53]. ZnO powder and polycrystalline films with an average particle size of 100 nm were used in experiments. Contrary to previous demonstrations, the strong scattering leads to the resonant feedback. After multiple scattering, light can make closed loops, so interference effects determine the laser frequencies. The resonant feedback results in narrow lasing spikes on top of the smooth gain profile, different spikes are attributed to distinctive lasing modes and appear randomly over the gain spectrum.

Since the initial demonstrations, a huge number of different types of random lasers operating in different gain and scattering media were reported. An excellent overview of random lasing features in systems with non-resonant and resonant feedback can be found in [37] and [26], respectively, as well as in recent review papers [27,38] and book [36]. Further in this section we discuss demonstrations of random lasing in different types of media.

2.3. Random lasers based on direct bandgap semiconductors

Direct bandgap semiconductors are widely used to achieve random lasing starting from the first demonstration of lasing in ZnO powder in [53]. Most of the random lasers in disordered semiconductor materials are reported on the base of ZnO samples in various forms — powders, films, nanowires and nanorods, nanoneedles. Many papers report on random lasing in ZnO powders, see, for example, early works in the field [53–57], as well as the review papers [26,37]. Different organic and inorganic polymer matrices could be used to host ZnO particles to facilitate material fabrication and processability in view of potential applications [58].

Other semiconductor materials could be also used. A random laser based on GaAs powder emitting near 880 nm is reported in [59,60]. Interestingly, in [61] an anti-Stokes GaAs-based random laser operating at 885 nm with two-photon pumping at 532 nm was realized demonstrating another mechanism for population inversion and gain in the system. The ZnSe powder based random lasers are reported in [62]. In [63,64] room-temperature pulsed random lasing from the single-crystalline compound Cr^{2+}:ZnSe powder is reported. Note that the laser emits in eye-safe infra-red region around 2.4 µm. Gold-nanoparticle-assisted random lasing from powdered GaN is demonstrated in [65].

Advances in ZnO structures manufacturing processes [66] result in the possibility of fabricating various ZnO based structures. Random lasing is observed in many of them. ZnO nanocrystalline films are widely used for random generation, see, for example, [52,67–71], as well as films combining different materials are used [72–74].

The application of nanowires and nanorods for random lasing is another interesting opportunity. UV lasing in a single ZnO nanowire under optical pump was demonstrated in the seminal paper [75]. The feedback mechanism is associated with axial Fabry–Pérot waveguide modes as the nanowire is well-faced, and the large refractive index difference between the semiconductor material and surrounding dielectric environment enables light confinement in the nanowire cavities. The threshold pump intensity of 40 kW/cm^2 is reported. Meanwhile, high pump intensities need to achieve random lasing in short nanowires having high cavity losses. In high-density arrays of vertically aligned ZnO nanorods, the random lasing threshold can be as high as $\sim$1 MW/cm^2 [76]. Random lasing is also achieved in ZnO nanoneedles [77,78]. Interestingly, it was found that random lasing is more easily implemented in disorder-grown oriented ZnO nanowires rather than in well-aligned ZnO nanowires [79]. Under 355 nm pumping, the lasing around 390 nm is achieved with randomly distributed lasing spikes of less than 0.4 nm linewidth.

The lasing threshold can be made sufficiently less when nanorods are accompanied by additional nanoparticles. For instance, TiO$_2$ nanoparticles ($\sim$10 nm in diameter) were deposited on ZnO nanorods surface ($\sim$100 nm in diameter) in [80]. The threshold is decreased almost twofold for random lasing in nanocomposites consisting of ZnO nanorods and TiO$_2$ nanoparticles as compared with the lasing in pure nanorods. The associated mechanism is the fluorescence energy transfer from TiO$_2$ nanoparticles to ZnO nanorods through the resonance effect of the excited electron–hole pairs contributing to the band edge emission. A similar strategy could be used to improve lasing properties of powder based random lasers. It was shown that a resonant energy transfer from the organic-dye molecule donor to the ZnO-nanopowder acceptor results both in increased lasing emission intensity and a reduced threshold power [81]. Further development in the field of random lasing in nanorods/nanowires involves lasing in different materials such as gallium nitride (GaN) [82,83], SnO$_2$ nanowires [84,85], randomly assembled ZnS nanosheets [86], composites consisting of photonic crystals and semiconductor nanowires [87], composites consisting of ZnO nanorods and SnO nanoparticles [88].

2.4. Dye and polymer based random lasers

Another widely used way to provide a gain in a random media is to exploit laser dyes and/or polymer active materials. Initially, random laser emission was observed in a laser dye dispersed in a strongly scattering medium in a solution containing TiO$_2$ or other types of micro- and nanoparticles [50,89–91]. A systematic study of the random laser properties dependence on the dye and metallic scatterers concentrations is presented in [92]. The topic is still under active studies, see, for example, recent works [93–95]. A laser dye could be hosted in various scattering matrices including polymeric films [96]. Films could contain additional nanoparticles to increase the scattering strength [97]. In this way, weakly-scattering dye-doped polymer films are designed to provide coherent random lasing [98,99].

There is a way to achieve a random lasing in polymer films without using laser dyes. This can be done in organic π-conjugated polymer films [100–104] providing high enough optical gain due to excitonic cooperative emission [105]. In the study presented in [106], Tulek et al. performed measurements of generation threshold probability density functions depending on the excitation area size and combined this data with a proposed technique of space/spectrum cross-correlation spectroscopy of the laser emission lines. They found that near the generation threshold, a single lasing mode is generated corresponding to a well defined laser resonator, thus confirming that the model of random resonators in the gain medium [107,108] explains random lasing in π-conjugated polymer films. In general, organic random lasers (based on organic based polymers) are extensively studied [108–111]. The random lasing was demonstrated both in two-dimensional organic thin films [112,113] and one-dimensional organic molecular nanofibres [114–116].

Combinations of laser dyes as active media and organic polymers as scattering media are also studied. It was demonstrated that the photosensitized polymers incorporating POSS (polyhedral oligomeric silsesquioxanes) nanoparticles dispersed at molecular level (1–3 nm) [117] can be used for coherent random lasing in slab waveguides in different spectral bands (depending on the dye used in the solution). As an example, lasing near 580 nm [118] and in the 660–740 nm band [111] was achieved in such organic random lasers. A similar approach is used in [119] to achieve random lasing in active waveguides having a high surface roughness because of the 2D island-like nanostructures obtained from a blend of a polymer and PMMA. A coherent random laser based on dye solution with POSS nanoparticles infiltrated into the hollow optical fibre core was demonstrated in [94].

Actually, laser dye or active organic polymers could be infiltrated in very different host materials. Lasing in opals infiltrated by *pi*-conjugated polymers or laser dyes was demonstrated [101,109,120,121]. In letter [39] random lasing in a dye-circulated polymeric structured microfluidic channel was achieved. The disorder arises from the limited accuracy of the microchannel photolithographic manufacturing process. Other examples of dye-doped solid-state hosts are silica gel powders [122] and polymer nanowire array embedded in a porous alumina membrane [123]

Using liquid crystals is also proven to be an efficient way to generate random laser light. In initial endeavours, see [124], liquid crystals were used to provide a scattering needed for the random generation and, at the same time, to tune the emission wavelength. To date, a number of liquid crystal based lasers was demonstrated [125–140] providing generating both via coherent and incoherent feedback. As the refractive index of liquid crystals can easily be controlled externally because of large anisotropy, liquid crystals based random lasers are easily tunable. Indeed, it was demonstrated that the

generation threshold and/or generation wavelength can be controlled by temperature [125,126,128,129,132,136], external voltage [133,134,141] or by optical means [137,138].

2.5. Plasmonic-enhanced random lasers

New interesting possibilities arise when metal nanostructures are used as scatterers. Indeed, the scattering efficiency of subwavelength sized metal particles could be enhanced due to the existence of surface plasmons. When metal particles are used in a random gain media, the laser performance can be substantially improved. A number of random laser systems based on the plasmon-enhanced scattering mechanism were demonstrated. In [142] plasmonically enhanced diffusive and subdiffusive random lasers made from a suspension of silver nanoparticles in a laser dye is reported. Surface plasmon resonance increases the scattering cross section keeping the gain volume large as the geometrical cross section of scattering particles remains small. Moreover, the localized electromagnetic field near the particle surface leads to enhanced absorption of excitation light and larger amplification of fluorescence. For silver particles of 55 nm diameter used in [142], the field enhancement near the particle is 3 times for a wavelength of 532 nm. As a result, the generation threshold is lower and the linewidth is smaller in the studied surface plasmon enhanced random laser as compared to a laser using dielectric nanoparticles.

Further, random lasing in Rhodamine 6G doped polymer films containing silver nanoparticles was achieved [143], as well as coherent random lasing in highly transparent polymer film doped by silver/metallic–dielectric core–shell nanoparticles was demonstrated [98,99]. The generation threshold and lasing intensity depend on the nanoparticle size. A waveguide-plasmonic scheme was proposed in [144]. The demonstrated random laser consists of the matrix of randomly distributed gold nano-islands coated by a layer of active waveguide made of dye-doped polymer providing strong confinement for the generated light. Another approach was realized in [145], where random lasing was demonstrated in a dielectric–metal–dielectric surface plasmon waveguide, in which top and bottom dielectric layers contain scatterers and provide optical gain. Some improvements of lasing properties can be achieved under the appropriate design of the waveguides [146].

It is important that surface plasmon resonance scattering peaks have to be matched with the gain spectrum to achieve a low-threshold surface-plasmon-enhanced random lasing. However, this is not necessary for a simple demonstration of random lasing. In [147] the authors managed to achieve random lasing near 575 nm by pumping a system containing silver nanowires and Rhodamine 6G far from a resonance peak of the nanowires at 380 nm. Similarly, resonant surface plasmon enhanced random lasing was obtained in gold–silica nanoshells in de-ionized water [148]. The system is pumped at 514 nm that is above surface plasmon resonance frequency. The random generation occurs at wavelengths from 720 to 860 nm corresponding to frequencies near and below the plasmon peak.

In semiconductor ZnO based random lasers, surface plasmons can be used if metal nanoparticles are added [149] or graphene nanoflakes are used [150]. In [65], gold nano-particles were used to improve efficiency of the powdered GaN random laser. Summarizing, a random scattering in active media combined with plasmonic effects is an efficient way to develop new classes of random lasers.

2.6. Other types of random lasers

Another possibility to produce random lasing is to use rare-earth doped powders. The most frequently used element is Nd, see examples in the nice book [36] and reference therein, as well as [151–155]. Random lasing is also achieved in Pr^{3+} and Ce^{3+}-doped δ-alumina nanopowders [156]. In early works laser crystals processed to a powder state were used to achieve random generation [47–49,157–159] as well as random generation was achieved in a powder of LiF crystal with colour centres [160].

In [161] a random microchip laser was presented. The laser comprises a transparent ceramic Nd:YAG microchip and a Nd:YAG powder tablet for additional feedback. The laser operated in quasi-continuous-wave regime. In the paper [162] colloidal quantum dot random laser is reported. In this laser the gain is provided by colloidal quantum dots randomly packed on the rough glass grooves having a disordered sub-micron structure. Paper [163] describes coherent random lasing in an aerosol of dye-doped microdroplets in the air.

Interestingly, the random lasing was demonstrated recently in a fluidic paper-based devices realized by conventional soft-lithography techniques on common paper [164–166].

Random lasing is demonstrated even in biological tissues including such an exotic ones as dye-infiltrated chicken breast [108]. In [167] it was experimentally shown that infiltrated with a concentrated laser dye solutions biological tissues, including human ones, provide coherent random lasing. Later, random lasing in bone tissue was achieved [168]. The main motivation of these works is to show that the random laser emission can potentially provide *in situ* information about structural and functional properties of the tissue under investigation. Indeed, it was found that malignant tissues show many more laser lines compared to healthy tissues taken from the same organ [167], and cancerous and healthy tissues have different light scattering properties that could be automatically detected in their random lasing emission spectra [169].

Promising results are obtained in the field of cold atoms. Random lasing in a cloud of cold atoms was theoretically predicted [170] and experimentally demonstrated in [171]. Cold-atom random laser could be a test bed system for further understanding of resonant scattering feedback in astrophysical lasers [172].

Most of random lasers generate in UV or visible range. However, mid-IR laser sources are of great demand in scientific and practical applications. Random lasing in the 2.4 μm band in the single-crystalline compound Cr^{2+}:ZnSe powder is reported in [63,64]. Generation near 2.18 μm was achieved in a random laser based on Cr^{2+}:ZnSe nanocrystalline particles [173]. Mid-IR random lasing is also possible in Cr-doped ZnS nanocrystals [174]. Interesting results are presented in [71], where the simultaneous generation of visible and ultraviolet light is reported in ZnO films. Other possibilities to obtain a generation in different spectral bands are the second-harmonic generation of a random laser radiation [175], the up-conversion of random laser frequency [176–178], and the anti-Stokes random lasing [61].

2.7. Electrically pumped random lasers

Random lasers are usually pumped optically. An important achievement in the field of random lasers was a demonstration of electrically pumped random laser diodes that opens the way to highly integrated optical devices. As a first step, the electrically pumped UV random laser diode was demonstrated in ZnO/dissimilar material heterojunction diodes [179] and the ZnO p–n junction [180]. Later, the electrically pumped random laser diode was demonstrated in Sb-doped p-type ZnO/Ga-doped n-type ZnO with quantum wells embedded in the junction [181]. The lasing mechanism is an exciton-related recombination and the feedback is provided by a close-loop scattering from densely packed nanocolumnar ZnO grains formed on Si. A room-temperature stable single-mode operation was obtained in arrays of random laser diodes [182]. Emission direction and the number of random lasing modes can be controlled by the presence of the rib waveguide in the random laser diode [183].

Electrically pumped random lasing can also be obtained in a simple ZnO based metal oxide semiconductor (MOS) structure [70], but an issue there is a relatively high generation threshold (68 mA). A high threshold could cause heating problems in potential applications. The low-threshold devices having a threshold of only 6.5 mA were demonstrated in ZnO nanocrystallite films grown on a glass substrate in an atomic layer-deposition technique [184]. Changing the structure of the material, the radiation wavelength can be tuned. As an example, in $Mg_xZn_{1-x}O$ films which are polycrystalline in nature with a random distribution of crystal grain, the central wavelength of random lasing spectrum becomes blue-shifted with the increase of Mg content [185]. Overall, the central wavelength of the random lasing spectrum is tuned from ∼377 to 352 nm with an increase of the x value in $Mg_xZn_{1-x}O$ from 0 to 0.35. Using ZnO nanorod arrays on Si substrate, the electrically pumped random generation was achieved at room temperatures [186]. Recently, electrically pumped ultraviolet lasing from ZnO in metal–insulator–semiconductor diodes based on ZnO films was achieved [187]. Generation properties of electrically pumped random lasers could be improved by using surface plasmon resonances [188].

Some other more exotic ways to pump random media do also exist. As an example, random lasers could be pumped by a *dc* electron beam of typical energy 1–10 keV. In this case, the pump beam penetrates deeply into the sample contrary to optical pumping where the surface scattering (usually strong in random materials) prevents optical pump penetration deep enough into the sample.

2.8. Control of random lasers emission

Random lasers characterized by a complex emission spectrum with many different spectral peaks on the top of the gain profile principally differ from conventional lasers with well-localized generation spectra. It is interesting to manage the emission properties of random lasers. Obviously, straight-forward approaches proved to be efficient in managing the radiation of the conventional lasers could be applied for random lasers also. For example, external mirrors can increase the output power in ZnO film based random lasers up to 10 times [54]. External mirrors are also proven to decrease the generation threshold in the Neodymium random laser [153,189]. In Nd random lasers, the intensity variation of a seeding light can be used to change the wavelength and the intensity of the random generation [190].

Random lasers can be tuned by temperature. In [124] temperature is used to switch a random laser below and above the threshold; a threefold change in the generation bandwidth was also observed. This was achieved by introducing liquid crystals to the dye solution to control the scattering strength. Indeed, the liquid crystal changes its phase from unordered to partially ordered while heated. As different phases have a different refractive index and, therefore, different scattering properties, the gain/loss balance in the random laser can be changed with temperature. Generation thresholds and output power of the random lasers with liquid crystals can be also controlled electrically [133,191]. Note that in random lasers based on dye-doped nematic liquid crystals polarization properties could be controlled by rotating the liquid crystal sample [139].

Random lasing properties of GaAs powders are also strongly dependent on temperature [60]. A model for a random laser tunable by a temperature through a three-dimensional random walk of photons in an active random medium has been developed in [192]. Both the intensity and the generation spectrum width are affected, because of the temperature-induced scattering mean free path changes.

The random laser properties could be effectively managed by using different particles added to the gain media. As it was numerically shown in [193–195], the resonant frequency of the monodispersed scatterers with externally introduced defects could be controlled by adjusting the Mie resonances of individual scatterers. Optimizing sizes and refractive indexes of the scatterers and the defects, random lasing can be initiated at points where defects are located. These findings were later confirmed experimentally [196]. Polymer particles were used as defects in monodispersed ZnO film. It was demonstrated

that in such a system the number of lasing modes is less and the generation threshold is lower compared to pure ZnO based random lasers. In organic polymer based random lasers, the emission wavelength can be shifted within 7 nm (in visible range) by controlling the mean diameter of monodisperse nanospheres forming photonic glass into which the π-conjugated active polymer is infiltrated [197].

Managing pump properties results in various changes of the random laser emission and is one of the most promising ways to control radiation of random lasers. Limiting the area illuminated by the pump beam, the generation threshold can be changed [154,198]. A local pumping also allows a selective excitation of individual localized modes in two-dimensional disordered systems in the localized regime [199,200]. An active control of the spatial pump profile results in the possibility to select any lasing mode from the overall random laser emission spectrum as demonstrated numerically in [40]. Further it was experimentally demonstrated, that random lasers can be tuned to any desired wavelength within the lasing spectrum under an appropriate optimization of the pump beam spatial profile [201]. By engineering the pump shape in order to excite different lasing modes, researchers even succeeded to observe a transition from the coherent to incoherent random lasing in the same sample [202]. Finally, by shaping the spatial pump distribution, authors of [203] numerically demonstrated that a random laser can be tuned to emit in specific predetermined directions, so highly directional emission can be achieved. What is important, is that this could be achieved in a weakly scattering regime for extended lasing modes.

A substantial step forward was made in paper [204] where a random laser with an a priori designed lasing peak within the gain curve was demonstrated. Contrary to the conventional route of using irregularly shaped or polydisperse scatterers having some average scattering strength being constant over the frequency, S. Gottardo et al. considered resonant scatterers. In randomly assembled monodisperse spheres there are scattering resonances determined by Mie resonances which shift the emission wavelength of the random laser by a value corresponding to several linewidths. The lasing frequency depends on the size and refractive index of the particles, so varying these parameters, generation wavelength can be precisely tuned. Later, it was shown that not only spectral position, but the generation threshold also can be controlled [205]. In paper [206] it was shown that control over the amount of absorption at the emission wavelength is another way to tune the random laser emission. To achieve that, a nonfluorescent dye is added to the gain medium. The nonfluorescent dye shifts the net gain curve, so the generation peak is also shifted.

In recent papers [202,207] the transition between different random regimes (from uncorrelated lasing modes of spiky spectrum to correlated lasing modes with a smooth spectrum) was observed while pumping conditions are changed. Under appropriate shaping of the pump, a shortening of the emission pulse is achieved that is accounted for the mode synchronization in a random laser. Control through spatial pump shaping demonstrated in [40] can resolve one of the major challenges in random laser technology — how to make a radiation with a predictable selective wavelength. The key approach proposed in [40] is to use a feedback loop to adjust the spatial profile of the pumping source. The pumping radiation was directed to the laser in perpendicular direction to the main laser axis. Before reaching the random laser medium, the pump wave was passed through a spatial light modulator that allows one to program the spatial shape of the pumping light. To control radiation of random lasers one needs to prepare spatial distribution of a pump wave that will hit different "random laser modes" (spatial parts of the lasing medium) in a pre-programmed way leading to selective lasing. This approach relies on the assumption that in a random laser there is a spatial (random) distribution of modes that amplifies photons of a specific wavelength. This method shows serious promise for the spectral radiation control through the spatial pumping profile programming [40].

2.9. Low-dimensional random lasers

Usually, the random nature of generation of radiation provides random lasers with special features compared to conventional cavity lasers, such as pulsed operation, complex non-localized emission spectra or an irregular and unstable angular dependence of the output beam. Low-dimensional random systems can be used to overcome these problems. In a theoretical paper [208] it was shown that in one-dimensional random laser operating in the regime of strong localization, the generation threshold decreases exponentially with the size of the system. Further, effectively one-dimension random lasing of directional output was realized in glass multi-layers doped with laser dye of randomly varying thickness [209]. Random lasing is also achieved in fully organic dye-doped flexible one-dimensional random multilayer photonic crystal [210].

Using optical fibres as a host for traditional random gain media provides a lot of possibilities. The first work in this direction was reported in [28] where a directional pulsed random lasing was demonstrated in the photonic crystal fibre with the hollow core filled with a suspension of TiO_2 nanoparticles in a Rhodamine 6G dye solution. In this way, the fibre waveguide properties are combined with traditional bulk random material (amplifying dye with randomly scattering nanoparticles) providing one dimensional random lasing. Further, a coherent random fibre laser operating in an extremely weakly scattering regime was demonstrated in [94,211]. The laser is based on a hollow-core optical fibre filled with a dispersive solution of polyhedral oligomeric silsesquioxanes nanoparticles and laser dye. The reduced generation threshold and increased directionality was demonstrated in this system. Another direction is to used polymer optical fibres. Dye-doped polymer optical fibre with nanoparticles incorporated into the core during manufacturing process was used for random generation in the visible range [212].

Another approach is based on using of a number of UV written in-core fibre Bragg gratings [213,214]. The array of randomly spaced gratings forms a complex cavity in an active Er-doped fibre, so the random lasing could be achieved under appropriate pumping. The reflection properties of the cavity and therefore lasing properties of a random laser depend on a
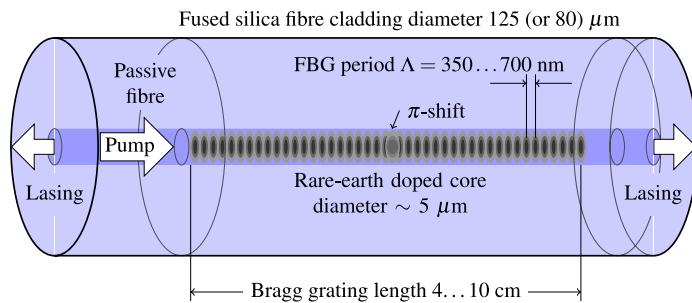
Fig. 3. Distributed feedback fibre laser cavity (not to scale).

number of gratings in the array. The theoretical mode analysis of a similar random laser in the presence of mode competitions is performed in [215]. A slightly different approach is used in [216] where a random Er-doped fibre laser based on a single long fibre Bragg grating having a large number of randomly distributed phase errors was demonstrated. The random fibre laser has a low threshold of 3 mW and a narrow bandwidth of 0.5 pm only. In general, UV light could be used to fabricate a disorder in a controlled way [217] with a potential for random lasing. Theoretical description of such random grating writing can be found in [218].

3. Distributed feedback fibre lasers

Fibre lasers represent a broad class of lasers that can be effectively treated as one-dimensional devices. In a single-mode fibre waveguide, the light is confined in a transverse direction that has a nearly Gaussian beam shape corresponding to the fundamental transverse mode of the fibre. Assuming that the effective mode area is constant along the fibre, the generated radiation dynamics is determined only by longitudinal variations of the optical power that is directly proportional to the intensity averaged over the mode area. This one dimensional spatio-temporal consideration has been shown to be well justified in a range of fibre-optic and fibre laser problems. However, though at very high powers the linear mode description can become a less adequate approach due to the impact of nonlinear effects on transversal field distribution.

Spatial variations of the refractive index in fibre cavity affect the properties of lasing. The simple design of fibre lasers with reflectors spread in space along light propagation direction is represented by the so-called distributed feedback (DFB) and distributed Bragg reflector (DBR) lasers. DFB lasers were first demonstrated by Kogelnik and Shank in 1971 [219,220] in gelatin films with induced refractive index or gain periodicity into which rhodamine 6G was dissolved to provide gain. It is interesting to note that those authors referred to DFB lasers as mirrorless.

This section focuses on the particular case of DFB fibre lasers [221]. The cavity of a DFB fibre laser is schematically depicted in Fig. 3. An optical pump is injected into the core of a single-mode optical fibre doped with rare earth elements. In transverse direction, the lasing mode is bound to the fibre core due to higher refractive index with respect to the cladding. Feedback originates from a slight refractive index modulation along the fibre axis; such a periodic structure is referred to as a fibre Bragg grating (FBG). In the longitudinal direction, the laser mode is localized around a specially introduced phase shift of the periodic structure.

Below we discuss several examples of DFB fibre laser applications and briefly overview types of DFB lasers and their history. Basic operational principles of DFB lasers will be illustrated through a discussion of distributed Bragg gratings and the influence of gain medium. Spectral properties are reviewed in the context of amplitude and frequency noise. We also examine DFB Raman lasers and gratings with complex structures due to their direct relevance to the main topic of our review.

Right from the earliest works in the field, studies of distributed feedback lasers have been stimulated by a strong industry demand for a compact and reliable narrow-band laser source that is appropriate for integrated devices. Semiconductor DFB lasers are now widely used for data transmission in high-speed fibre-optic networks. DFB laser diodes and DFB fibre lasers are successfully used in optical sensing, high-resolution spectroscopy of atoms and ions, for interrogating and cooling in experiments with optical traps including the most precise techniques in metrology. A range of impressive experiments have been conducted with various gain media and structure types that form laser cavities with distributed feedback.

Among the unique scientific applications of the DFB lasers are experiments on memory storage. Temporal cavity solitons may store information during seconds within a passive optical cavity approximately around one kilometre in length [222]. To compensate for cavity loss, a single frequency source with kilohertz linewidth needs to be locked to the cavity resonance. The DFB fibre laser was employed for this purpose in [222] and subsequent experiments.

In another impressive experiment, the Max-Planck-Institut für Quantenoptik in Garching and the Physikalisch-Technische Bundesanstalt (PTB) in Braunschweig, both in Germany, were connected by a 920 km long fibre link to compare frequency standards within some parts of 10^{-18} [223], which has better precision than that achievable with GPS satellites. At both locations, the DFB fibre lasers locked to ultra-low expansion cavities provided CW signals that were transmitted to

another site as a frequency reference. Finally, we note that the megajoule-class laser setup, the National Ignition Facility, incorporates CW ytterbium-doped DFB fibre lasers as the seed source [224,225].

3.1. Brief history of DFB lasers

We start by clarifying the difference between distributed feedback and distributed Bragg reflector lasers, even though they are indistinguishable in some cases. The medium with periodically alternating refractive index (modulated gain or waveguide with a periodic structure as the alternatives) has a set of diffraction resonances at certain wavelengths that known as Bragg scattering. A key feature is in the presence of sharp peaks in the backward reflection at resonant wavelengths. DBR lasers consist of volume or waveguide Bragg reflectors with a short-length gain medium between them that is comparable in size with the thickness (length) of Bragg gratings. Examples of active media include electrically pumped semiconductor structures and optically pumped fibre waveguides doped with rare-earth elements. The advantage of Bragg gratings over conventional mirrors is their narrow reflection spectrum, which makes it possible to achieve generation in a single longitudinal mode, even in the case of a wide luminescence spectrum of the active medium.

The main feature of distributed feedback lasers is that the gain medium and Bragg gratings are superimposed in the same volume. Backscattering due to grating provides enough feedback to compensate for a power leakage from the cavity by its amplification in the gain medium. A phase shift of refractive index modulation is usually induced in the central part of the DFB cavity, which makes it possible to divide it in two adjacent mirrors that form a high-quality resonator. This kind of cavity has just one laser mode with a low threshold, unlike the traditional Fabry–Pérot cavity, which has a set of equally spaced in frequency modes. As a result, DFB lasers do not suffer from longitudinal mode hopping and may be tuned continuously; for example, by heating or stretching the cavity.

Both of the above-mentioned early experiments with dye-infused gelatin film with periodic index [219] and derivation of the coupled wave theory of distributed feedback lasers [226] were pioneered by Kogelnik and Shank. A cavity formed by gain modulation was demonstrated in 1971 with a dye cell placed at the interference area of two crossed-pump laser beams [220]. Two years later, semiconductor lasers with optical pumping [227,228] and electrically pumped structures [229] were demonstrated.

An important step in the development of DFB lasers was the mentioned above invention of a cavity with an incorporated phase shift in the middle. This defect removes the degeneracy of two frequencies in cavities with refractive index modulation. A half-wave shift of the modulation phase (that equals to a quarter-wavelength of the light) significantly improves the cavity finesse as well, allowing it to achieve lasing in media with lower gain per unit length. This ideas was conceived in early work [230] but only implemented much later in semiconductor lasers [231].

On the other hand, continuous periodic Bragg structures with a significant imaginary contribution to the refractive index (gain or absorption) do not have either bandgap or degeneracy of modes with respect to lasing threshold; therefore, a reliable operation is possible without a phase shift in certain types of semiconductor lasers.

The first documented idea of a fibre DFB laser appeared in the mid-1970s [232] and was very different from the first practical implementation demonstrated decades later [221]. Instead of the initially proposed flash lamp wound in a spiral around the fibre, this first DFB laser experiment used in-core pumping by a single-mode laser diode. The technology of fibre Bragg grating inscription by an ultraviolet laser is much more convenient than the initial proposal to corrugate cladding surfaces, thereby forming a periodic structure. Thus, practical modern DFB fibre lasers hardly resemble the devices proposed in the first patent [232], though using the key design idea. Nowadays, erbium–ytterbium [221], erbium [233,234], ytterbium [235] and thulium [236] DFB fibre lasers have been demonstrated. Apart from the usual case of active medium with ground and excited energy level, it is possible to exploit nonlinear phenomena in passive fibres, namely gain due to stimulated Raman [237] or Brillouin [238] scattering (SRS or SBS).

We would like to mention the relevant review of Coles and Morris [239] in the rich field of liquid crystal lasers. This kind of medium resembles photonic crystals with a wide bandgap, and in most cases gain is a result of a combination of dye and pulsed optical pumping. Lasing has been achieved in different phases of liquid crystals, and mostly they are bandedge lasers, although defect-mode lasers (with phase shift inside the cavity) are also possible. The possible applications of liquid crystal lasers include holographic displays and medical diagnostics.

An electrically pumped plasmonic DFB laser has also been realized in a metal–insulator–semiconductor–insulator–metal structure [240].

It was demonstrated recently that bunches of cold atoms may provide sufficiently high feedback and gain for optical parametric oscillation when they are arranged is in a one-dimensional optical lattice in superimposed fields of magneto-optical and dipole traps [241].

The family of vertical cavity surface-emitting lasers (VCSEL) that are essentially semiconductor distributed Bragg reflector lasers includes mature devices for industry and laboratory prototypes that extend the operational parameters range. Their generation wavelengths spread from near ultraviolet to 2000 nm. Single-mode or multi-mode high-power single emitters, 1D, and 2D arrays with efficiency of more than 50% have been developed for the lighting and pumping of solid states and fibre lasers. Development of 1300 and 1550 nm lasers is stimulated by applications in telecommunications. In general, electrically pumped VCSELs are superior, but lasers with optical pumping may also be of interest for some applications. We do not have the opportunity to provide a comprehensive overview of VCSELs history or current state of the art here, as there is literature dedicated to these subjects [242–244]. Overall, a comprehensive overview of the fundamentals, properties, and technology
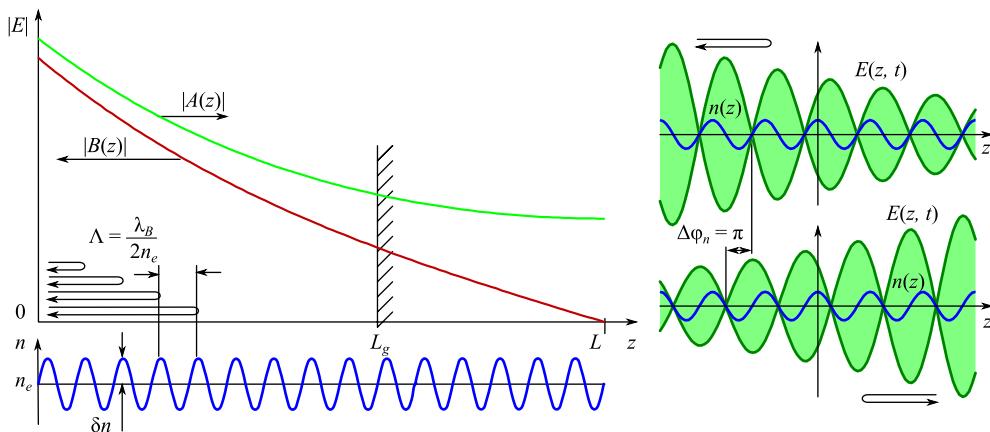
Fig. 4. Left: field amplitude of incident wave *A* and scattered wave *B* along the Bragg grating (top). Refractive index modulation parameters (bottom). L_g marks the distance to equivalent reflector for wavelengths close to the resonance. Right: standing wave envelope $E = A + B$ phase with respect to the refractive index modulation phase for the waves incident from the left side (top) and from the right side (bottom).

of semiconductors DFB and DBR lasers is beyond the scope of this section since there are many excellent review papers and books in this field [245,246].

Although DFB fibre lasers have a comparable impact with semiconductor DFB lasers review literature on DFB fibre lasers is relatively limited. Cranch's paper contains one of the best discussions of the key physical phenomena in the form of a brief review [247], even though the scope was limited to only erbium DFB fibre laser and their applications for sensing. The important result is the theory of spectral noise in a low-frequency range [248]. The review paper [249] presents an analysis of early experimental works and numerical simulations. The DFB fibre lasers are also discussed in the introductory book [250], though without much detail. The recently published paper by Zervas [251] presents an overview of current research in this field.

3.2. DFB laser cavity

The cavity of a distributed feedback fibre laser is formed by periodic modulation of the refractive index known as fibre Bragg grating. Although the reflected wave is formed by light scattered over the whole grating length, it is convenient to introduce an effective point of reflection that determines cavity length that will be used further.

Kogelnik's coupled wave theory is a convenient way to describe the interaction of light waves travelling in both (opposite) directions [252]. Specific properties of fibre gratings may be found in the brief review [253] or the books [254,255]. The case of the fibre laser allows us to consider a one-dimensional problem. Resonance reflection of the guiding mode is a particular case of Bragg scattering. We start the analysis from the general wave equation for an electric field

$$\frac{\partial^2 E(z,t)}{\partial z^2} - \frac{\epsilon \partial^2 E(z,t)}{c^2 \partial t^2} = 0. \tag{1}$$

Ignoring polarization, we assume that E is a scalar function. Instead of dielectric permittivity ϵ we will use the effective refractive index $n = \sqrt{\epsilon}$, where modulation along the fibre axis is presented (see Fig. 4) as

$$n(z) = n_e + \delta n \cos[2\pi z/\Lambda + \phi]. \tag{2}$$

Here n_e and δn include fibre geometry parameters, core and cladding refractive indices, therefore, for the sake of clarity, we operate with the effective (average) values. Λ denotes the grating period. Let us make the Fourier transform of Eq. (1) and consider evolution (in z-direction) of the monochromatic wave $E(z, t) = E(z) \exp(-2\pi i c t/\lambda)$ with a wavelength λ. This allows us to eliminate time dependence and reduce the problem to the Helmholtz equation for each the spectral harmonics:

$$d^2 E(z)/dz^2 + (2\pi n(z)/\lambda)^2 E(z) = 0.$$

Refractive index modulation leads to energy exchange between waves travelling along the z axis in opposite directions; further, they will be referred to as left and right travelling waves. It is convenient to introduce complex amplitudes of incident $A(z)$ and scattered $B(z)$ waves, slowly varying over wavelength scale, as follows

$$E(z) = A(z)e^{iz\delta - i\phi/2 + ik_0 z} + B(z)e^{-iz\delta + i\phi/2 - ik_0 z},$$

where $k_0 = 2\pi n_e/\lambda_B$ is a wavenumber at the Bragg resonance $\lambda_B = 2n_e\Lambda$ and $\delta = 2\pi n_e(1/\lambda - 1/\lambda_B) - \frac{1}{2}d\phi/dz$ is a wavenumber detuning from the resonance $\delta \ll k_0$. Substituting $E(z)$ to the Helmholtz equation, neglecting second

derivatives of $A(z)$ and $B(z)$, and averaging over fast oscillations, we come to the set of the two first-order linear differential equations. It is convenient to write relation of amplitudes at the points z and $z + L$ as follows [256]

$$\begin{pmatrix} A(z) \\ B(z) \end{pmatrix} = \begin{pmatrix} \cosh qL - i\frac{\delta}{q}\sinh qL & -i\frac{\kappa}{q}\sinh qL \\ i\frac{\kappa}{q}\sinh qL & \cosh qL + i\frac{\delta}{q}\sinh qL \end{pmatrix} \begin{pmatrix} A(z+L) \\ B(z+L) \end{pmatrix}, \tag{3}$$

where the parameter $q = \sqrt{\kappa^2 - \delta^2}$ takes complex values for detuning greater than grating strength $\kappa = \pi\delta n(z)/\lambda_B$. Taking $B(z + \Delta L) = 0$, which corresponds to the absence of an incident wave at the right edge of the FBG, we may readily get the following amplitude transmission t and reflection r coefficients:

$$t = \frac{A(z+L)}{A(z)} = \frac{q}{q\cosh qL - i\delta\sinh qL}, \qquad r = \frac{B(z)}{A(z)} = \frac{-\kappa\sinh qL}{\delta\sinh qL + iq\cosh qL}.$$

Close to the resonance, the phase of reflection coefficient has linear dependence on detuning

$$\arg r \approx \frac{\pi}{2} + \arctan\left(\frac{\delta}{q}\tanh qL\right), \quad \delta \ll \kappa.$$

After comparing the reflection coefficient $r = r_0 e^{2ik_0 L}$ to a thin mirror placed at some distance L, it may be concluded that for detuning $\delta \ll \kappa$ the grating is equivalent to a localized mirror placed at the distance $L_g = (2\kappa)^{-1}\tanh\kappa L$ and having a reflection coefficient (with respect to power) $R = \tanh^2\kappa L$. When considering DFB fibre lasers, we are interested in strong Bragg gratings $R \approx 1$ that may also be expressed as $\kappa L \gg 1$. This feature is a result of a relatively low gain compared to dye or semiconductor media.

As illustrated in Fig. 4, a wave propagating through Bragg grating is reflected from each layer of the grating. Incident wave $A(z)$ accumulates some phase on each grating layer. For detuning $\delta < \kappa$, the waves scattered at different points z interfere constructively, so the incident wave decreases along the grating with rate q. Condition $\delta < \kappa$ defines the stop band of Bragg gratings, where coupling wave equations have exponential solutions $e^{\pm qz}$. Outside the stop band q takes imaginary values and amplitudes A and B become oscillating functions $\exp iz\sqrt{\delta^2 - \kappa^2}$.

The spectral width of a Bragg grating may be estimated as minimal detuning when the reflection coefficient takes zero value

$$\delta_{\text{FBG}} \sim \sqrt{\kappa^2 + (\pi/L)^2}.$$

For example a grating with refractive index modulation of $\delta n = 10^{-4}$ has the width of $\delta_{\text{FBG}} \approx 0.05$ nm for the resonance wavelength of 1000 nm. A grating length of several cm makes a negligible contribution to the Bragg grating width. Unfortunately, full width at half maximum parameter convenient in practice does not have such a simple analytical presentation.

In a lasing regime there are no incident waves at both edges of the cavity ($A(z) = B(z + L) = 0$). For the fixed L and κ, the condition may be satisfied for a set of complex eigenvalues $\delta = \delta_{\pm n} - ig_n/2$, where g_n are gain for each lasing mode with respect to power. On the spectrum of the Fabry–Pérot resonator reflection, the modes are identified as minima. The spectrum of Bragg grating having length of $L = 2$ and strength of $\kappa = \pi$ is shown in Fig. 5. We will only to consider the case of strong gratings $\kappa L \gg 1$. Zeros lie outside of the stop band at detuning $\delta_{\pm n} = \pm\sqrt{\kappa^2 + (\pi n/L)^2}$. The gain necessary for lasing of $\pm n$ mode may be estimated as $g/2 \approx \pi^2(\delta_n L)^{-2}/L$. So that each spatial mode is two-fold degenerated with respect to frequency (sign of detuning), the modes for $n = 1$ have the lowest threshold. Power in dependence on coordinate z along the grating for the left and right travelling waves for $n = 1, 2$ are shown in Fig. 5. In the left part of the figure, lasing modes are marked as crosses and their ordinates reflects the required gain. They have detuning slightly less than $\delta_{1,2}$ in absolute values. Frequencies of adjacent modes are separated by approximately π/L, but the intervals are not exactly the same.

Historically, the first DFB lasers correspond to continuous uniform Bragg gratings described above. The main disadvantage of this kind of cavity is the possibility of lasing on the two degenerate frequency modes on the bandgap edges. It is usually easier to form a continuous grating, so the first demonstrations in various media usually happened in this way; for example, [219,220,227–229,241]. Another approach to avoid degenerate frequencies is to use complex coupling (gain or absorption modulation). This is suitable, for example, for semiconductor DFB lasers, but not for the considered fibre lasers.

In a high-quality linear laser cavity radiation is captured between two mirrors. A similar scheme may be realized with Bragg gratings. At the resonance wavelength, the wave reflected by the grating has the phase of $\pi/2$ with respect to the incident wave. The round trip phase must be a multiple of 2π, which means that two Bragg gratings have to be separated by some distance. It is similar to tuning a Fabry–Pérot interferometer to a specific wavelength. Alternatively, such a structure with the minimal grating separation may be considered as a single Bragg grating with the change of refractive index modulation phase in the central region. The phase shift of π maximizes the quality of the distributed cavity and is equivalent to the grating separation of $\lambda_B/4$. As a result of a compensated round-trip phase, spatial mode is localized around the introduced defect in the periodical structure.

We now take a closer look at the fundamental mode of the π-shifted DFB cavity. We will assume that the localized phase shift may have lengths ranging from parts of a millimetre to several millimetres, either intentionally or due to technology
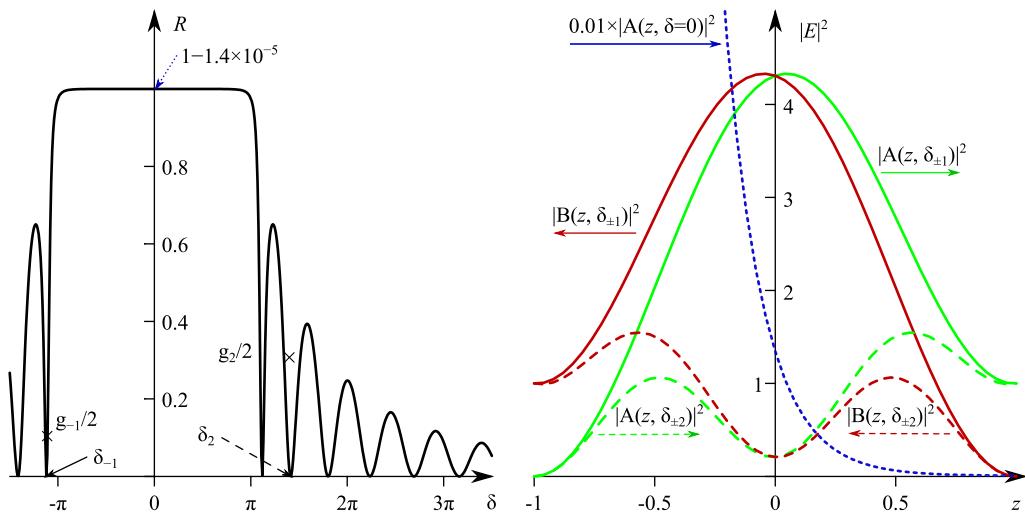
Fig. 5. DFB laser with continuous uniform grating. Spectrum of Bragg grating (left). Power distribution along the grating for the first- and the second-order modes, left and right travelling waves A and B (right). Scattered wave power for resonance wave $\delta = 0$ added for comparison.
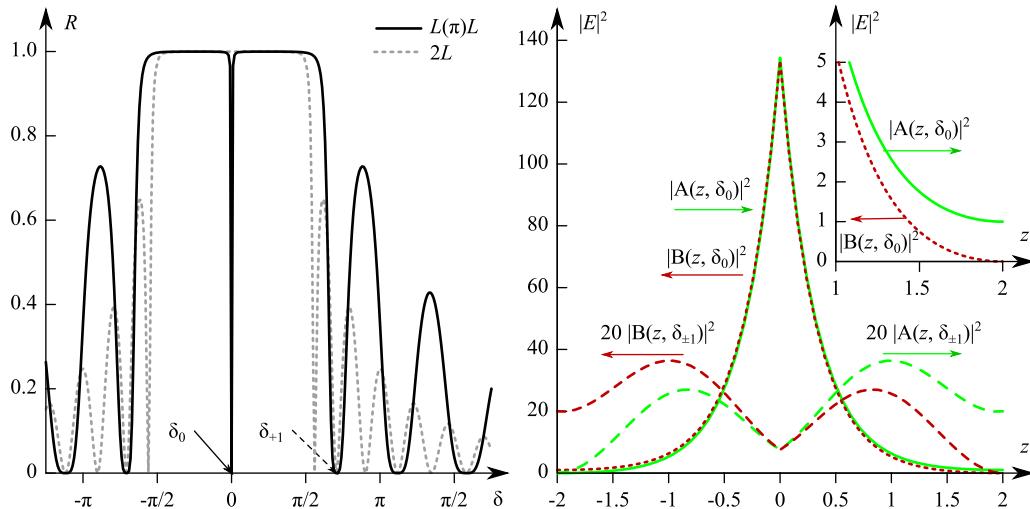

Fig. 6. DFB laser with π-shifted grating. Spectra of phase shifted grating and of the continuous grating of the same length (left). Fundamental δ_0 and first order $\delta_{\pm 1}$ mode power distribution along the grating length (right). Left A and right B travelling waves at the grating edge for the fundamental mode (inset).

limitations. The intensity of a resonant signal wave exponentially drops with distance from the phase shift location. We have introduced a grating effective length above, so the effective length of the cavity takes the form

$$L_{e,\text{DFB}} = 2L_g = 1/\kappa.$$

Cold-cavity resonance width (FWHM) for a DFB laser may be written using the expression for the Fabry–Pérot interferometer, having two mirrors of reflection and transmission coefficients (with respect to power) R_1, R_2 and T_1, T_2 in the following form (for the sake of simplicity we neglect signal absorption in the cavity medium):

$$\Delta \nu_{\text{FWHM}} = \frac{c(1 - \sqrt{R_1 R_2})}{2\pi n_e L_e \sqrt[4]{R_1 R_2}} \approx \frac{c}{4\pi n_e L_e}(T_1 + T_2).$$

The grating reflection spectrum and the mode profile along the fibre are shown in Fig. 6. They are plotted for a laser with a total grating length of $L = 4$ cm and grating strength $\kappa L = 2\pi$. These values correspond to $L_e = 0.64$ cm effective cavity length, $T_1 = T_2 = 0.7\%$ reflector transmission, and resonance width $\delta_{\text{FWHM}} = 0.012/\text{cm}$ or $\delta \nu_{\text{FWHM}} = 38$ MHz.

An analogy with a Fabry–Pérot interferometer is valid only for the fundamental longitudinal mode of a π-shifted DFB laser. Unlike an equally spaced spectrum of the modes that have the same quality factor, higher modes of a distributed feedback cavity lie outside the grating stop band, which means they have much lower quality and oscillating longitudinal profiles. In Fig. 6 the profile of the first mode is vertically scaled by a factor of 20. Higher-order modes have significantly
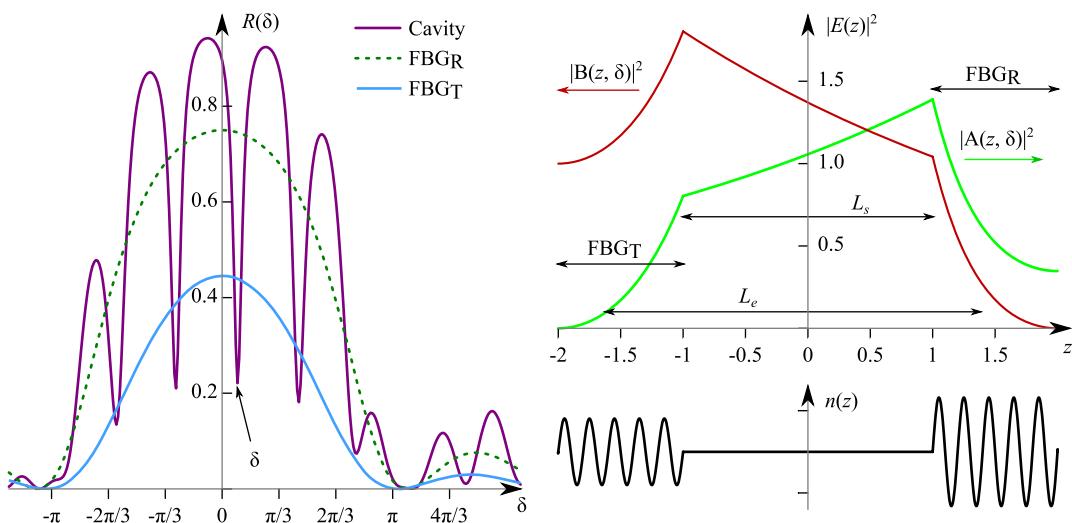
Fig. 7. Distributed Bragg reflector laser. Spectra of the cavity and the Bragg gratings (left). Power of the right and left travelling waves of the lasing mode and refractive index profile (right). FBG$_T$ and FBG$_R$ are output and dense Bragg gratings, respectively.

higher thresholds, which means that DFB lasers possess stable single frequency operation. It should be noted that this threshold may be reached in fibres that have excessively high gain since the fundamental mode saturates only the central region of the grating.

Another option is to write a couple of Bragg gratings with a distance between them that is comparable to the length of the gratings. The rationale for this kind of structure, referred to as a distributed Bragg reflector (DBR) laser, is that a piece of active fibre may be spliced in between pigtails with enhanced sensitivity to UV exposure. An example of a cavity that has a different mirror reflectivity is presented in Fig. 7. The laser emits mostly from the side of the weaker grating. DBR cavities often have significantly lower quality factors than DFB lasers. The optical path between the gratings must be maintained because the lasing mode wavelength must be at the maximum of their reflection spectra; otherwise, longitudinal mode hops and frequency instabilities may appear. It may be noted from the cavity spectrum that it supports more than one longitudinal mode having the close quality factors. The plotted longitudinal profiles represent the case of the medium with high enough gain. Note that DBR fibre lasers based on phosphate fibres with extremely high active ion concentration have been demonstrated in experiments [257].

Formally, any Bragg gratings in the laser cavity provide distributed feedback. In fact, the effect is noticeable while the separation distance L_s is not too large. The effective length of laser cavity is equal to

$$L_{e,\text{DBR}} = 2L_g + L_s = 1/\kappa + L_s.$$

When cavity parts with refractive index modulation are significantly shorter than the intermediate region, the system becomes a traditional linear laser cavity with localized mirrors. Any dielectric mirror is a case of a thin (or short in terms of this section) Bragg reflector. For sufficiently long lasers, the cavity may be considered as a Fabry–Pérot interferometer almost for the full bandwidth of the Bragg grating, and this spectral region is filled by equidistant cavity modes. A discrete lasing mode structure is a consequence of deterministic coherent feedback provided by Bragg reflectors. In cladding-pumped fibre lasers which generate the power of Watts level and have a cavity length of several metres, the nonlinear effects come into play, that means cladding-pumped fibre lasers simultaneously generate multiple longitudinal modes. This case is outside of the scope of this section, however.

It is well known that for a Bragg grating with a rectangular profile of refractive index modulation, the reflectivity drops quite slowly with an increase of detuning $R(\delta) \sim 1/|\delta|^2$ for $|\delta| \gg \kappa$. This is unacceptable for a series of DFB fibre lasers that are incorporated sequentially into a single fibre line. Such a chain of lasers with slightly different wavelengths may be used as a set of fibre sensors. A smooth refractive index profile at the grating edges suppresses an amplitude of side lobes. Similar to window functions in signal processing, this technique is known as apodization. An important specific requirement for DFB fibre lasers is both the grating edges and the phase shift are made smooth. This can be achieved either by gradual change of phase or modulation amplitude [258]. This point has not been fully recognized by some other researchers [259].

Since the main part of this review is devoted to the Rayleigh scattering, it is worth noting that any sort of external optical feedback sources may deteriorate conventional DFB fibre laser performance. Increased frequency and amplitude noise, their cross-coupling or even self-pulsation are especially important in remote sensing where long spans of fibre are inavoidable [247].

Therefore, in Eq. (2) an amplitude of refractive index modulation $\delta n(z)$, average index $n_e(z)$ and phase $\phi(z)$ may be functions that are slowly varied over the grating period Λ. In this case, the Bragg grating can be approximated by a stack

of short gratings with constant parameters; in other words, a rectangular profile. Similar to Eq. (3) it is possible to describe the tapered grating by the product of matrices representing rectangular gratings. This is a variant of the fundamental or *F*-matrix approach proposed by Yamada and Sakuda [256], which is referred to as the transfer or *T*-matrix method. A FBG with an arbitrary profile may be represented as a product of matrices describing short gratings with almost constant parameters (fundamental or transfer matrix approach). This is a sufficiently accurate and dramatically faster approach than a direct treatment of the Helmholtz equation, which requires integration with sub-wavelength steps.

When considering cavity modes, we have neglected nonlinear refractive change due to the Kerr effect. This assumption is valid for a typical DFB fibre laser, but the effect must be taken into account for Raman DFB fibre lasers, which are discussed in [260] and further in Section 3.5.

The fibre DFB lasers feature a refractive index Bragg grating with phase shift and achievable grating strength that determines a device length of several cm. Fibre Bragg grating may be written by CW frequency-doubled argon ion lasers operated at 244 nm or by excimer lasers; for example, at 193 nm. The presence of Ge_2O_3 in the fibre core makes it possible to modify the refractive index through UV exposure. Alternatively a B/Ge ring around the core may be formed if Ge ions degrade the performance of rare-earth active ions. An oscillating pattern of UV intensity is formed by the interference of two beams. The laser beam is split by a special diffraction grating (referred to as a phase mask) working in transmission and designed for enhanced ±1 diffraction orders while suppressing the zero-order beam. An active fibre is placed just behind the phase mask. In long gratings used in DFB fibre lasers, the focused UV beam is scanned along the fibre and the phase mask. The phase shift is induced by a longitudinal shift of the phase mask relative to the fibre, (for details, see [254]). The DBR fibre laser cavity may be also written by point-by-point technique using a femtosecond laser that has been reported in [261].

We have considered in this section some basic properties of laser cavities with distributed feedback formed by Bragg gratings. For the cavities with refractive index coupling, the phase shift in the middle of the grating dramatically increases cavity finesse and removes degeneracy of the longitudinal modes. The low threshold mode makes DFB lasers inherently stable single-frequency sources with no mode hopping. The distributed nature of optical feedback plays a crucial role, while the total effective cavity length is comparable to the effective length of the Bragg reflectors. The intensity of the lasing mode varies along the cavity by orders of magnitude; for DFB fibre lasers it is determined solely by Bragg gratings with a negligible contribution of gain. Lasing with a narrow spectrum is possible due to deterministic coherent feedback with smooth dispersion characteristics close to the peak of Bragg grating reflectivity.

3.3. Steady-state models of DFB fibre lasers

Numerical models are often considered to be an easier way to analyse DFB FLs than the analytical approach. Signal power variation along the cavity, spatial hole burning and excited state absorption make it difficult to provide useful analytical expression for laser parameters.

A reasonable agreement with experimental data was achieved for a numerical model of an ytterbium DFB fibre laser [262]. The local energy state population was expressed through pump power and signal fields. After averaging saturated gain to encounter spatial hole burning, a set of differential equations for the signal wave's envelope and pump power in dependence of the coordinate along the fibre was obtained and solved numerically.

Linear signal loss was introduced to a similar model of erbium DFB FL in order to find the optimal parameters of FBG strength and the phase shift position [260,263]. Limited by cross-relaxation erbium concentration, leads to low pump absorption and signal gain. Increasing grating strength to enhance signal field and pump–signal interaction works until signal loss (induced, for example, during UV exposure) becomes important.

The case of erbium–ytterbium DFB fibre lasers requires an extension of the rate equations to take into account the energy transfer between ytterbium and erbium ions. Pump absorption at 980 nm is enhanced by a high concentration of Yb ions, while erbium makes it possible to achieve lasing of approximately 1550 nm. To fully exploit advantages of versatile Bragg grating writing techniques [264,265], a grating strength was varied to obtain the highest Er:Yb DFB laser power [266–268]. A DFB cavity with optimal strength resembles a Fabry–Pérot cavity with mirrors concentrated on both sides of the active medium; this makes it possible to maximize cavity effective length and improve pump–signal energy exchange.

A detailed theory of DFB fibre lasers was developed by Scott Foster. The description of the longitudinal mode profile and erbium laser slope efficiency are given in [269–271]. Other groups have slightly corrected definitions of Er-doped fibre parameters [272] and discussed specific properties of thulium [273] and ytterbium lasers [274].

Whether the laser threshold can be reached is determined by the obvious relations for effective cavity length L_e, unsaturated gain g_l, mirror transmissions $T_{1,2}$ and unsaturable linear losses owing to scattering and defects α_0

$$g_l L_e > \frac{1}{2}(T_1 + T_2) + \alpha_0 L_e.$$

For the cavity with abrupt π phase shift $L_e = 1/\kappa$, where κ is FBG strength. If the total FBG length is L and the phase shift divides it into even parts, then $T_{1,2} = 1/\cosh^2(\kappa L/2) \approx 4e^{-\kappa L}$. The right part may be determined in the experiment by tuning similar DFB laser over the resonance of the FBG under the test since total cavity losses are proportional to resonance linewidth.
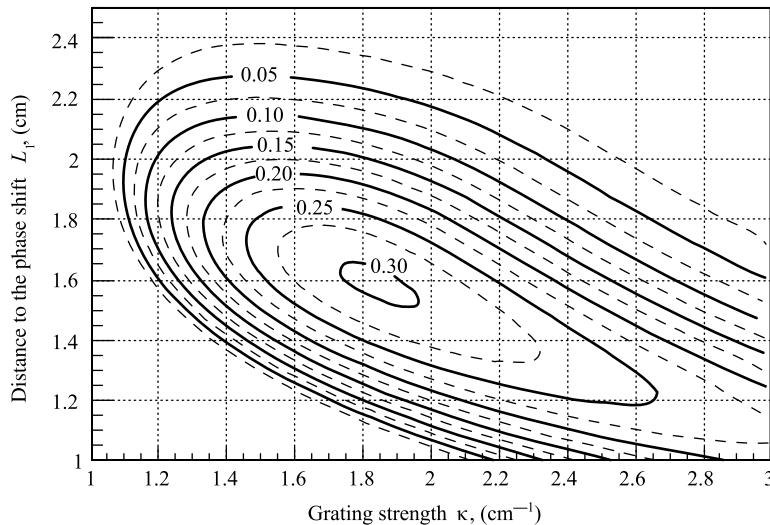
Fig. 8. Ytterbium DFB fibre laser slope efficiency in dependence on grating strength and phase shift position. The total grating length is 4 cm, its strength is constant, phase shift is localized, background signal loss $\alpha_0 = 0.028$ cm^{-1}, lasing wavelength is $\lambda_l = 1030$ nm, pump wavelength is $\lambda_p = 976$ nm.

The threshold gain for a 4-cm long DFB cavity having FBG strength $\kappa = 2$ cm^{-1} is equal to $g_t = 2.7 \times 10^{-3}$ cm^{-1} = 1.2 dB/m. This number may be compared with the minimal gain (with respect to power) required for lasing with continuous FBG [226]. Assuming strong index coupling and negligible gain coupling, we get an approximate number $g_t = (2/L)[\pi/(\kappa L)]^2 = 7.7 \times 10^{-2}$ cm^{-1} = 33 dB/m. This shows that DFB cavities with π-shift have a significantly lower threshold.

In order to express the slope efficiency of DFB fibre laser we must introduce some fibre properties (see [275] for details). Amplification in ytterbium and erbium (neglecting excited state absorption) doped fibre may be described by quasi two-level system with excited state lifetime τ_2. Below, l and p subscripts denote laser and pump beams with according wavelengths. $\alpha_{p,l}$ are absorption coefficients (per unit length) due to pump/lasing transitions at zero inversion, and $g_{p,l}$ are gain values at full inversion. These quantities are defined with respect to power (not amplitude). Note that $\alpha_i \neq g_i$ due to levels splitting and broadening. The pump-lasing energy exchange is actually characterized not by g_l and α_p, but by the $d_l = (g_l\alpha_p - \alpha_l g_p)/(\alpha_p + g_p)$ and $d_p = (\alpha_p g_l - \alpha_l g_p)/(g_l + \alpha_l)$ parameters. Therefore, in this sense, the above expressions with g_l are not strictly correct. To reduce subscripts usage, let us denote for the purpose of this section the *power* at the lasing wavelength as I, and the pump beam power as just P. We can introduce a saturation power $I_t = hcn_{Re}A_{n_{Re}}[\lambda_l\tau_2(g_l + \alpha_l)]^{-1}$ where n_{Re} is the volume concentration of rare-earth ions and $A_{n_{Re}}$ is the doped area cross-section. The similar expression is valid for pump saturation power P_t. Amplification of a travelling wave is given by the expression $I^{-1}dI/dz = (d_l P/P_t - \alpha_l)/(1 + I/I_t + P/P_t) - \alpha_0$. The saturated gain for the standing wave in the DFB fibre laser has the following form for a laser with rectangular FBG profile and localized π-shift $(d_l P/P_t - \alpha_l)[1 + P/P_t]^{-1}[1 + Xe^{-2\kappa|z|}\cos^2(kz + \phi)]^{-1}$, where X denotes saturation factor. Assuming that I_0 and P_0 are powers of the lasing and pump waves at the phase shift, yields $X = 2I_0 P_t/(P_0 I_t)$. Lasing powers at the grating edges $I_{1,2}$ are $I_{1,2} = I_0 T_{1,2}/2$.

The key equation that makes it possible to determine saturation parameter is given in above-cited works of Foster [269, 270]

$$\frac{4d_l}{\kappa X} \ln \frac{\sqrt{X+1}+1}{2} = \frac{T_1 + T_2}{2} + \frac{\alpha_0}{\kappa}. \tag{4}$$

For an arbitrary FBG profile the left-hand side can be written in the following generalized form

$$G(X)\frac{d_l}{\kappa} = \frac{d_l}{\kappa} \int_{z_l}^{z_r} \frac{|e(z)|^2}{1 + XL_e|e(z)|^2/2} \, dz \tag{5}$$

which may be considered as definition of the function $G(X)$ that will be used later. Here, $e(z)$ is a normalized longitudinal mode profile. Finally, the slope efficiency (for each edge) reads:

$$\eta_{1,2} = \frac{XI_t T_{1,2}}{4P_t} \quad \text{or} \quad \eta_{1,2} \approx \frac{2\lambda_p d_p T_{1,2}}{\lambda_l \kappa (T_1 + T_2 + 2\alpha_0/\kappa)} \ln \frac{\sqrt{X+1}+1}{2}. \tag{6}$$

A weak saturation approximation may be found in Foster's works. As an example, Fig. 8 demonstrates the slope efficiency of an Yb-doped DFB fibre laser when grating strength and π-shift position are varied. The calculations include correction for pump absorption along the laser cavity [269,274].

3.4. Temporal dynamics and noise properties

After studying steady-state parameters, the next step is to examine the impact of ambient noise and fundamental fluctuations on the laser power and its spectrum.

The relative intensity noise (RIN) of an erbium DFB fibre laser was calculated within the numerical model in [276]. Steady-state distributions of signal waves and inversion population were derived from a numerical model of DFB cavity [260].

An experimental study and an analytical description of amplitude and frequency noise components were performed by Rønnekleiv in [277]. He considered erbium-doped DFB fibre laser within a phenomenological model. Values of cavity parameters such as a round-trip time, a gain, reflection coefficients of mirrors were chosen to be close to experimental ones. However, the model does not take into account a strongly nonuniform longitudinal distribution of the power in the DFB fibre laser.

In the following Sections 3.4.1–3.4.3, we present ideas and results from works published by Foster dedicated to the theory of DFB fibre lasers [248,269,278]. It includes a dynamic laser model and a contribution of the spontaneously emitted photons to the relative intensity noise and frequency fluctuations [269], equilibrium heat transfer fluctuations which have higher impact on spectral noise below the relaxation oscillation frequency [278], and, finally, a $1/f$ contribution to the low-frequency spectral fluctuations was attributed to temperature fluctuations owing to spontaneous photons which are not related to lasing [248].

For lasers having a spectral linewidth of order of 1 kHz, external noise sources become important: pump noise, ambient temperature changes, vibration, and acoustic noise. So it is instructive to provide expressions for the fundamental noise limits (assuming a pump laser without any noise and a properly isolated laser cavity) and for the response functions to the perturbations by external sources.

Let us establish important numbers in the frequency scale for DFB fibre lasers. An effective cavity length of about of 1 cm determines a cavity round trip time of 10^{-10} s, so the perturbations should be considered as adiabatic. Excited state lifetimes for rare-earth ions are 10^{-2} s for erbium and approximately 10^{-3} s for ytterbium. In the rate equations, lifetime is accompanied by the ratio of saturation power and pump or signal power within the cavity, so the actual time-scale should be divided by 100 or 1000. As a result, relaxation oscillation frequency may be of the order of 100 kHz (perhaps 10 times lower or higher dependent on dopant and cavity quality). Below we determine time-scale of thermal processes that are slower than relaxation oscillation.

To clarify the meaning of the term noise, it is instructive to consider measurement techniques. Amplitude noise in a signal of power P (relative intensity noise (RIN)

$$\text{RIN} = \Delta P / \langle P \rangle$$

may be measured directly (through corresponding transform) with a photodiode and a radio-frequency (RF) spectrum analyser. The regions of interest are relaxation oscillation resonance and level of fluctuations at low frequencies. Note that noise in the pump source and effects inherent to gain medium such as an absorption of the excited state and cross-relaxation for the active (erbium-doped) fibre may deteriorate laser performance.

The DFB laser spectrum is too narrow for spectrum analysers based on diffraction gratings, and also for Fabry–Pérot interferometers with moderate finesse. Straightforward for semiconductor lasers, the self-heterodyne technique is suitable for determining spectrum linewidth [279]. The signal is split into two parts. One beam is delayed using a fibre spool by a time greater than coherence time, and in the other path frequency is shifted by an acousto-optic modulator. The laser linewidth is obtained from the beat signal spectrum of the two interfering beams. A 100 km long delay line (0.5 ms time) is unable to provide a reliable result for a linewidth of less than 2 kHz.

A fibre interferometer with $l = 1$–100 m path difference allows to obtain a spectral noise power density function that is indispensable for the characterization of fibre sensors. Let us consider electric fields in the laser field with negligible amplitude variation

$$E(t) = E_0 e^{-i\omega t - i\phi(t)}$$

where ω is a constant optical circular frequency and ϕ describes phase noise in the wave. The normalized low-frequency interference signal detected by a photodiode is

$$|E(t) + E(t-\tau)|^2/(4E_0^2) = \frac{1}{2}(1 + \cos[\phi(t) - \phi(t-\tau)]) \approx \frac{1}{2}[1 + 2\pi\tau\delta\nu(t)\sin(\omega\tau + \pi/2)].$$

Here $\delta\nu(t)$ is a deviation of optical frequency from the optical carrier ($\tau\delta\nu \ll 1$). Either τ or ω may be tuned to ensure $\sin(\cdot) \approx 1$, so the time evolution of frequency deviation may be determined by recording the power variation in time

$$\delta\nu(t) = \frac{c\delta P(t)}{2\pi nl\langle P\rangle},$$

where we have substituted $\tau = ln/c$. To obtain frequency noise probability density function samples of $\delta\nu(t)$ of certain length T are recorded. After the Fourier transformation, the power at each frequency f is normalized to the time T and averaged over samples. Different versions of this technique are summarized in [247].

Either Michelson or Mach–Zehnder fibre interferometers may be used in the measurement. The former, used with polarization independent Faraday rotating mirrors, is advantageous because it helps avoid signal fading due to polarization rotation in the spools of the fibre. Orthogonal polarization came back to the coupler from both arms, so maximum fringe visibility is ensured.

We will use the following definition for Fourier transformation here. Please note, that other definitions are often used in the signal theory literature.

$$F(\omega) = \int_{-\infty}^{+\infty} F(t)e^{i\omega t}\, dt, \qquad F(t) = \int_{-\infty}^{+\infty} F(\omega)e^{-i\omega t}\, \frac{d\omega}{2\pi}.$$

This notation is convenient with respect to integrals in the frequency domain $d\nu = (2\pi)^{-1}\, d\omega$. Parseval's theorem (having the meaning of energy conservation) has the form

$$\int_{-\infty}^{+\infty} |F(t)|^2\, dt = \int_{-\infty}^{+\infty} |F(\omega)|^2\, \frac{d\omega}{2\pi}.$$

Further we will use double-sided power spectral density functions that are related to correlation functions

$$S_F(\omega) = \left| \int_{-\infty}^{+\infty} \langle F(t)F(t+\tau) \rangle_t\, e^{i\omega\tau}\, d\tau \right|, \qquad \int_{-\infty}^{+\infty} S_F(\omega)\, \frac{d\omega}{2\pi} = \langle |F(t)|^2 \rangle.$$

If $S_\nu(2\pi f)$ is the power spectral density of the laser frequency noise, then

$$\langle E(t)E(t+\tau) \rangle = \frac{E_0^2}{2} \exp\left[-4\pi\tau \int_{-\infty}^{+\infty} S_\nu(\omega') \frac{\sin^2(\omega'\tau/2)}{(\omega'\tau/2)^2}\, d\omega'\tau \right].$$

For example, for the constant S_ν we have $\langle E(t)E(t+\tau) \rangle = (E_0^2/2)\exp(-4\pi^2\tau)$ and a Fourier transformation of the correlation functions gives us the Lorentz function as having FWHM of

$$\delta\nu_{\text{FWHM}} = 4\pi S_\nu. \tag{7}$$

We should reiterate that S_ν is defined as a double-sided noise spectrum.

3.4.1. Impact of spontaneous emission

In this section, we will discuss the impact of spontaneous emission of photons to the lasing mode on the amplitude and spectral noise of DFB fibre lasers. Essentially, this problem is close to the seminal Schawlow and Townes' consideration of the laser linewidth [280] and a problem of the contribution of the amplitude noise to frequency fluctuations in semiconductor lasers which was considered through the complex susceptibility by Henry [281,282]. Spontaneous emission determines the amplitude noise that will be referred to as a relative intensity noise (RIN). However, spontaneous emission is not the primary noise source for the spectral fluctuations.

Actually, we start with a transfer function that describes the amplitude and frequency modulation in response to pump wave power perturbations. The similar approach in which amplitude fluctuations are considered as an excitation force, will further result in the description of the laser noise spectra.

In general we will follow the theory developed in [269]. Due to the different time scales of cavity round trip time and laser power variation time, the wave equation may be treated by the separation of variables to the time-varied factor and normalized longitudinal mode profile

$$E(z, t) = A(t)e^{i\omega t+\phi(t)}e(z), \qquad \int |e(z)|^2\, dz = 1.$$

Local saturated gain coefficient $g(E, t)$ is time-dependent as well. It is sufficient to retain just the first derivatives of A, q and ϕ in the decomposition (with respect to time) of the wave equation. Complex and real parts give us the equations for the field amplitude and its phase, respectively. Time-dependent variations may be considered as small corrections to the steady state solution, so generation amplitude $A(t)$ becomes $A(1 + \epsilon_A(t))$.

Considering a weak modulation of the pump beam power $P(t) = \hat{P} + P^{(1)}(t)$, where $\hat{P}$ is averaged pump power, we define modulation transfer function $H_P(\omega)$ for the frequency domains where $\epsilon_A(\omega)$ and $P^{(1)}(\omega)$ do exist from the following equation:

$$\epsilon_A(\omega) = H_P(\omega) \frac{P^{(1)}(\omega)}{\hat{P}}. \tag{8}$$

To write down the expression for $H_P(\omega)$, it is convenient to introduce the relaxation oscillation frequency ω_0 and the term $D(\omega\tau_g)$ that determines the resonance width of the relaxation oscillations:

$$\omega_0^2 = \frac{c}{n_e\tau_2}\left(d_l \frac{P}{P_t} - \alpha_l \right), \qquad D(\omega\tau_g) = G\left(\frac{\hat{X}}{1+i\omega\tau_g} \right) - G(\hat{X}).$$
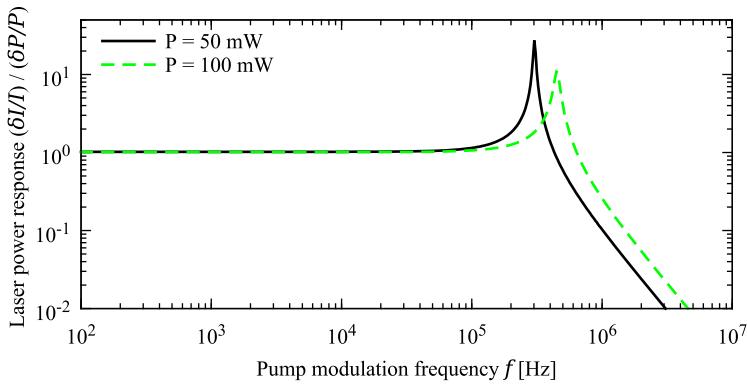
Fig. 9. Relative laser power variation in response to pump modulation.

So $H_P(\omega)$ can be found from

$$H_P(\omega) = -\frac{i\omega d_l c}{2n_e(1 + i\omega\tau_g)[\omega^2 - \omega_0^2 D(\omega\tau_g)]} \left\{ G\left(\frac{\hat{X}}{1 + i\omega\tau_g}\right) + \frac{(q_c + \alpha_0)}{i d_l \omega \tau_g G(\hat{X})} \left[D(\omega\tau_g) - i\omega\tau_g G(\hat{X}) \right] \right\}. \tag{9}$$

Here $G(X)$ is the ratio of space averaged gain to the unsaturated value in dependence on the saturation parameter X and defined by Eq. (5), $q_c = (T_1 + T_2)/(2L_e)$ is cavity losses normalized per unit length (see Eq. (4)), parameters d_l, α_l and τ_2 are given in Section 3.3, $\tau_g = \tau_2/(1 + P/P_t)$.

The response function is plotted in Fig. 9. The expression given above is not as compact as in [269], but it does provide the proper value of 1 when $\omega \to 0$. It is a consequence of the linear relation of the pump and the laser power.

The same transfer function describes the laser frequency modulation that appears if gain variation leads to changes in the refractive index (see, for example, [283]). By introducing $\mu = d\mathrm{Re}\chi/d\mathrm{Im}\chi$ as the ratio of real and imaginary parts of complex susceptibility associated with active ions, we may write

$$\frac{\delta\nu}{\delta P}(\omega) = -\frac{i\mu\omega H_P(\omega)}{2\pi\hat{P}}, \tag{10}$$

where ν is the laser frequency. Since steady-state round trip gain does not depend on the pump and laser power, the frequency response function goes to zero at low frequencies. The factor μ depends on the laser wavelength. Equating its value to 1, we get the functions shown in Fig. 11. Relaxation oscillation frequency increases with growth of the pump power.

The same approach allowed Foster to take into account the process of spontaneous emission into the lasing mode. An idea how to calculate the power of the noise source may be found, for example, in Yariv's textbook [284]. If there are n_l photons in the lasing mode, each spontaneously emitted photon changes the phase of the field by $\delta\phi^2 = 1/(2n_l)$, and the amplitude by $\delta\epsilon_A = (1/N)e^{i\psi}$, where ψ is a random phase. The rate of such events is dn_{sp}/dt. The photon loss rate is $dn_l/dt = -n_l c/n_e(q_c + \alpha_0)$. We intentionally drop the contribution of the gain or, in other words, the contribution of the stimulated emission, and consider a cold-cavity photon loss rate. Stimulated emission compensates photons loss, so the number of photons is kept almost constant. If T_1 is the transmission of the output coupler (the grating half), we will see a laser power of

$$I = -\frac{T_1/2}{L_e(q_c + \alpha_0)} \cdot \frac{dn_l}{dt} h\nu.$$

So we may obtain the mean number of photons $n_l = IL_e[c/n_e T_1 h\nu]^{-1}$.

To calculate the ratio $\delta n_{sp}/\delta n_l$ of stimulated to spontaneous photons emission rates, we will use the following relation being equivalent to the power amplification: $dn_l/dz = (n_l + 1)N_2\Gamma_l\sigma_e - n_l(\Gamma_l N_1\sigma_a + \alpha_0)$. Spontaneously emitted photons are described by the additive factor 1 in $(n_l + 1)$. Here N_1 and $N_2 = n_{Re} - N_1$ are populations of lower and upper levels, respectively; Γ_l is overlap integral between pump and generation transverse fibre modes; and σ_e and σ_a are cross-sections of emission and absorption processes. By performing an integration with the weight of $|e(z)|^2$ and taking into account that the single pass gain is equal to the losses $q_c + \alpha_0$, we get the relation between the number of spontaneous emitted photons, δn_{sp}, and the number of stimulated photons, δn_l. The different factors at $N_2(z)$ results in $g_l/(g_l + \alpha_0)$ factor. The details of Foster's model are given in [269]. Note that, due to some typos, the expressions there should be critically examined.

For the sake of brevity we introduce a factor that accounts for the inversion population in a lasing regime and reflector transmission in relation to the total cavity losses $\zeta = g_l(g_l + \alpha_l)^{-1}[1 + \alpha_l/(q_c + \alpha_0)](T_1/2)[L_e(q_c + \alpha_0)]^{-1}$. Since the power of the noise source is proportional to $(2n_l)^{-1}dn_{sp}/dt = [\delta n_{sp}/\delta n_l](2n_l)^{-1}dn_l/dt$, we may write an expression for the power spectral density (double-sided) of the relative intensity noise

$$S_{RIN} = \frac{h\nu c^2(q_c + \alpha_0)^2 \zeta \omega^2}{I_1 n_e^2 |\omega^2 - \omega_0^2 D(\omega\tau_g)|^2}.$$
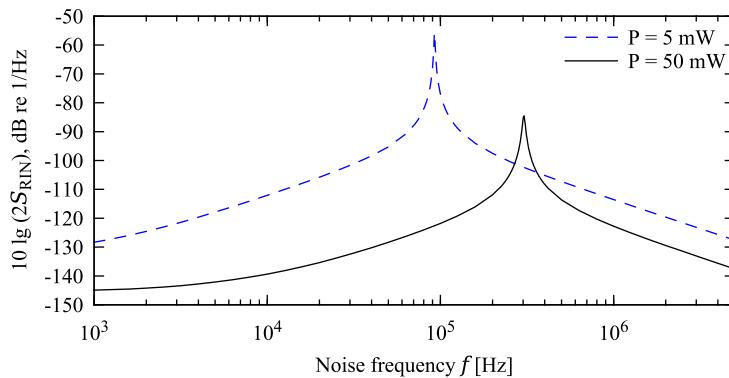
Fig. 10. DFB fibre laser RIN spectra (theory). Pump powers are 5 and 50 mW; the generation threshold is ~0.7 mW.

The direct contribution of the frequency noise to the phase noise from spontaneous photons has following form:

$$S_\nu = \frac{h\nu c^2 (q_c + \alpha_0)^2 \zeta}{16\pi^2 n_e^2 I_1} \left[1 + \mu^2 \frac{\omega_0^4 |D(\omega\tau_g)|^2}{|\omega^2 - \omega_0^2 D(\omega\tau_g)|^2} \right]. \tag{11}$$

The examples of the calculated RIN spectra are plotted in Fig. 10. Contribution of this effect to the frequency noise a shown as curves 3 and 4 in Fig. 12.

The expression for the laser linewidth (FWHM)

$$\Delta\nu_{\text{las}} = \frac{2\pi h\nu (\Delta\nu_c)^2}{I} \zeta \tag{12}$$

that is often referred to as Schawlow–Townes formula [280], may be obtained by setting $\mu = 0$, using Eq. (7), and introducing the full width of the cold-cavity resonance $\Delta\nu_c = c(q_c + \alpha_0)/(2\pi n_e)$. Actually the expressions are different by the factor of two, and the same discrepancy may be found in the Yariv's textbook [284] while using different ways to obtain the expression for the $\Delta\nu_c$. As it was pointed by Lax in [285], the smaller factor appears if the laser is properly considered as a Van der Pol oscillator, and the value larger by the factor of 2 originates from a harmonic oscillator excited by a random force which model describes a laser below the generation threshold.

Experiments with early DBR erbium fibre lasers [286] demonstrated that the frequency noise spectrum at high enough frequencies (above 50 kHz) is consistent with Schawlow–Townes limit (about 35 Hz for 95% reflectivity mirrors, 2 cm long cavity and 150 µW power).

In this section we have considered dynamic model of the DFB fibre laser [269], namely its behaviour under weak pump modulation and linewidth limit and frequency noise due to spontaneously emitted photons in the lasing mode.

3.4.2. Contribution of thermal effects to noise properties

Any change of FBG length leads to a deviation in laser frequency. It may be due to an intentional strain by the piezoelectric transducer or an impact of ambient noise on the laser package. The effect is noticeably mitigated by the refractive index's dependence on elastic tension in the media. Laser frequency is also affected by transverse pressure on the fibre cladding (for example, by high frequency acoustic waves in the air [287]). The DFB cavity is especially sensitive to perturbations localized close to the phase shift position. It may even affect laser power if resonance is shifted far enough from the FBG maximal reflection.

Another effect, which is often exploited for wavelength tuning (1 nm to provide some impression) and leads to frequency noise, is temperature dependence of the refractive index. For fused quartz it is an order of magnitude greater than thermal expansion. The cumulative effect may be estimated as $q = \delta\lambda/(\lambda\delta T) = 0.7 \times 10^{-5}$ K^{-1} or 1.4 GHz/K at 1550 nm.

Time-dependent laser frequency variations due to temperature instabilities may be described through a response function that depends on modulation frequency. Thermal time scales are defined by the relation of circular frequency of a thermal wave ω and its wavenumber

$$k_h^2 = \omega c_v / \kappa_t,$$

where $\kappa_t = 1.37$ W/(m K) is thermal conductivity and $c_v = 1.67 \times 10^6$ J m^{-3} K^{-1} is specific heat per unit volume. For 125 µm cladding we get 330 Hz, for 5 µm core it is 200 kHz.

Thermal oscillations in low-frequency acoustic waves affect laser frequency [287]. Pump absorption is accompanied by heating the fibre. It was somewhat unusual for laser spectral line-width to grow with increasing pump and signal power [288] and this finding attributed to pump noises [289].
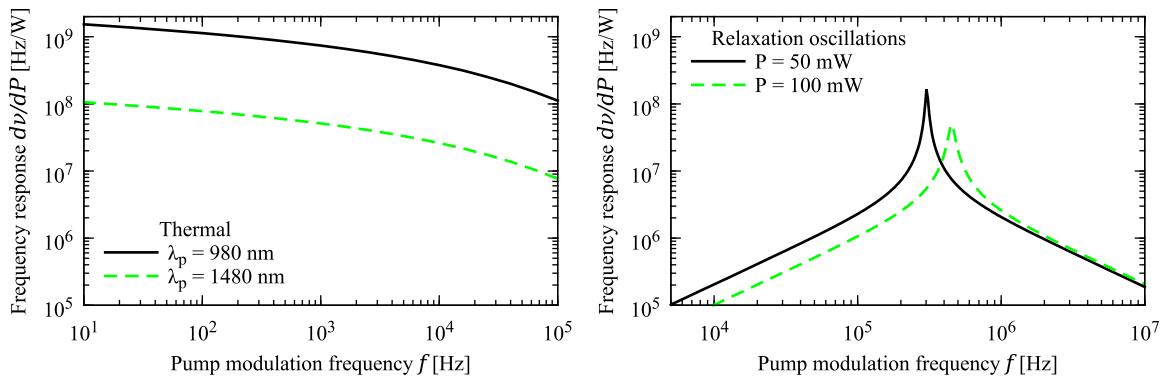
Fig. 11. Frequency response to pump power modulation for an Er DFB fibre laser (theory).

In detail, the effect of pump noise/modulation onto laser frequency has been studied theoretically and experimentally by Foster and Tikhomirov [290]. Assuming mode field distribution $e(\mathbf{r})$ (normalized by $\int |e(\mathbf{r})|^2 \, d\mathbf{r} = 1$), laser frequency deviation may be expressed through medium temperature deviation from the mean value $T(t, \mathbf{r})$

$$\delta\nu(t) = \nu q \int T(t, \mathbf{r}) |e(\mathbf{r})|^2 \, d\mathbf{r}.$$

Thus, we must solve the heat equation in the presence of heat sources $Q(t, \mathbf{r})$

$$c_v \frac{\partial T}{\partial t} - \kappa_t \nabla^2 T = Q(t, \mathbf{r}). \tag{13}$$

For efficient lasers written in fibres with high ytterbium concentration, heat generation caused by pump–signal exchange plays a crucial role. The following analysis is limited to erbium lasers where pump power P remains almost constant along the cavity and heat is generated due to some residual losses μ_h attributed to erbium ions with concentration n_{Re}. Instructive results may be obtained on the assumption that infinite cladding fibre and uniform ion concentration within the laser mode of radius a has a transverse profile $e(\rho, \varphi) = a^{-1}\sqrt{2/\pi}e^{-\rho^2/a^2}$. Therefore, heat deposition is z-independent and has the form $Q(t, \mathbf{r}) = \mu_h n_{Re} P(t) e(\rho)$.

A formal solution for the heat equation may be written in the $(\omega, \mathbf{k})$ domain. We are mostly interested in a frequency-dependent response function, so the backward Fourier (or Hankel) transformation shall only be performed for a wave vector. The procedure includes averaging the weighted by transverse mode profile, and the result is

$$\delta\nu(\omega) = P(\omega) \frac{\mu_h n_{Re} q_t \nu}{2\kappa_t} E_1(ik_h^2 a^2/4) \exp(ik_h^2 a^2/4),$$

where $E_1(\cdot)$ denotes an exponential integral [291,292]. Since the thermo-optic coefficient represents relative change of the refractive index, the expression does not contain effective cavity length. Spectral dependence of response to pump modulation looks similar to random heat flux contribution to the noise spectrum. In the low-frequency limit, the border conditions at the fibre surface play the crucial role; specifically, the cavity may be fixed at the heatsink with thermal conductive grease or, conversely, the conditions may be closer to insulating.

To provide an example, we will assume a high-quality fibre and low population of the metastable level, so thermal deposition may be expressed through the pump absorption coefficient and the quantum efficiency $\mu_h n_{Re} = g_p(1 - \lambda_p/\lambda_l)$. A frequency response function $d\nu(f)/dP$ in dependence of modulation frequency f is shown in Fig. 11 for two pump wavelengths $\lambda = 980, 1480$ nm. A relatively low pump absorption coefficient has been taken ($g_p(980 \text{ nm}) = 5$ dB/m and $g_p(1480 \text{ nm}) = 3$ dB/m). The order of magnitude difference appears due to a significant difference in the quantum defect. Pump power fluctuations at the microwatt level lead to a frequency modulation of kilohertz levels. The effect is much more prominent for Yb and Er:Yb fibres that have higher pump absorption coefficients.

In further discussions on frequency noise we will assume that the pump source has no any noise, a fibre-based cavity is effectively isolated from vibration, ambient acoustic noise and temperature fluctuation. In the experiment, this may be achieved by placing the cavity in the groove of heatsink mounted on a thermoelectric cooler with an appropriate control circuit.

Heat transfer fluctuations present one of the sources of frequency noise that is more important than spontaneous emission noise at low frequencies. The problem of thermal noise due to random heat fluxes in fibre interferometer (for passive fibres) was discussed by Wanser [293]. Rønnekleiv discussed the impact of thermal noise on the laser frequency noise in [277]. Foster calculated thermal noise, taking into account a longitudinal profile of the lasing mode [278]. This provides a description of spectral noise PDF in the intermediate range of 10–100 kHz. To derive an expression for spectral noise, one should substitute into heat equation (13) random heat currents

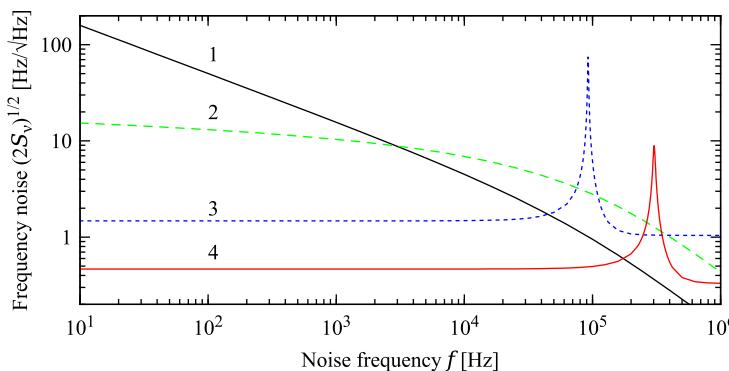$$Q(t, \mathbf{r}) = \nabla \mathbf{h},$$

Fig. 12. Contribution of different mechanisms to the power spectral density of the frequency noise in the erbium-doped DFB fibre laser. 1. A heat dissipation due to spontaneous transition not associated with lasing, see Eq. (15) and Section 3.4.3. 2. Fluctuations of the equilibrium heat transfer, see Eq. (14) and Section 3.4.2. 3 and 4. Spontaneous emission into the lasing mode for the pump power of 5 and 50 mW, respectively, see Eq. (11) and Section 3.4.1.

with the following expression for the correlator

$$\langle h_i(\omega, \mathbf{k}) h_j^*(\omega', \mathbf{k}') \rangle = \frac{\kappa_t K T^2}{8\pi^4} \delta_{ij}\delta(\omega - \omega')\delta(\mathbf{k} - \mathbf{k}'),$$

where $K = 1.38 \times 10^{-23}$ J/K is Boltzmann's constant. Depending on the laser's purpose, fixed temperature or thermal insulating boundary conditions must be considered on a cladding surface. Following Foster, we provide an expression for infinite cladding approximation. In general, the steps to derive it are similar to those mentioned with respect to pump modulation impact. However, a longitudinal mode profile should be taken into account.

$$2S_\nu(\omega) = \frac{2\nu^2 q_t^2}{L_h} \frac{KT^2}{2\pi\kappa_t} \text{Re}\big[E_1(ik_h^2 a^2/4) \exp(ik_h^2 a^2/4) \big], \tag{14}$$

where $L_h = 2/\kappa = 2L_e$, see [278] for details. The curve 2 in Fig. 12 is an example of frequency noise spectrum calculated from the last expression.

In this section we have presented the results from [278,290] and described laser frequency fluctuations owing to thermal effects, namely pump power perturbations and heat transfer fluctuations within the fibre medium.

3.4.3. 1/f spectral noise

In the frequency range 10 Hz–10 kHz the power spectral density of the frequency noise is dominated by $1/f$ contribution. Such behaviour is not specific to DFB fibre lasers and could be found in semiconductor and solid state lasers. It cannot be described neither by spontaneous photons in the laser mode nor by fluctuations of the heat transfer considered in the previous section.

To resolve the $1/f$ problem, Foster pointed to the statistics of spontaneously emitted photons in heavily doped fibres that are not connected with the lasing mode [248]. The discussion of the effect provided below aims to be somewhat complementary to the original paper [248].

Heat Q_1 dissipated on each photon emission event gives us another kind of a source in Eq. (13). This process is assumed to be instantaneous $Q_1\delta(t - t_j)$ at some time t_j. If n_{Re} is a volume concentration of rare-earth ions, than an average heat dissipation per unit volume is expressed by $\langle Q(t, \mathbf{r}) \rangle = Q_1 n_{\text{Re}}/\tau_2$ multiplied by some factor due to the partial inversion. A mean heat dissipation leads to a temperature shift and does not affect temperature variations. Further we are interested in fluctuations only. The Poisson statistics, that is usually assumed to be a case, have the following relation of the variation and the mean value for photon number, $\langle \delta N^2 \rangle = \langle N \rangle$ in the case of independent in time events with additive probability. The correlation function is described by $\langle Q(t, \mathbf{r}) Q(t', \mathbf{r}') \rangle = Q_1^2 n_{\text{Re}}\tau_2^{-1}\delta(t - t')\delta(\mathbf{r} - \mathbf{r}')$ or $\langle Q(\omega)Q^*(\omega') \rangle = 2\pi Q_1^2 n_{\text{Re}}\tau_2^{-1}\delta(\omega - \omega')$ Unfortunately, it is not sufficient to describe fluctuations of the laser frequency due to heat associated with photons absorption or emission.

The superposition of photons is described by the sum of complex-valued amplitudes. The state with many photons may be approximated as a random walk of an amplitude on the complex plane. Therefore, the amplitude is described by a two-dimensional Gaussian distribution. Thus, the intensity has a corresponding exponential distribution. In terms of the photons number it may be expressed as $\langle \delta N^2 \rangle = \langle N \rangle^2$. Considering some small volume ΔV and taking a luminescence spectral width of $\Delta\lambda \sim 50$ nm, we get the number of photon modes of $\rho_\lambda = 8\pi \Delta\lambda \Delta V/\lambda^4$ and the number of active ions per photon number of $n_{\text{Re}}\lambda^4/(8\pi \Delta\lambda)$ in the same volume. The last number determines heat dissipation fluctuations. Assuming some relaxation or decoherence time τ_r, we write correlation function in the each mode of the volume ΔV as $\langle Q(t)Q(t') \rangle \Delta V^2 = (Q_1 n_{\text{Re}}\Delta V)^2(\rho_\lambda \tau_2)^{-2} e^{-|t-t'|/\tau_r}$. The corresponding function in the spectral domain has the form

$\langle Q(\omega)Q^*(\omega')\rangle \Delta V^2 = (Q_1 n_{Re}\Delta V)^2(\rho_\lambda \tau_2)^2\tau_r\delta(\omega-\omega')$. We are interested is total fluctuations per unit volume, so the result should be multiplied by the number of modes. Emission rates from different points are independent so

$$\langle Q(\omega,\mathbf{r})Q^*(\omega',\mathbf{r}')\rangle = \frac{(Q_1 n_{Re})^2\lambda^4}{8\pi\Delta\lambda\tau_2^2}\tau_r\delta(\omega-\omega')\delta(\mathbf{r}-\mathbf{r}').$$

If one excludes saturation effects, a partial ions excitation could be estimated by $\alpha_l/(\alpha_l+g_l)$. Foster assumed $\tau_r=\tau_2$. Heavily doped fibres could have a concentration of 10^{19} cm^{-1} or even more. This results in a number of excited ions per photon mode as high as 5×10^7. In this case the fluctuations are dominated by the $\langle N\rangle^2$ term.

Omitting the details of the heat equation integration [248], the result for the power spectral density of the frequency noise is the following

$$S_\nu(2\pi f) = -\frac{\nu^2 q^2}{8\pi L_h\kappa_t^2\kappa_h^2}\cdot\frac{(a_l N_{Re}\lambda^2 Q_1)^2}{8\pi(\alpha_l+g_l)^2\Delta\lambda\tau_2}\text{Im}\left[E_1\left(\tfrac{ik_h^2a^2}{4}\right)\exp\left(\tfrac{ik_h^2a^2}{4}\right)\right]\approx\frac{(a_l Q_1 N_{Re}\lambda^2)^2}{128\pi^2\Delta\lambda(a_l+g_l)^2\tau_2\kappa_t c_v f}. \tag{15}$$

A random heat deposition instead of the fluctuations of heat transfer in Eq. (14) results in a different frequency dependence. An example of the frequency noise spectrum calculated using the presented theory is shown in Fig. 12, curve 1.

Foster estimated heat deposition per spontaneous photon Q_1 as $Q_1=KTs_1$ using an argument of the entropy difference of excited and ground levels; here s_1 is a factor of value ~ 1. Another point of view may be argued since Q_1 should depend on branching ratios of spontaneous transitions from/to sub-levels. That means Q_1 should have a temperature-independent contribution that was likely observed in [294], but not realized. Although temperature affects equilibrium distribution within sublevels of ground and excited levels, a heating (or cooling for some crystals) happens due to probability of transitions to higher (lower) states of the ground level in comparison to the equilibrium distribution.

Note that the considered phenomenon of the fluctuations enhancement for the spontaneous emission should not be confused with cooperative effects, such as, Dicke superradiance [295] that have coherent nature.

In support of this hypothesis, Foster provides arguments that in the erbium-doped DFB fibre lasers, the amplitude of the frequency noise does not depend on the pump power and even remains the same for 1480 and 980 nm pump wavelength.

It may be questioned if it is correct to assume $\tau_r=\tau_2$ or in other words to state that the correlation time is equal to the spontaneous emission lifetime. There are other time scales that may dramatically shorten this time and, consequently, suppress the effect. For the medium that acts as an active medium of a laser, the transition time between the ground and the excited states may be approximated as the relaxation oscillations period (for example, 1 μs). Strong coupling of active ions to phonons in the amorphous fibre media leads to the thermal equilibrium between sublevels in less than 1 ps. It is doubtful that some correlations could live longer.

There is a similar $1/f$ behaviour of the phase noise in fibre interferometers; some related theory is developed in [296]. The effect associated with thermal length fluctuations is too weak to play noticeable role in DFB fibre lasers even though the elastic beam approximation is more suitable for the DFB fibre laser than for a coiled fibre interferometer.

Although some questions arises to his theory, Foster achieved quantitative agreement to experimental data [248,294].

The stimulated Brillouin scattering is another way to achieve a light amplification in passive fibres, and a Brillouin DFB fibre laser was demonstrated in 2012 [238]. Due to the negligible detuning from the pump wavelength (10–15 GHz), this method does not extend the spectral range available for single frequency fibre lasers. The Brillouin DFB fibre lasers may be advantageous with respect to the frequency noise: Indeed, much less heat dissipation occurs there in comparison with rare-earth DFB fibre lasers. However, the heat transfer fluctuations should be the same. Previously, the pump noise suppression were demonstrated for ring-cavity Brillouin fibre lasers [297].

In this section, we have presented the Foster's idea to describe $1/f$ frequency noise spectrum of the DFB fibre laser [248,294]. In conclusion of the sections dealing with the noise in the DFB fibre laser, we would like to mention several works on experimental measurements of the noise in DFB fibre lasers [247,277,294].

3.5. Raman DFB fibre lasers

Since the emergence of both Raman fibre lasers and rare-earth doped DFB fibre lasers, the possibility of developing a Raman DFB fibre lasers has attracted a great deal of attention. However, the low Raman gain, meant that the task of implementation such a laser was challenging. Perlin and Winful published a first theoretical analysis in 2001 [298,299]. The proposed continuous 1-m long Bragg grating was obviously difficult to implement. Several years later, the numerical simulation was conducted for the feasible 20-cm long gratings with localized or distributed phase shift [300]. A small core fibre ($A_{\text{eff}}=2$ μm^2) leads to the threshold power of order of magnitude of 1 W or even less. Slope efficiency of more than 50% was predicted. It was noted that Kerr nonlinearity significantly distorts the longitudinal power profiles.

Two groups experimentally demonstrated Raman DFB lasers in 2011. The first laser manufactured in the OFS laboratory [237] had the threshold of 35 W and generated a power of 150 mW only at pump power 70 W. A smaller core made it possible to decrease the threshold to approximately 4 W and obtain 350 mW at 35 W pump power. The phase-shifted FBG had the length of 124 mm, the lasers operated near 1584 nm.

Longer gratings (30 cm) and special care to avoid extra losses in the fibre originated from UV exposure (used to increase the fibre photosensitivity) allowed to achieve a threshold of 1 W for an unpolarized pump [301], and the threshold of 0.5 W

only for polarized pump [302]. The pump and the lasing wavelength were 1064 and 1110 nm, respectively. The measured linewidth of 2.5 kHz is close to the limit of the self-heterodyne technique. Four-wave mixing has been also observed within the cavity of Raman DFB fibre laser [303]. A pump spectrum was transferred to longer wavelengths symmetrically with respect to the lasing frequency.

The slope efficiency in relation to the incident pump power is still close to 10%, which probably indicates severe nonlinear grating distortion since the pump wave is almost unabsorbed in the cavity. The power of the pump beam passed through the cavity increases as the launched pump power is raised — this means that average gain and therefore also round-trip gain increases with pump power. The only way to maintain the balance between the gain and the total losses is to increase mirror transmission, either by nonuniform heating or by grating distortion (and magnitude of the phase shift as well) due to Kerr nonlinearity. Otherwise, a noticeably higher slope efficiency may be expected close to the threshold accompanied by a drop of unabsorbed pump power with the increase of power of the incident pump beam. The simulation results [300] do not contradict the hypothesis that linear pump-lasing power dependence is a result of Kerr nonlinearity; however, the slope efficiency 50%–80% is much higher than the values obtained in the above-cited experiments. The effect of gain saturation inherent to rare-earth doped lasers is inapplicable to Raman gain that does not depend on Stokes component power (confer the gain terms $dI/dz = g_0 I (P/P_t)(1 + I/I_e)^{-1}$ and $g_R IP$ for Raman and rare-earth lasers, respectively. Here $I_e = I_t P/P_t$).

Like other Raman fibre lasers, DFB Raman fibre lasers make it possible to extend wavelength range to regions that lie outside of the rare-earth ions luminescence spectra. Unlike the conventional Raman fibre laser, DFB cavities provide narrow linewidth generation that is unavailable in long cavities with a large number of interacting longitudinal modes. We believe that the field of DFB fibre lasers is yet to be fully explored.

3.6. DFB fibre lasers with sampled FBG

Besides continuous phase shifted fibre Bragg grating cavities, there are variants of DFB fibre lasers with cavities based on sampled FBGs.

FBG with many π shifts, separated by the constant period D along the fibre, has two resonances separated in the spectral domain by $\Delta\lambda = \lambda^2/(2n_e D)$ [304]. This makes it possible to obtain lasing at two wavelength with controlled difference (1 mm corresponds to 100 GHz) [305]. This is why Moiré gratings have advantages in microwave generation over cavities formed in high-birefringence fibre [306]. Unlike a conventional DFB cavity, in longitudinal directions the mode is localized around the skipped phase shift. A continuous fragment of double length resembles the π-shift in an ordinary grating. Since lasing wavelengths lay out of the stop band, the resonance may be compared with quasi phase matching. The effective grating is significantly weaker than continuous FBG at the resonance wavelength.

Another variant of a structured grating which could be more tolerant to positioning errors is several short pieces of FBG written with some duty cycle [307]. Coupling of a fundamental mode to cladding modes breaks the symmetry in spectral domain and leads to lasing at longer wavelength. Although the structure of such gratings is more complicated than for continuous gratings, they still provide coherent feedback.

Finally, randomly embedded multiple or single gratings with random shifts inscribed in Er-doped fibres have also been studied [213,216]. Because of the grating randomness, performances of such lasers differ substantially from regular or sampled DFB fibre lasers. The number of emitted modes is observed to be a function of the length of the grating and of the pump power. The spectrum is narrowing and may even approach an effectively single-mode one. The linewidth of 0.5 pm at a wavelength of around 1534 nm is demonstrated. This kind of laser in some aspects (strong random grating in an amplifying medium) could be treated as a specific example of random lasers, see Section 2.9, and also has some similarity (random gratings embedded in the fibre) with random DFB fibre lasers, see Fig. 1.

4. Random DFB fibre lasers

4.1. Operation principles of the random DFB fibre laser

The concept of a random distributed feedback (DFB) fibre laser briefly described in the introduction can be treated as a convergence of two distinct types of lasers, namely random lasers, see Section 2, and DFB fibre lasers, see Section 3. The basic scheme of the random DFB fibre laser is very simple comprising only a pump laser and a piece of a passive fibre directly connected to the laser diode. Further in this section we focus on the properties of the random DFB fibre laser operating via Raman gain (other gain mechanisms are discussed in Section 4.12). The random DFB fibre laser converts the pump radiation into new spectral range defined by the pump wavelength and the Stokes shift of a particular Raman gain media. At the same time, the quality of the radiation could be sufficiently improved as compared to one coming from the pump source: As an example, a radiation of cheap low-quality laser diode pumps being multi-mode both in longitudinal and transverse directions is converted to the single transverse mode generation (details are discussed in the Section 4.9). In general, the random DFB fibre laser generates very stable narrow-band radiation similar in properties to output from DFB fibre lasers. The random fibre laser has neither *regular* cavity formed by either point-action reflectors, as in conventional lasers, nor *regular* distributed reflection, as in DFB fibre lasers. In this sense, random fibre laser is similar to other types of random lasers, see Section 2. However, the random feedback in the random DFB fibre laser is distributed over the fibre length, so the laser is
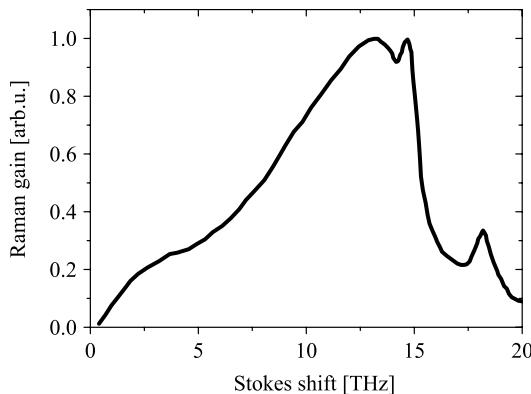
Fig. 13. A Raman gain spectrum of a silica-based optical fibre. After Ref. [308].

similar to the DFB fibre lasers, Section 3. The distributed random feedback in optical fibres is originated from the Rayleigh scattering on a natural disorder of the fibre core's refractive index. Although a randomness in other random systems usually means a stochastic behaviour of output beam in temporal, spatial and spectral domains, the radiation of the random DFB fibre laser is well-confined in spectrum and stable over time, see further discussion in Section 4.3. Amazingly, random DFB fibre lasers can even outperform conventional fibre lasers of a similar kind in several aspects, as it will be demonstrated below.

Before going into details of the random DFB fibre laser operation, we make here a brief excursion into the principles of the Raman gain and Rayleigh scattering in optical fibres. The gain mechanism is based on the stimulated Raman scattering. A pump light of frequency ν_p incident on a medium excites a quantum of molecular vibrations of the silica glass during an inelastic scattering process and loses some small part of its energy. Residual energy is carried out by a so-called Stokes photon possessing lower frequency ν_s than the pump photon. The frequency difference between pump and Stokes photons is called a Stokes shift. The Stokes shift value is determined by a structure of vibration levels of the host media. In the amorphous medium of silica glass with a variety of different collective vibrations, Stokes phonons of the wide energy range following the Raman scattering spectral profile could be spontaneously emitted. If there are some spontaneously scattered photons in the media, the stimulated Raman scattering can take place. The stimulated Raman scattering rate depends on the pump wave, P_p, and the Stokes wave, P_s, powers and can be described as $dP_s/dz = g_R P_p P_s$, where g_R is the frequency-dependent Raman gain coefficient, Fig. 13. The total amplification acquired by the Stokes wave in the fibre span of length L can be found as $\exp(g_R P_p L)$, meaning that the total gain is exponentially increases over the fibre length. However, in practice the gain is limited by the pump wave attenuation, $P_p(z) \sim \exp(-\alpha_p z)$. As a result, the total gain is limited by $\exp(g_R P_p L_{\text{eff}})$, where $L_{\text{eff}} = 1/\alpha_p$ is the approximate expression for the effective length in the very long fibres; $L_{\text{eff}} \sim 20$ km in SMF-28 fibre. At pump power level of 1 W, the total gain could be as high as 10^5–10^6.

The Rayleigh scattering used in the random DFB laser as a feedback source is an elastic scattering process. While propagating in the fibre, the light scatters on the random (in strength and position over the fibre, but unchanging in time) fluctuations of the density in the fibre core obeying the Rayleigh law. Such density fluctuations are "frozen" during the fibre's manufacturing process. The Rayleigh scattering contributes sufficiently to the total linear losses α of optical fibre in the wavelength range below 1.55 μm. Small part of the light scattered at angles close to π is recaptured by the fibre waveguide and propagates in direction opposite to the direction of the incident light. The backscattered part of the radiation is equal to $\varepsilon = \alpha_s \cdot Q \sim 5 \times 10^{-5}$ km^{-1} being extremely small. Here the geometrical factor $Q \sim 0.001$ is defined by a numerical aperture and geometrical dimensions of the fibre [30].

Despite the Rayleigh backscattering is extremely small, the backscattered signal can be detected that is widely used in optical time domain reflectometry since 1970s [309]. In the 1990s it was shown that the presence of the RS feedback in a Brillouin fibre lasers improves laser's performances, namely its output line-width is narrowed by three orders of magnitudes [310]. In 2000s the effect of double Rayleigh scattering was observed in long-haul fibre-optic transmission lines [311]. The double Rayleigh scattering manifested itself as irregular spikes of lasing that occurred at high values of the distributed Raman gain in the system. In 2009 it was pointed out for the first time that the Rayleigh scattering based random feedback may be sufficient for lasing in ultra-long fibre lasers ($\simeq$270 km), [19]. In cavities of such length, the Rayleigh scattering based random feedback has a lower threshold compared to the lasing threshold of the corresponding FBG-based linear cavity, see Section 5.2. After that, intensive endeavours directed at the development of self-consistent Rayleigh scattering based lasing in passive fibres have resulted in the invention of a new class of lasers — random DFB fibre lasers.

The first scheme of a random DFB fibre laser exploited to prove the concept of the random generation via weak random Rayleigh backscattering is shown in Fig. 14a, left scheme; see also Fig. 1. The laser was made up of two equal spans of standard telecommunication fibre SMF-28 with total length of $2L = 83$ km. The linear losses α_s for the generation wave are $\alpha_s \sim 0.045$ km^{-1}. Therefore the total reflection in the very long fibre span due to the Rayleigh scattering amounts to
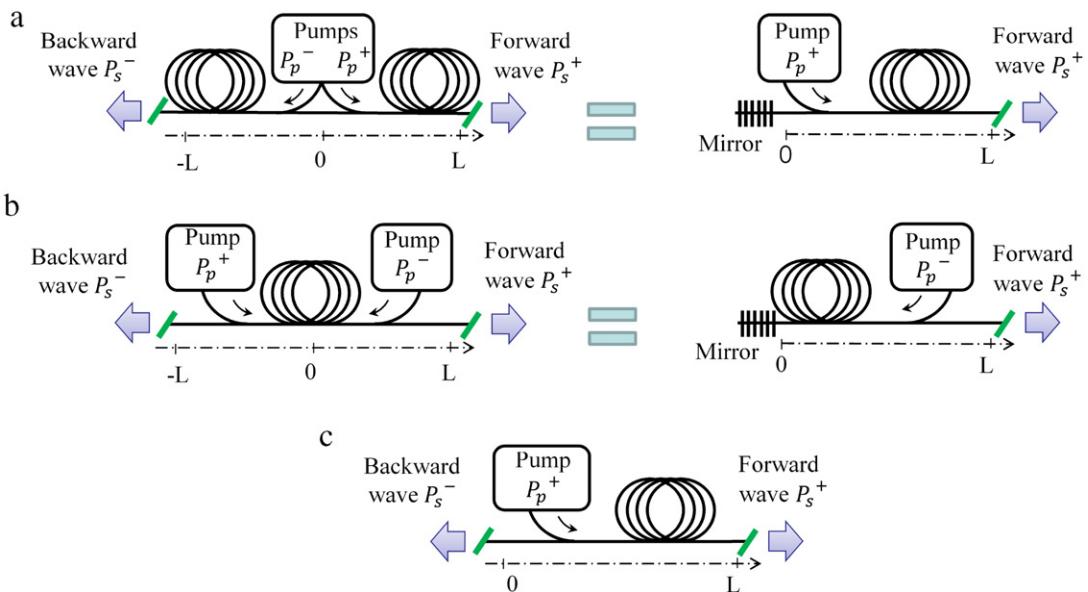
Fig. 14. Random distributed feedback fibre laser configurations: (a) forward-pumped laser, (b) backward-pumped laser and (c) single-arm configuration.

a small value of $R \sim Q \sim 0.1\%$. The gain mechanism is relied on the stimulated Raman scattering. Two pump waves at 1455 nm were used to achieve a Raman gain near 1550 nm. At the power level of each pump unit $P_{th} \sim 0.8$ W, the net amplification at the round trip amounts to $G \sim \exp(4g_R P_{th} L_{eff}) > 10^6 \sim R^{-2}$ which is enough to obtain a generation [31]. Here $g_R \sim 0.4$ (W km)$^{-1}$ is the Raman gain coefficient in SMF-28 fibre, $L_{eff} = (1 - \exp(-\alpha_s L))/\alpha_s$ is the effective length. Note that fibre ends were cleaved at the angle of $\sim 10°$ to avoid additional feedback caused by Fresnel reflection. In this case, the light reflected at the glass–air interface of the angle-cleaved fibre leaks out of the waveguide and does not propagate in the backward direction.

4.2. Laser design

There are 3 different basic configurations of the random DFB fibre laser. The first one is the so-called forward-pumped configuration, as the generation wave out-coupled from the laser is co-propagating with the pump wave, Fig. 14a, left diagram. This configuration could be realized in two technical ways. The first one, is a symmetrical scheme based on 2 fibre spans of length L, two pump lasers coupled to the fibre centre, at $z = 0$, and 2 laser outputs at $z = L$ and $z = -L$. This scheme was used in the first demonstration of the random DFB fibre laser, [31]. Thanks to the symmetry in the system, this scheme is equivalent to a configuration in which only one fibre span of length L and only one pump laser is used with a mirror of 100% reflection placed at $z = 0$, Fig. 14a, right diagram. Physically, the latter laser has only one output, at $z = L$, but its power performances are identical with a symmetrical configuration because of the full symmetry in the system. This was experimentally checked in [312]. The advantage of the reduced scheme is two times less fibre length and only one pump unit needed for the random generation.

The pump wave could be coupled from fibre ends, i.e. at points $z = -L$ and $z = L$, Fig. 14b, left diagram. This scheme is called the backward-pumped configuration of the random DFB fibre laser, as the output generation wave is counter-propagating with the pump wave. In this configuration again, there is an equivalent scheme based on one fibre span, one pump source coupled at $z = L$ and an additional point-based highly reflecting mirror placed at $z = 0$, compare left and right schemes on Fig. 14b. Note that further in our theoretical considerations of forward- and backward-pumped random DFB fibre lasers, we consider schemes from the right column of Fig. 14a, b.

Finally, the third scheme comprises a fibre span of length L with one pump laser coupled at point $z = 0$. However, there is no any point-based reflector, so the laser is operated via the random distributed feedback only. We call this scheme as the single-arm configuration.

4.3. Generation properties

Here we briefly describe the main generation properties of a random DFB fibre laser. The random DFB fibre laser has a clear generation threshold in all configurations. As an example, the power performance in the forward-pumped configuration of Fig. 14a is shown in Fig. 15. The key laser features — a generation threshold and the almost linear growth of the output power above the threshold are clearly seen. The experimentally measured laser threshold in the forward-pumped laser is close to a value of 0.8 W for one pump. The output power value of 160 mW is limited by the available pump power. The random DFB
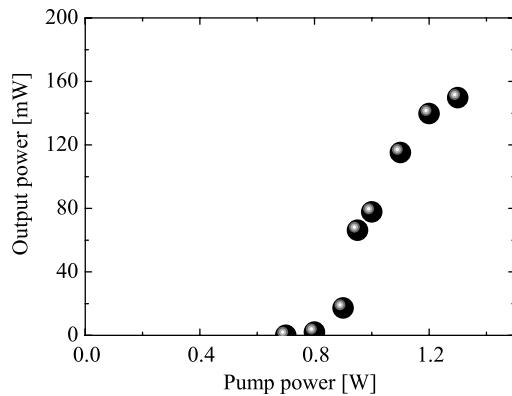
Fig. 15. Typical output power performances of the forward-pumped random DFB fibre laser. After Ref. [31].
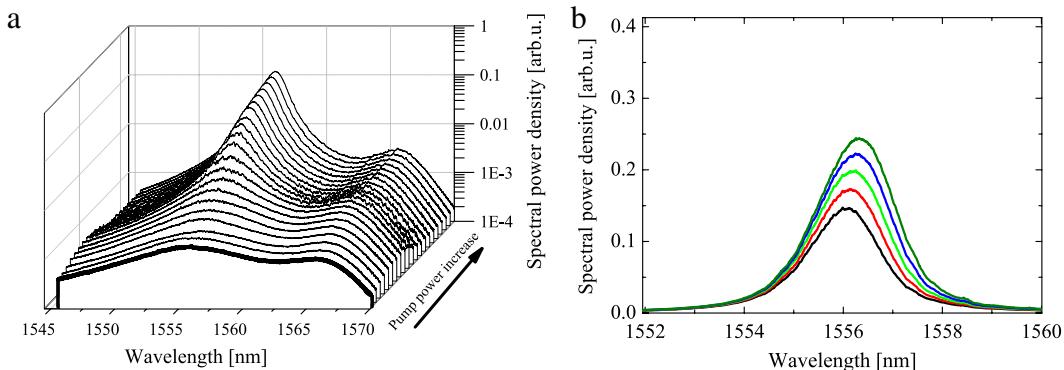

Fig. 16. Generation spectra of the random DFB fibre laser measured at different power levels in (a) logarithmic scale and (b) linear scale. The thick black curve in (a) is a Raman gain spectral profile measured below the laser generation threshold.

fibre laser can easily emit several Watts of output power under appropriate pumping. A detailed theoretical description of generation thresholds and output power in different configurations is presented in Sections 5.2 and 5.3.

The random DFB fibre laser generates a well-confined optical spectrum with a typical width of 1 nm. When the pump power is below the generation threshold power, the spectrum is broad and corresponds to the amplified spontaneous emissions spectrum, Fig. 16a, black curve. However, above the threshold, the generation spectrum becomes much narrower (1 nm) than the spectral profile of the Raman gain (∼10 nm), Fig. 16. The abrupt narrowing of the spectrum above the threshold is the important criteria for that the real lasing is achieved in contrast to the amplified spontaneous emission. This narrowing is similar to the classical Schawlow–Townes line narrowing considered for DFB fibre lasers in Section 3.4.1, but there is a difference defined by dissimilar mechanisms of narrowing. In the conventional laser having cavity mode(s), the spectral profile of an individual mode providing its reflection at each round-trip leads to narrowing after many round-trips, whereas in the random DFB fibre laser with broadband RS reflection only the gain spectral profile defines narrowing at each round trip. So one can effectively treat this laser as a single-mode one with a continuous spectrum of the width and central frequency defined by the gain profile. As the Raman gain profile has a double-peak structure with two maxima near 1555 nm and 1565 nm, Fig. 16a, black curve, the lasing could be achieved in two wavelength bands (near 1555 and 1565 nm), either separately or simultaneously depending on the system configuration and the pump power level. Well above the threshold the generated spectrum exhibits power broadening: the higher is the pump power, the broader is the generation spectrum, Fig. 16b. The observed spectral broadening is similar to spectral broadening in conventional Raman fibre lasers [313].

Random DFB fibre lasers have a directional output as the light is confined in the fibre core. The beam profile is nearly Gaussian, Fig. 17. Moreover, even for the systems based on the multi-mode fibres, the radiation is still nearly single-mode with a Gaussian profile because of the beam clean-up effect, see Section 4.9 for details.

The random DFB fibre laser operates in the quasi-CW regime. The intensity dynamics measured with a 300 MHz bandwidth photodetector reveals almost steady output at ms time scale, Fig. 18. However, radiation should comprise fluctuations on the time scale inversely proportional to the optical spectrum width (1 nm), i.e. the laser output could be highly irregular on the time scale of several tens of ps. The intensity dynamics of random DFB fibre lasers in broad frequency range have not studied in details yet. However, it is known that near the generation threshold the temporal behaviour could be very different from the steady-state, because of the pronounced stimulated Brillouin scattering [31,312]. Indeed, near the threshold irregular pulses are generated with pronounced components in radio-frequency signal at 11 and 22 GHz
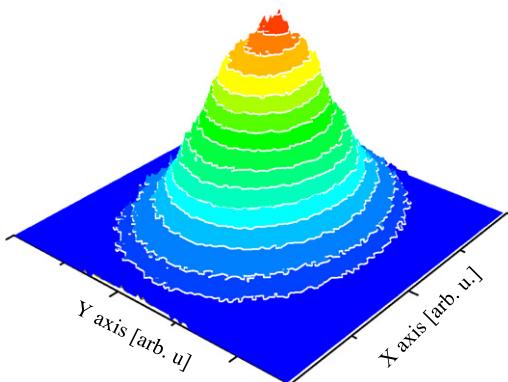
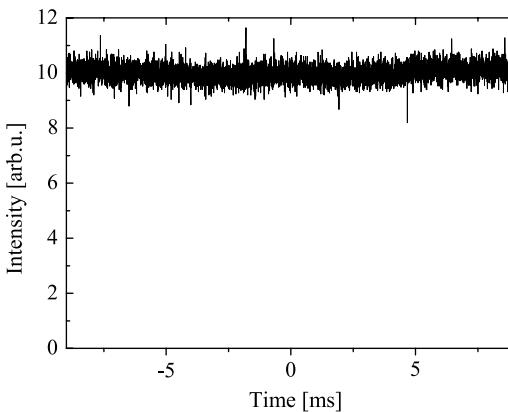**Fig. 17.** Beam profile of the random DFB fibre laser measured in far field.

Fig. 18. Intensity dynamics of the random DFB fibre laser experimentally measured within a 300 MHz bandwidth.
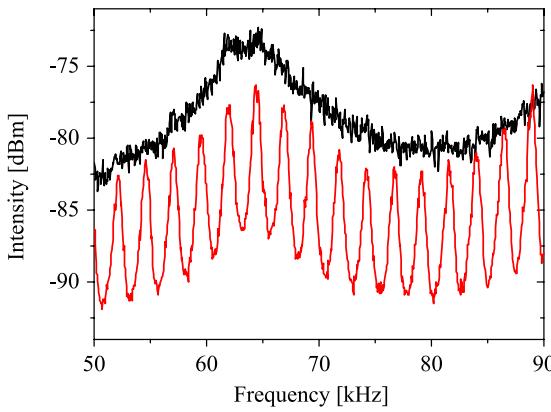

Fig. 19. Radio-frequency spectra of the random DFB laser (black) and a laser with conventional cavity of the same length (red). After Ref. [317]. ©American Physical Society.

corresponding to the Brillouin shift [31]. The pulsed behaviour of the random DFB fibre laser in this regime is similar to a self-Q-switched laser with combined RS–SBS feedback [310,314]. Note that the acoustic waves and, therefore, SBS-induced irregular pulses could be suppressed by external noise, so the generation of the random DFB fibre laser could be stabilized. Moreover, the SBS–RS instability could be self-suppressed high above the generation threshold. The most probable reason for that is the cross-phase-mixing (XPM) induced spectral broadening [314].

The measured radio frequency (RF) spectrum shows that there is no indication of longitudinal mode beating corresponding to any cavity of fixed length in contrast to the conventional cavity Raman fibre lasers, Fig. 19, where longitudinal modes are always observed in RF spectra [315]. As a result, the random DFB fibre laser could be treated as mode-less. However, some auxiliary peaks in rf-spectrum could be observed in some cases on frequencies not equivalent to the inter-mode
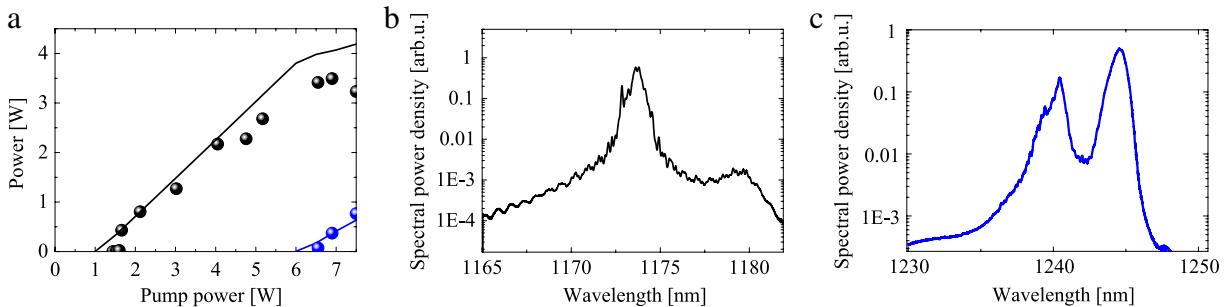
Fig. 20. Performances of the cascaded random DFB fibre laser. (a) Output powers of first (black) and second (blue) Stokes waves. Experimental data is shown by circles, numerical simulations within balance equation set (26) is shown by lines. (b) and (c)—Optical spectra for first and second Stokes waves, respectively. After Ref. [321].

frequency of the conventional resonator, $c/2Ln$. A possible reason could be associated with relative intensity noise transfer from the pump wave to the generation wave similar to conventional Raman fibre lasers [316].

4.4. Operation in different spectral bands

Most of the demonstrated random DFB fibre lasers emit in the 1550 nm spectral band as they use Raman gain induced by 1455 nm pump lasers. This is a typical telecom configuration for distributed Raman amplifiers operating at wavelengths with minimal losses both for the pump and the signal. However, the magnitude of the Rayleigh scattering coefficient scales with wavelength as λ^{-4}, so the random feedback based on the Rayleigh scattering could be more intense at shorter wavelengths. At the same time, the optical losses increase nearly proportionally at shorter wavelength. Generally, since the Raman gain is always related to the pump frequency with a constant shift, the random DFB fibre laser could be designed to operate at any wavelength under appropriate pumping. As an example, a random DFB fibre laser generating at 1455 nm while pumped at 1365 nm is reported in [318]. In [319], a random DFB fibre laser generating in the 1.2 μm spectral range is reported. The single-arm laser is pumped at 1115 nm by an Ytterbium-doped fibre laser. The output power of up to 1.5W is obtained in the 2-km long fibre. Up to date, it is the shortest demonstrated random DFB laser. The range of possible wavelengths was extended in [320], where the authors applied pumping at 1064 nm to obtain generation at 1115 nm of output power up to 280 mW at 4.5 W pump power. The relatively low generation efficiency is related to a rather long (for this wavelength) 50 km fibre span used in the laser, see Section 5.3 for theoretical considerations of the lasing efficiency. Note that in paper [320] the laser generated at a wavelength below the cut-off wavelength of the used fibre, so the generation could be spatially multi-mode. However, in the [321] it was verified that in a random DFB fibre laser operating below the cut-off wavelength of the fibre, the radiation is still single-mode and has a Gaussian diffraction limited beam profile. The same effect is observed in random DFB fibre lasers based on the highly multi-mode fibres pumped by multi-mode laser diodes, see Section 4.9 for details.

4.5. Cascaded operation

A cascaded generation is a process in which the Stokes wave acts as a pump wave for higher order Stokes waves shifted further to the long wavelength region. Cascaded Raman fibre lasers are widely used to generate in the range from 1.1 to 2.2 μm [322]. A traditional way to achieve a cascaded generation in a Raman fibre laser is to form a resonator for higher Stokes waves using mirrors resonant to higher Stokes wavelengths. In the random DFB fibre laser, the Rayleigh backscattering provides feedback both for the first and the higher-order Stokes waves. The cascaded operation in the random DFB fibre laser was demonstrated in [321], where both the first and the second Stokes wave were generated simultaneously in the same fibre span. At 7.5 W of the pump power at 1115 nm, about 4 W power for the first Stokes wave at 1175 nm and 1 W for the second Stokes wave at 1240 nm were generated in the backward direction in the single-arm configuration, Fig. 20.

A cascaded generation of the second Stokes component at 1555 nm was obtained in a backward-pumped random DFB fibre laser based on 50 km of SMF-28 fibre with 1366 nm pump and FBG at 1454 nm in [323]. Pump power thresholds for the first and second order were 0.7 and 2 W, respectively; maximum output powers — 100 mW and 130 mW. Note that the claimed generation threshold of 0.7 W means that some parasitic point-based reflections were affected the system performances, as the minimal threshold in the laser with pure random feedback is 0.8 W, see Section 5.2 for details. Authors of [324] added two FBGs for 1454 and 1550 nm and 1 km of DCF fibre, which has a rather high Raman gain coefficient. This allows to decrease the length of SMF-28 down to 9 km only and to obtain the cascaded generation at 1550 nm at 2.5 W pump power.

A generation of the third-order Stokes wave at 1670 nm was achieved in ∼100 km long fibre under pumping at 1365 nm [325]. To form the cavity for all Stokes waves simultaneously, a wavelength-division-multiplexer was used as a broad-band reflector at one fibre end. A threshold power for the third Stokes wave was as low as ∼2.5 W.
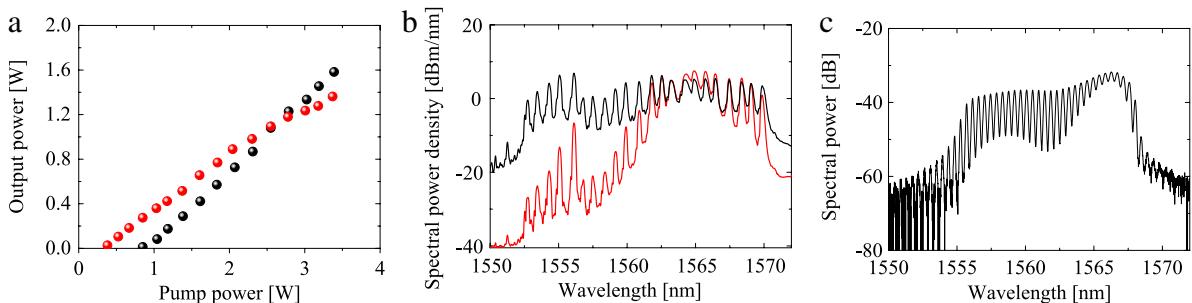
Fig. 21. Multiwavelength generation in the random DFB fibre laser based on (a, b) the set of 22 FBGs and (c) the all-fibre Lyot filter. (a) Output powers and (b) optical spectra of a multiwavelength random DFB fibre laser operating via random feedback only (black) and using additional 4% Fresnel reflection (red). (c) Generation spectrum in all fibre Lyot filter based multiwavelength random DFB fibre laser. After Ref. [326,327].

4.6. Multiwavelength operation

Since the RS-based random feedback is broad-band, it is possible to use it together with multiple spectral filters thus providing a multi-wavelength operation of the random DFB fibre laser. The first realization of a multi-wavelength random DFB fibre laser was based on the backward-pumped configuration of the random DFB fibre laser, Fig. 14b, where an array of 22 FBGs with different central wavelengths is used at the end of the ∼22 km fibre span [326]. In this instance, a simultaneous generation at 22 wavelength defined by the wavelengths of the corresponding FBGs was achieved. The generated radiation covered the span of 1552–1570 nm with spacing of ∼0.8 nm, Fig. 21b. It is interesting, that spectral and power performances of multiwavelength random DFB fibre lasers overpass those of conventional lasers based on a 4% Fresnel reflection. Namely, the total generation efficiency of the multiwavelength random DFB fibre laser is found to be higher in the case of a laser operating via pure random feedback than for a laser operating via conventional feedback, Fig. 21a. Moreover, the power distribution between different generation lines is flatter in the case of pure random feedback, Fig. 21b. The improved generation efficiency and flatter power distribution among the different lines are caused by the suppressed competition between the lines. This fact may be treated as a manifestation of self-organization in the case of random feedback that depends on spatial power distribution for all waves.

Another approach to obtain a multi-wavelength generation is to use an all-fibre Lyot filter in the central point of the symmetrical scheme [327]. The all-fibre Lyot filter comprises two 45° tilted fibre Bragg gratings inscribed into a polarization maintaining fibre along its principle axis and a polarization maintaining fibre as cavity [328,329]. The filter has both filtering and polarizing functions, and its bandwidth and free spectra range could be adjusted by changing the length of the polarization maintaining cavity. All-fibre Lyot filters are used in various types of fibre lasers [330,331]. A Lyot filter with a 0.2 nm bandwidth and 0.4 nm free spectral range (FSR) was incorporated in the random DFB fibre laser cavity. The random DFB fibre laser generates multiple wavelengths simultaneously in the whole range of the Raman gain spectral profile, Fig. 21(c). Near the Raman gain peak, the power distribution of generated lines is flat with only about 0.5 dB of variation over a 4 nm region comprising 8 lines. The higher the pump power, the flatter is the power distribution between the lines and the more lines are generated within ∼33 dB intensity variation range. Note that each line has a typical spectrum width of about 0.07 nm, which is 3 times less than a spectral width of the Lyot filter transmission peak and much less than a spectral width in the case of FBGs based multiwavelength random DFB fibre laser. It is possible to control the spectral properties of the generated radiation during the Lyot filter manufacturing process. For instance, spacing between the generated lines can be controlled by adjusting the length of the polarization maintaining fibre in the Lyot filter. Linewidth of the individual lines can be controlled by employing a cascade of such Lyot filters. It is also possible to control these parameters of generation in a different way, as the polarization maintaining fibre in the Lyot filter can be replaced by any suitable birefringent device, allowing room for possibility of wavelength and spacing tuning.

Other schemes could be also implemented to achieve multiwavelength generation in random DFB fibre lasers. In the papers [332,333], multiwavelength generation was obtained in the forward-pumped configuration, Fig. 14a, using a Sagnac loop mirror with a high-birefringence photonic crystal fibre, which works as a multiwavelength filter and results in a modulation of the Sagnac loop mirror reflection spectrum. This element allows to obtain a multiwavelength generation with mode spacing depending on the photonic crystal fibre length. Up to 16 nm span around 1550 nm was filled by multiple lines with a spacing of 0.09 nm only. The Sagnac multiwavelength filter is also used in the symmetrical scheme [334] and in the scheme with a Raman gain fibre inserted into the Sagnac fibre loop together with a high-birefringence fibre [335].

4.7. Tunable operation

Broadband nature both of the Raman gain and the Rayleigh backscattering also opens a possibility to tune the generation wavelength of the random DFB fibre lasers in a wide range. An idea of the tunable generation in the random DFB fibre laser was implemented in [317]. To make a radiation tunable, a tunable acousto-optic filter of spectral width 1.5 nm and 2 dB
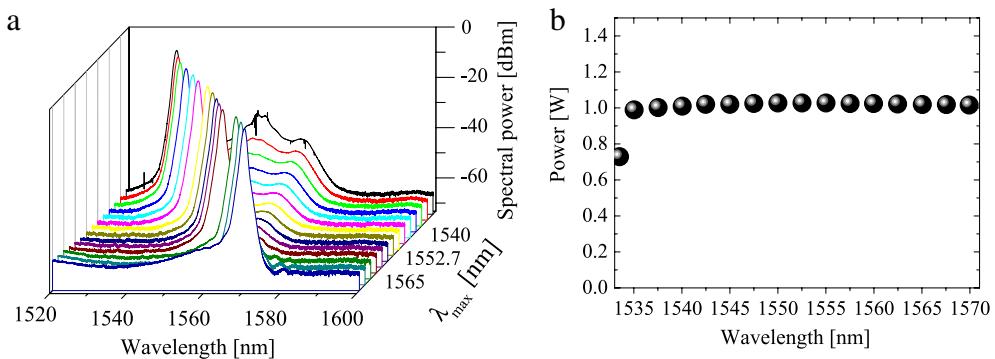
Fig. 22. Tunable random DFB fibre laser. (a) Generation spectra while tuning the spectral filter. (b) Output power depending on the generation wavelength. After Ref. [317]. ©American Physical Society.

insertion losses was placed at the central point, $z = 0$, of the symmetrical scheme, Fig. 14a. The generation power at $z = 0$ point in the symmetrical scheme is below 100 mW even at the multi-Watts level of the output laser power (see details about longitudinal power distributions in Section 5.4), so low-power handling wavelength selective elements could be used to control the high power radiation of the random DFB fibre laser. Also the authors reduced the fibre length of each arm down to $L = 20$ km to increase the efficiency (theoretical background about efficiency and power optimization can be found in Section 5.3). As a result, a radiation tunable within the range of 1530–1575 nm is generated, Fig. 22a. Note that the lower the generation power, the more pronounced is the amplified spontaneous emission near the Raman gain maxima limiting tunability at low powers. The achieved tuning range is comparable with those in Raman fibre lasers based on conventional cavities [336–339].

Another impressive result here is that the power variations within the tuning range 1535–1570 nm do not exceed 3%, Fig. 22b. The obtained flatness of the tuning curve is much better than that in the conventional linear cavity as measured in [317] or in ring lasers where the power flatness is around 20% within the similar tuning range [340,341]. Excellent flatness of power over the generation wavelength is caused by the fact that the total generation efficiency of the random DFB fibre laser barely depends on the wavelength and the value of the Raman gain (see details in Section 5.3 and also see Eq. (37)).

A similar approach was implemented in [342], where the forward-pumped configuration with a fibre loop mirror was used, Fig. 14a. For wavelength selection a FBG-based tunable filter of 0.2 nm spectral width was used at some point within the fibre loop mirror. A small part of the generated radiation propagating in a backward direction was out-coupled by using a 1% coupler. Tuning over 21 nm within a range of 1550–1571 nm was achieved with power variations of less than 3 dB. However, because most of the radiation in this scheme is generated in a forward direction (see Section 5.4.2 for the details) and due to the small coupling ratio of the output coupler, the power efficiency was relatively low in this scheme.

4.8. Narrow-band generation

In the random DFB fibre laser, the radiation spectrum is usually quite broad having a typical spectral width of 1 nm and more, Fig. 16. It is of practical interest to suppress the linewidth of the random DFB fibre laser. A narrow-band emission down to ∼0.05 nm was achieved by inserting narrow-band spectral filters between two spans of 40 km standard single-mode fibres in the central point $z = 0$ of the symmetrical scheme in [343]. Two types of filters were used: a FBG (spectral width is 0.05 nm) and fibre-coupled Fabry–Pérot filter (a spectral width of 10 pm for every transmission peak). It is important that the spectral filters are inserted at the point $z = 0$ there the generation power is low (around 10 mW at output power level of 1 W) because of the specific non-uniform longitudinal power distribution in the random DFB fibre laser, see Section 5.4.2.

With a FBG as a spectral filter, spectral width of the generated wave is almost constant at a level of around 0.05 nm and follows the spectral width of used FBG up to the pump power 1.2 W. However, at a higher pump power, the spectrum becomes broader than the filter spectral width: up to 0.3 nm being still narrower than in the case of a random DFB fibre laser without any spectral filters. Similar results are obtained with FPF as a spectral filter. Namely, narrow-band generation of spectral width below 0.02 nm is generated. Note that using an all-fibre Lyot filter as a spectral element results also in narrow-band multiwavelength generation, see Section 4.6, with a spectral width being less than a spectral width of the individual peak of the Lyot filter transmission profile.

In general, the random DFB fibre laser can be operated in any mix of tunable, multiwavelength and narrow-band regimes. As an example, a tunable multiwavelength generation of small spectral width of each individual line was demonstrated in [344]. The authors used a Mach–Zehnder interferometer based on two long-period FBGs as a tunable broadband filter (tuning is provided by bending the interferometer). At the same time, a Fabry–Pérot filter was used for a fine selection of 12 different wavelengths within the Mach–Zehnder interferometer bandwidth. As a result, the multiwavelength generation with tuning range 1553.9–1565.4 nm and individual line spectral width of 0.034 nm only was achieved.
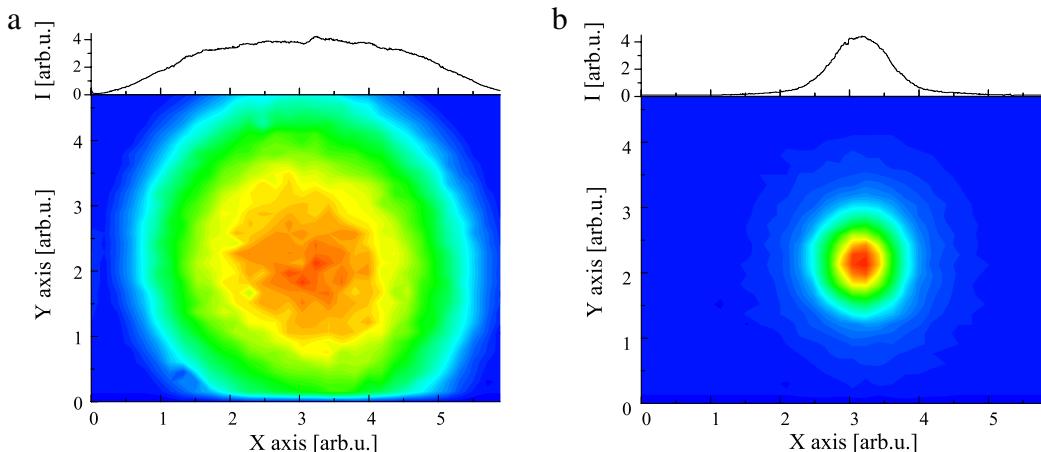
Fig. 23. Output beam profile of a multi-mode random DFB fibre laser pumped by a multi-mode pump laser: (a) pump beam (b) generation beam.

The described above narrow-band lasers are not obviously single-frequency. However, the Rayleigh backscattering could be used to improve performances of single-frequency lasers. The Rayleigh backscattering in the Erbium-doped ring fibre laser was employed to achieve single longitudinal mode generation in [345]. To preliminary narrow down the generation spectrum, a 3 GHz tunable filter was used in the cavity. The Rayleigh backscattering signal was harvested and re-injected co-directionally with generation wave. It was shown that additional seed signal provided by Rayleigh backscattering enhances the generation of the mode with a maximum gain and suppresses the generation of other modes. As a result, a spectral line of only 4 kHz width was obtained being additionally tunable in the 0.5 nm range.

The impact of the Rayleigh feedback in a ring cavity Raman fibre laser was investigated in [318]. The laser comprised 123 km of SMF-28 fibre and was pumped ad 1365 nm. The authors proved significance of the Rayleigh scattering by means of numerical simulations of output power. Presence of Rayleigh feedback has proven not to alter the threshold level, but to sufficiently change generation power characteristics above the threshold. Besides, it results in a vanishing of mode structure in the Stokes wave spectrum, as in ultra-long linear cavity fibre lasers [19].

Note that in general a ring cavity laser operating via only pure random distributed feedback is not possible. Indeed, if the cavity length is short enough to allow light to make round-trips over the ring cavity, the conventional longitudinal modes will immediately appear and the laser could not be considered as a random laser. If one elongates the cavity sufficiently to prevent making round-trips and make random feedback to work, the laser scheme will be equal to the linear random DFB fibre laser. However, the generation properties could differ in fine details.

In random DFB fibre lasers based on the Brillouin gain instead of the Raman gain, much narrower line-width could be achieved just because the bandwidth of the Brillouin gain ($\sim$100 MHz) is much less than the bandwidth of the Raman gain (few THz), see Section 4.12 for details.

4.9. Random DFB fibre lasers directly pumped by a multi-mode laser diode

A random laser based on 4.5 km of multi-mode fibre directly pumped by a multi-mode laser diode at 940 nm was reported in [346]. Random lasing was obtained at 980 nm via the Rayleigh backscattering as a feedback mechanism and the stimulated Raman scattering as gain. The threshold pump power was above 40 W, and the generation power was 0.5 W at 45 W pumping. In addition, this scheme has a prominent feature enabling a radical beam quality improvement. The measured divergence of the output beam at 980 nm is 4.5 times lower than that of the pump beam, Fig. 23. The main mechanism of the beam quality improvement is the well-known Raman clean-up effect [347] based on the radial-coordinate dependent Raman gain in gradient-index multi-mode fibres. However, Rayleigh scattering based feedback could also have some impact on the clean-up due to the radial variation of the refractive-index and its fluctuations as well. It was indirectly confirmed in experiments with linear-cavity Raman lasers made of the same fibre [348]: The observed divergence of the output beam was 1.5 times larger than that for the random laser.

The demonstrated approach seems to be attractive for a high-power generation in the short-wavelength spectral domain ($<1\,\mu$m), where generation of rare-earth doped fibre lasers is challenging. For example, using a commercially available high-power laser diode around 800 nm one can generate a high-quality beam at 830 nm in conventional multi-mode passive fibres

4.10. Random DFB fibre lasers for telecom applications

In random DFB fibre lasers long fibre spans are usually used to generate a light, so random fibre lasers are natural candidates for distributed Raman amplification in quasi-lossless transmission systems [20,349–352] requiring homogeneous
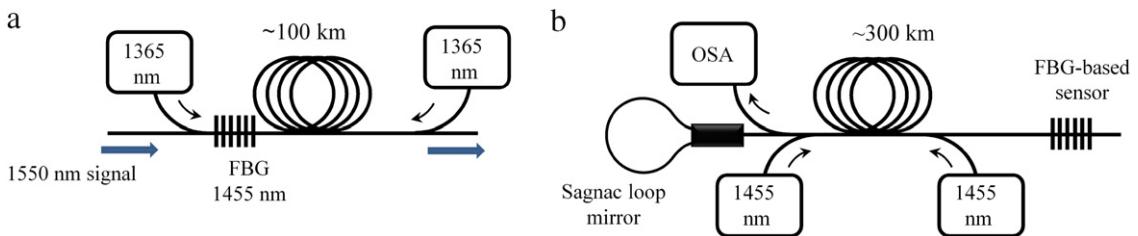
Fig. 24. Examples of random DFB fibre laser applications in (a) distributed Raman amplification [354] and (b) remote temperature sensing [365].

distribution of laser power along the fibre that is then utilized as a Raman pump. The random DFB fibre laser operating at 1455 nm was used as a pump in distributed Raman amplifier and performances of the scheme was compared with performances of the conventional bi-directional 1st-order and 2nd-order distributed Raman amplifiers its performance [353,354]. Random lasing was initiated in a 100 km fibre span used as the transmission link simultaneously. Different configurations of random DFB fibre laser were tested. It was found that in some configurations, Fig. 24a, the transmission scheme based on the random laser exhibits ∼2.3 dB lower effective noise figure as compared to conventional bi-directional 1st-order and 2nd-order distributed Raman amplifiers, but larger average gain and gain fluctuation levels. To address this issue, in the subsequent paper [355] the authors suggested to incorporate an additional 1st order low-noise pump that proved to retain noise figure while reducing potential nonlinear impairment. They demonstrated the operation of the Brillouin optical time-domain analysis system in a 154 km transmission link operated via a random DFB fibre laser based amplification. Earlier the Brillouin optical time-domain analysis system improved by an implementation of the random DFB fibre laser was demonstrated in 142 km ring cavity [356].

Random DFB fibre laser design could also be used for remote pumping of Erbium-doped fibre amplifiers. In [357], the tunable forward-pumped random DFB fibre laser based on 41 km fibre span was used to simultaneously pump the Erbium-doped fibre amplifier and support signal transmission via Raman gain. It was shown that net gain in such setup is larger than in the scheme of the remote Erbium-doped fibre amplifier pumping based on the conventional laser design.

4.11. Random DFB fibre lasers for remote sensing

Distributed fibre sensor systems [358–360] could also benefit if the random DFB fibre lasers are used. For instance, in paper [361,362] a backward-pumped 100 km long random DFB fibre laser was used to interrogate remotely a FBG-based temperature sensor. In this case, the generated wavelength serves as a signal sensitive to the FBG temperature and strain. The authors also suggested a second-order random DFB fibre laser to improve the signal to noise ratio. A forward-pumped random DFB fibre laser with two FBGs of slightly different central wavelengths providing two-wavelength generation was used for scanning of the temperature sensor based on a fibre Fabry–Pérot interferometer [363]. A temperature sensor based on lasing provided by the combination of the Fabry–Pérot cavity and the Rayleigh backscattering was proposed in [364]. The Fabry–Pérot cavity fabricated by the splicing of a single mode fibre with a small piece of suspended-core fibre was used simultaneously as a laser reflective mirror and a temperature sensing element.

A tunable random DFB fibre laser in a forward-pumped configuration was used to interrogate 11 FBG temperature sensors placed at a distance of 200 km. In [365], a FBG sensor placed as far as 300 km apart was interrogated in a two-wavelength random DFB fibre laser configuration: the scheme comprises a fibre loop mirror at one fibre end and the FBG-based sensor at the other end of the 300 km fibre span, Fig. 24b. In this scheme the temperature or strain can be calculated from the power ratio between 2 different lines generated in the random DFB fibre laser. A more complicated interrogation scheme based on the two-wavelength random DFB fibre laser was presented in [366]. The laser has a forward-pumped configuration with two FBGs at one fibre end. One of the FBGs experienced tension while another was kept undisturbed as a reference, so that the FBGs were equally sensitive to the ambient temperature. Information about the strain was derived from the measurements of wavelength difference between idler and signal waves in a four-wave mixing scheme involving two generated wavelengths. A random DFB fibre laser was also used to improve performances of a distributed temperature sensor based on the Brillouin scattering. In a 122 km long fibre span, the Brillouin signal at 1550 nm was amplified owing to the random generation at 1455 nm, that allowed to improve signal-to-noise ratio in comparison with a conventional first-order Raman amplification scheme. As a result, spatial and temperature resolutions of ±2 m and ±1 C, respectively, were achieved.

For sensing applications, the modulated interrogation signals are frequently required. In [367], the first implementation of the internal modulation of the generated power in random DFB fibre laser was demonstrated. To do this, the reflection of the fibre-loop mirror was modulated with a frequency of up to 12 GHz. Unlike conventional internally modulated fibre lasers, where the presence of the longitudinal modes determines a repetition rate of the pulses and can, therefore, sufficiently alter modulated output signal, there were distortion of the modulation frequency or self-mode-locking effects in the random DFB fibre laser in the entire 12 GHz range. This features random DFB fibre lasers as a source that can be easily modulated for remote sensing and other applications.

4.12. Random DFB fibre lasers based on the Brillouin gain

In all the discussed configurations of the random DFB fibre lasers, the gain mechanism is based on the Raman scattering. However, it is well known that the Brillouin scattering in fibres, i.e. wave scattering on an acoustic wave in a fibre core, has a much higher gain coefficient [368]. The Brillouin gain coefficient is a thousand times higher, which makes it possible to provide necessary amplification at very weak random feedback, so the fibre span needed to achieve the random generation could potentially be made much shorter. In early works it was shown how drastically small Rayleigh backscattering could change the properties of laser radiation, however random lasing was not achieved [310,369]. In more details, self-Q-switching in the Yb-doped fibre laser was achieved by replacing the output reflector by just a few metres of passive fibre [310]. Random Rayleigh scattering based feedback from the fibre was amplified by the process of stimulated Brillouin scattering that resulted in the modulation of cavity finesses and finally in strong pulsations in the output radiation. The influence of the Rayleigh scattering on the performance of a Brillouin fibre laser was studied in [310]. A short fibre span of only 300 m was pumped by a single-frequency laser at 1.06 μm. To compare the laser properties with and without the influence of Rayleigh scattering, the pump wave was modulated at 100 kHz frequency by means of an electro-acoustic modulator. In this case the Rayleigh feedback could not grow because of pulsations in the pump wave that were too fast. It was found that Rayleigh backscattering results in the narrowing of the generation spectrum from 10 MHz to less than 100 kHz. What is interesting, is that statistical properties of the radiation are also changed from exponential statistics with a maximum at the zero intensity to Gaussian statistics with non-zero mean value [370]. The authors performed numerical simulations and found good agreement with the experimental data.

In further works, pure random DFB fibre lasers operating via Brillouin gain were demonstrated [371,372]. In a forward-pumped laser scheme comprising 20 km of fibre and FBG, the Brillouin lasing was achieved via random feedback based on the Rayleigh backscattering. 1550 nm pumping was realized by a single-mode (spectral width of 100 kHz) tunable laser of 150 mW output power. The wavelength of the laser was chosen to be detuned from the FBG reflection wavelength by 15 GHz, so the grating could reflect one Brillouin Stokes component only. Similar to [310] a co-existence of two regimes was found — usual Brillouin process with broad exponential intensity statistics and the regime of the random lasing via Brillouin gain due to Rayleigh backscattering with Gaussian statistics. Note that difference in statistical properties of radiation are studied on a time scale of hundreds nanoseconds, that makes these two different regimes principally different from laminar and turbulent lasing regimes in Raman fibre laser recently experimentally demonstrated in [25] and theoretically discussed in [373,374]. Indeed, during the transition from the laminar to the turbulent regime in a quasi-CW fibre laser, statistical properties are changed on sub-ns time scale because of the destruction of the coherent condensate via the generation of dark and grey solitons. One can find out more about turbulent generation in conventional quasi-CW fibre lasers in the review [375] as well as in papers [313,376–378]. Note that methods of optical wave turbulence are now widely applied to different problems in fibre optics, see, for example, [379–383].

Other schemes of Brillouin-gain based random DFB fibre lasers do exist. In paper [384], a resonator of the laser was formed with three different fibre spans, spliced together. The middle fibre span of high Brillouin gain was used for Brillouin Stokes wave amplification, while other fibre spans were inserted to additionally increase random feedback produced by the Rayleigh backscattering. Above the generation threshold, the Stokes wave starts to lase with spectral width of 3.4 kHz that is 3 order of magnitude smaller than the spectral width of the Brillouin gain profile. Even better results are reported in [385], where the highly stable pump laser of 3.5 Hz linewidth was used. The generated of the Brillouin Stokes component had a very narrow spectrum of ∼10 Hz width. In further work [386], the frequency jitter was suppressed to the level of 40 kHz per 3 h of operation. A propagation model governing the dynamics of distributed feedback Brillouin lasers based on a p-phase shifted grating in a highly nonlinear silica fibre [238] and chalcogenide was presented in [387].

The Brillouin scattering can be also used to achieve a high-dense multiwavelength generation in a cooperative Raman/Brillouin fibre laser. Demonstrated in [388] the multiwavelength laser generates a number of Brillouin-Stokes components near the maximum of Raman gain spectrum. A resonator is formed by a broadband mirror from one side and random RS-based feedback from another side, that decreases the threshold for the cascaded generation of the Brillouin Stokes waves and increases the full span of the Brillouin comb up to 57 nm. An impact of the Rayleigh backscattering on the Brillouin comb generation was studied in [389]; it was confirmed that the generation efficiency and the total generation bandwidth could be increased via the random feedback. A similar approach of a cooperative Raman/Brillouin laser was used in papers [390,391], where 210 uniform Brillouin Stokes lines with 0.08 nm spacing in the bandwidth of 16.8 nm from 1550 to 1567 nm were generated. Eleven Brillouin Stokes components in the shorter wavelength region around 1516 nm were generated under the 1425 nm pump provided directly by laser diodes in [392].

Finally, a very different laser was demonstrated in paper [393], where the authors managed to achieve a generation in the fibre due to stimulated Rayleigh scattering as an amplification mechanism while using regular spontaneous Rayleigh scattering as a distributed feedback in the same fibre span. As in conventional fibres the stimulated Rayleigh scattering threshold is normally higher than that of SBS and hence unobserved. The authors used a specially designed non-uniform fibre with a continuous change of a core diameter, that raises the SBS threshold and makes the stimulated Rayleigh scattering generation possible. With high enough pump laser power, having 6 MHz linewidth at 1549 nm, generation signal at the same wavelength, observed in the opposite direction relative to the pump, narrows dramatically down to 4 kHz due to cooperative stimulated and spontaneous Rayleigh scattering operation.

5. Theory and modelling of random DFB fibre lasers

In this section we introduce mathematical models governing the operation of the random DFB fibre lasers. The first theoretical approach is based on the analysis of the system of equations describing average power evolution. This model takes into account all important physical effects, including fibre losses, Raman gain, pump depletion, amplified spontaneous emission, Rayleigh backscattering and propagation through the fibre. The model works rather well for describing of the key features of the random DFB fibre lasers and is also widely used for the design and optimization of Raman fibre lasers and amplifiers, including distributed Raman amplification schemes. We will apply a power average model to demonstrate the impact of Rayleigh scattering on lasing. We derive the generation threshold of the random DFB fibre laser, and analyse output power, generation efficiency and longitudinal power distribution of generated waves in different schemes. However, an average power model is not capable of providing information about dynamics of the spectra during propagation in fibre medium. Changes in the spectrum of radiation during propagation in fibre occur due to the nonlinear Kerr effect and fibre dispersion. Therefore, for an analysis of the spectral evolution in the random DFB fibre lasers, we apply a model based on the amplitude evolution equations.

5.1. Average power balance model

The generation of radiation due to the Raman gain and the propagation of the generated waves in the fibre cavity in terms of the time averaged optical power is given by the system of differential equations, often called the power balance model [368]. This model works very well for predicting a generation threshold, an output power and a power balance between the pump and generation waves in conventional Raman fibre lasers [394–398] and Raman amplifiers [349]:

$$
\pm \frac{dP_\nu^\pm}{dz} = -\alpha_\nu P_\nu^\pm + P_\nu^\pm \sum_{\mu>\nu} g_{\mu\nu} \left(P_\mu^+ + P_\mu^- \right) - P_\nu^\pm \sum_{\mu<\nu} \frac{\nu}{\mu} g_{\nu\mu} \left(P_\mu^+ + P_\mu^- \right) + \varepsilon_\nu P_\nu^\mp
$$
$$
+ 2h\nu \sum_{\mu>\nu} g_{\mu\nu} \left(P_\mu^+ + P_\mu^- \right) - 4h\nu P_\nu^\pm \sum_{\mu<\nu} g_{\nu\mu}, \tag{16}
$$

where μ and ν are optical frequencies, $P_\nu^\pm$ represents average (within the infinitesimal bandwidth around ν) powers of the forward $(+)$ and backward $(-)$ propagating relative to the z-axis direction waves; α_ν is an attenuation coefficient, $g_{\nu\mu}$ is an effective Raman gain parameter at frequency ν induced by a pump at frequency μ, h is the Planck's constant. This system models the key physical effects affecting optical power generation and propagation, including: fibre losses, nonlinear Raman effects that can be divided here into subclasses, such as, pump-to-pump, pump-to-signal, and signal-to-signal interactions, pump depletions due to energy transfer from pump to signal, Rayleigh backscattering, amplified spontaneous emission noise and thermal noise. As it was pointed out in [399] a factor of two in the noise terms is due to a lack of correlation between signal and noise and polarization scrambling leading to mixing of signal and noise during propagation.

To describe the random DFB fibre laser within the power balance model, we take into account the Rayleigh backscattering at the signal frequency by adding the term proportional to ε_ν (an effective Rayleigh-backscattering coefficient): Although the Rayleigh backscattering is a random process on a sub-micron scale [310], its effect on the optical power can be taken into account through an average energy income to the generated wave from the backscattered wave. The same approach is efficiently used in Raman amplifiers [349]. Note that the introduced full system of equations is very generic and can be applied in a variety of fibre laser systems including random DFB fibre lasers.

For particular laser configurations, the full set of equations can be substantially simplified. For instance, for a laser generating narrow signal from the pump waves at a single pump frequency, the master equations read:

$$
\pm\frac{dP_p^\pm}{dz} = -\alpha_p P_p^\pm - g_R \frac{\nu_p}{\nu_s} P_p^\pm \left(P_s^- + P_s^+ + 4h\nu_s \Delta\nu \right),
$$
$$
\pm\frac{dP_s^\pm}{dz} = -\alpha_s P_s^\pm + g_R \left(P_p^+ + P_p^- \right) \left(P_s^\pm + 2h\nu_s \Delta\nu \right) + \varepsilon P_s^\mp. \tag{17}
$$

Here P_p, P_s denote the pump and the first Stokes wave powers, respectively; $\nu_{s,p}$ are frequency of the Stokes and pump waves, respectively; $\alpha_{s,p}$ are losses at the signal and pump frequencies, g_R and ε stand for the Raman gain coefficient and Rayleigh scattering coefficients, respectively at the Stokes wave frequency. The impact of the Rayleigh backscattering at the pump wave frequency is not taken into account. The parameter ε is defined here as $\varepsilon = \alpha \cdot Q$, where $Q \sim 0.001$ is the geometrical factor [400], accounting for the part of the scattered radiation, that is further recaptured by the fibre waveguide. This value may vary depending on the fibre numerical aperture and a fabrication method [401]. Despite the smallness of the parameter ε, the Rayleigh backscattering plays the major role in the operation of the random fibre lasers. The small amount of the backscattered radiation is amplified by the Raman effect leading to the formation of an effective distributed reflector providing for a feedback. Also note that in telecommunication even double backscattering is known to be important in distributed Raman amplification. We add to the equation set the term corresponding to the spontaneous Raman scattering, $h\nu_s \Delta\nu$, where $\Delta\nu \sim 10$ nm is a Raman gain spectral profile width. Despite the fact that the term with the spontaneous Raman scattering is small compared to other terms, it plays an important role of a seed source, otherwise the equations give

zero solutions in numerical simulations. In all further numerical modelling, we take into account this term, however, we do omit it in some appropriate analytical considerations. The value of the wavelength-independent Raman gain g_R is taken at the maximum of the Raman gain spectral profile. It is justified by the fact that the typical width of the Raman gain spectral profile is ~10 nm, while the typical width of the generation spectrum in the random DFB fibre laser is ~1 nm, [31].

To solve the equation set (17), one should add boundary conditions which do depend on the specifics of the random DFB fibre laser scheme. We would like to stress here, that we consider equivalent schemes from the right column in Fig. 14. For example, in the forward-pumped configuration, there is no reflection at one fibre end, $z = L$, and the full reflection at the another fibre end, $z = 0$:

$$\begin{cases} P_s^-(L) = 0, \\ P_s^-(0) = P_s^+(0), \\ P_p^+(0) = P_0. \end{cases} \tag{18}$$

Here P_0 is the input pump power.

Boundary conditions for backward-pumped configuration differ by the opposite pump direction only: $P_s^-(L) = 0$, $P_s^-(0) = P_s^+(0)$, and $P_p^-(L) = P_0$. In the single-arm scheme, there is a zero reflection from both fibre ends: $P_s^+(0) = 0$, $P_s^-(L) = 0$, and $P_p^+(0) = P_0$.

Note that in conventional Raman fibre lasers with a cavity made of point-based mirrors, boundary conditions are defined by the reflectivity profile of the laser mirrors. Because spectral profiles of mirrors are obviously frequency-dependent, it is challenging to take them into account in the frequency-independent power balance model. Indeed, in most cases one cannot treat the spectral profiles of the cavity mirrors as frequency-independent because of the huge spectral broadening making the generation spectrum comparable in width to the spectral width of the mirrors [377]. As a result, the power balance model could fail to quantitatively describe the generation power in conventional Raman fibre lasers. To resolve this issue, different phenomenological approaches are used to take into account frequency dependence of boundary conditions, namely the effective transmission of laser mirrors is introduced [396,402,403]. In the random DFB fibre laser, boundary conditions are wavelength-independent (within the generation bandwidth), so the power balance model should provide good predictions for power performances of the random DFB fibre laser.

5.2. Generation threshold

Firstly, we use the Eq. (17) to calculate the generation threshold P_{th} in different configurations Fig. 14 of the random DFB fibre laser. The dependence of the generation threshold on the laser length for the forward-pumped random DFB fibre laser is shown by the red line in Fig. 25. The threshold is calculated for the 1550 nm generation in a SMF-28 fibre, see parameters in Section 4.2. As expected, when the cavity is short the Rayleigh backscattering is negligible, therefore the generation threshold is high. However, the longer the fibre the more pronounced the random distributed feedback is, thus the generation threshold rapidly decreases reaching the almost constant value of 0.8 W at the fibre length of ~40 km. Further increase of the fibre length over this value should have no impact on the generation performances of the laser, as the additional fibre length does not provide an amplification, but only attenuates the generated light. Indeed, the pump wave creates the Raman gain higher than optical losses for the generated wave only in a certain spatial region, namely, for distances $|z| < L_{RS}$, where L_{RS} is the amplification length defined by the gain/loss balance condition:

$$g_R P_p^+(L_{RS}) = \alpha_s. \tag{19}$$

At the generation threshold, there is no Stokes wave generation, so the pump wave distribution over the fibre is determined by the linear losses only, $P_+(z) = P_+(0)e^{-\alpha_p z}$, that means the following expression for the amplification length is valid at the threshold:

$$L_{RS} = \frac{1}{\alpha_p} \ln \frac{g_R P_{th}}{\alpha_s}. \tag{20}$$

For the $P_{th} = 0.8$ W, the calculated value of the amplification length is $L_{RS} \approx 40$ km. The threshold value of 0.8 W is in good agreement with experiments, see Section 4.2.

It is obvious that in the limit of very short fibre, the generation threshold of the backward-pumped DFB fibre laser should coincide with the forward-pumped scheme. This is due to the fact that in the short lasers the pump power is almost undepleted, therefore, both schemes are identical. Numerical calculations prove this observation, Fig. 25, blue and red curves. At the same time, when the backward-pumped laser is very long, the generation threshold should be higher than that in the forward-pumped laser, because the pump wave does not reach the other fibre end. The system acts as two independent single-arm lasers with two different pumps (in the case of the symmetric configuration, see Fig. 14b, left scheme). Indeed, for the backward-pumped laser, the generation threshold coincides with the value calculated for the single-arm laser based on a long fibre span, Fig. 25, green curve. The minimal generation threshold for a single-arm configuration, 1.6 W, is exactly two times higher than that for the forward-pumped configuration. Note that in the backward-pumped laser, there is an optimal laser length $L \approx 30$ km, at which the generation threshold takes its minimal value of 1.1 W, nevertheless being higher than 0.8 W achieved in the forward-pumped laser.
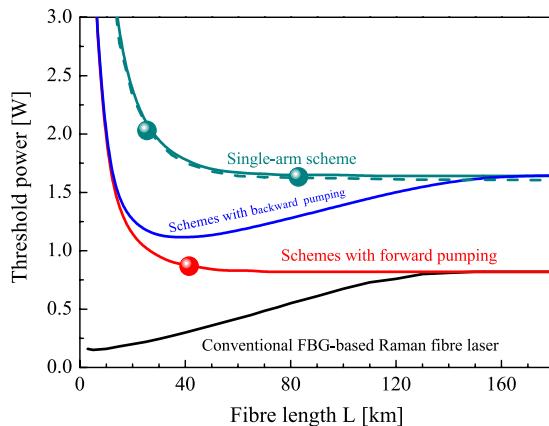
Fig. 25. Generation threshold for random DFB fibre lasers of different configurations in comparison with that of the conventional Raman fibre laser. The total laser length and pump power correspond to the schemes presented at right column in Fig. 14. Solid lines — numerical calculation of Eq. (17), dashed line — numerical calculation from equation set (23), dots — experimental data. All data is for the generation near 1550 nm in a SMF-28 fibre.

Finally, we calculate the threshold for the conventional Raman fibre laser with a cavity formed by two point-based highly-reflective mirrors. We consider a laser of the total length $2L$ pumped from both fibre ends. As expected, the generation threshold in the case of the conventional cavity grows linearly with the cavity length increasing, Fig. 25, black curve, as more pump is needed to overcome total losses in the longer cavity. Indeed, if one neglects the effect of the Rayleigh scattering, the generation threshold is defined by the condition of the total losses being equal to the total gain in the cavity:

$$\exp\left(-2\alpha_s L + g_R \int_0^{2L} P_p(z)dz\right) = 1.$$

Here P_p is the total pump power from both pump sources. The generation threshold can be found as $P_{th} = \alpha_s \alpha_p L / [g_R(1 - \exp[-2\alpha_p L])]$, that results in $P_{th} = \alpha_s \alpha_p L / g_R$ in the limit of the long fibre length. Note that P_{th} is defined as a power needed from the one pump source to achieve the generation, so the total pump power is twice higher. The generation threshold increases linearly with the increase of the system length L. In reality, this simple consideration fails at long lengths because of the Rayleigh backscattering. Indeed, one can numerically calculate the generation threshold from the full model, Eq. (17), with boundary conditions specific to the conventional point-based cavity design, and taking into account the Rayleigh backscattering. It is found that while increasing the cavity length over 100 km, the numerically calculated threshold value becomes lower than predicted by the simple analytical consideration without Rayleigh backscattering, see black curve in Fig. 25. This means that the feedback mechanism is gradually shifted from pure lumped reflector feedback to the random distributed feedback. Moreover, at $L_{max} > 150$ km meaning the total laser length is over 300 km, the generation threshold power becomes independent of the fibre length, thus the laser of such cavity length operates via random distributed feedback only. This means, in particular, that fibre lasers with conventional cavities made of highly reflecting mirrors/gratings have a principal limitation in length of $2L_{max} \approx 300$ km that is in the agreement to the experimentally demonstrated limit of 270 km [19]. For cavities longer than $2L_{max}$, there is no difference which cavity type to use to generate the light — with or without point-based mirrors as the light would be generation in all cavity designs via the random distributed feedback. Thus, none of them should have a longitudinal mode structure.

The influence of small point-based reflections (for example, of 4% Fresnel reflection from a flat-cleaved fibre end) on the generation threshold of ultra-long Raman fibre lasers operating via combined point-based and random DFB feedback is discussed in [312].

One can also calculate the threshold analytically from an equality condition for integral gain and losses [31,311]. Let us consider a fibre as a vast number of low-finesse cavities, each formed by Rayleigh backscattering on the fluctuations of the refractive index. The intensity of the light making round-trips in each of these cavities increases after each round-trip by a gain/loss factor

$$\varepsilon dz \cdot \exp\left(-2\alpha_s z + 2g_R \int_0^z P_p(x)dx\right).$$

Here εdz is the reflection coefficient of a virtual mirror placed at the point z. Another mirror with 100% reflectivity is placed at $z = 0$, i.e. forward- and backward-pumped configurations are considered. An integral condition of the equality of the gain and the losses means that the net amplification in the sum of all cavities should balance the total losses:

$$1 = \varepsilon \int_0^L \exp\left(-2\alpha_s z + 2g_R \int_0^z P_p(x)dx\right) dz. \tag{21}$$
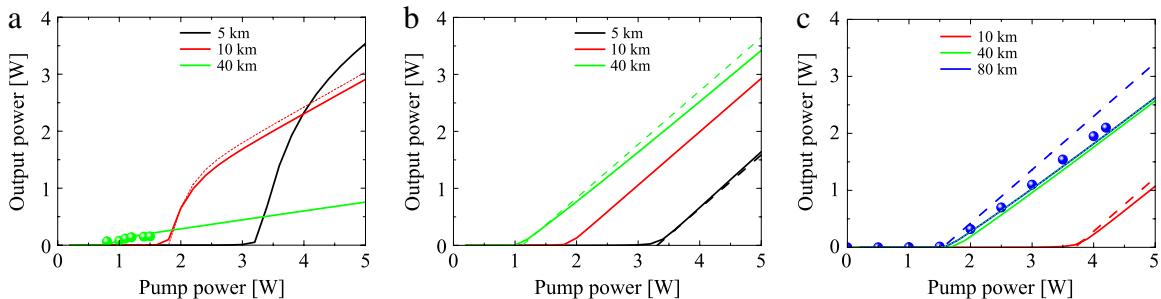
Fig. 26. Output powers in random DFB fibre lasers of different configurations: (a) forward-pumped laser, (b) backward-pumped laser, (c) single-arm laser (for backward waves). Solid lines — numerical calculation from the power balance model, Eq. (17). Dash lines — analytical predictions: (a) calculation from Eq. (30) using Eq. (35), (b) and (c) calculation from Eq. (25) with P_{th} taken from Eq. (21). Different colours correspond to different system lengths. Dots — experimental data.

In the long-length limit, $L \gg L_{RS}$, one can apply saddle-point approximation to (21). As a result, the threshold power P_{th} can be found from the following transcendental expression:

$$P_{th} = \frac{\alpha_s}{g_R}\left(1 + \ln\left(\frac{g_R P_{th}}{\alpha_s}\right)\right) + \frac{\alpha_p}{2g_R}\ln\left(\frac{1}{\varepsilon}\sqrt{\frac{\alpha_s\alpha_p}{\pi}}\right). \tag{22}$$

Expression (22) gives a threshold value $P_{th} \approx 0.8$ W for the experimental parameters of Section 4.2 being in excellent agreement both with experimental data and results of numerical calculations within power balance model (17). From Eq. (22) it follows that the threshold power can be reduced by increasing the strength of the backscattering factor $\varepsilon = Q \cdot \alpha_s$. This could be potentially achieved, for example, by using a fibre with a higher numerical aperture and factor Q, respectively.

In the single-arm scheme each virtual cavity having length l consist of two random mirrors: a left mirror of strength εdz placed at z and a right mirror of strength εdl placed at $z + l$, [319]. So the gain/losses factor per round-trip takes the form:

$$(\varepsilon dz \cdot \varepsilon dl)\exp\left(-2\alpha_s z + 2g_R\int_0^z P_p(x)dx\right).$$

Integrating over such "effective cavities" and setting the condition of total gain is equal to the total losses, one gets:

$$1 = \varepsilon^2 \int_0^L dz \int_0^{L-z} dl \cdot \exp\left(-2\alpha_s l + 2g_R\int_z^{z+l} P_p(x)dx\right). \tag{23}$$

Eq. (23) gives a value twice bigger than that in the forward-pumped configuration, Fig. 25, dots, in the agreement with numerical calculations and experimental data [312]. In general, Eq. (23) provides a good prediction of the generation power in all ranges of fibre length, compare dots and green line in Fig. 25.

5.3. Output power and generation efficiency

We can further use the power balance model, Eq. (17), to numerically calculate the output power of the random DFB fibre laser. In different laser configurations, the output power depends on the pump power differently, Fig. 26. Indeed, in the forward-pumped configuration, the highest output power and conversion efficiency are reached in a short fibre, despite the generation threshold in short lasers is relatively higher. In long fibres, the conversion efficiency and output power are very low, Fig. 26a. This can be understood from the simple consideration in terms of amplification length, L_{RS}. Indeed, if the fibre length $L \gg L_{RS}$, most of the fibre acts as a lossy media for the wave generated at $|z| < L_{RS}$, so the output power is exponentially attenuated, see more details in Section 5.4. Note that the slope (differential) efficiency in the short fibre could be higher than the formal quantum efficiency $\eta = \lambda_p/\lambda_s$. As an example, for a laser based on the 5-km long fibre, almost 3 W of output power is generated at 1 W power above the generation threshold (i.e. the total pump power is 4 W, while the generation threshold is 3 W), see black curve in Fig. 26a. The output power curve is sufficiently nonlinear consisting of two different regimes: a high slope efficiency generation just above the generation threshold and the generation at a lower slope efficiency and higher absolute efficiency at higher pump power.

In the case of a backward-pumped configuration, a simple analytical consideration can be made. We assume that the power of a forward-propagating generation wave is much higher than the power of the backward-propagating wave, $P_s^- \ll P_s^+$. Note that this assumption is further validated in numerical simulations of longitudinal power distribution, see
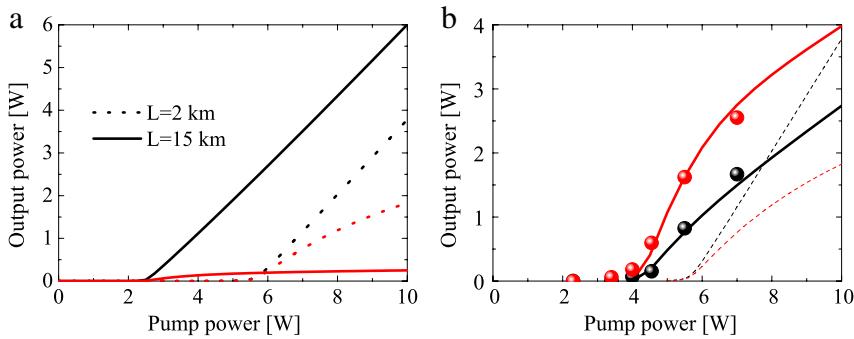
Fig. 27. (a) Numerically calculated output power for backward- (black) and forward- (red) propagating generation waves in the single-arm random DFB fibre laser based on 1060-XP fibre and operating at 1.2 μm for different cavity lengths. The solid and dotted lines are calculations for different fibre lengths. (b) Influence of parasitic reflections on the power balance between forward- (black) and backward- (red) propagating generation waves in 2 km-long laser. Numerical data is shown by lines: solid lines correspond to the case where parasitic reflections of ~10^{-4} are used, dotted lines — calculations without parasitic reflections. Experimental data is shown by dots. After Ref. [404].

Section 5.4 for details. In this case Eq. (17) is reduced to the following equation set:

$$
\begin{cases}
\dfrac{dP_p^-}{dz} = +\alpha_p P_p^- + g_p P_p^- P_s^+, \\[2mm]
\dfrac{dP_s^+}{dz} = (g_R P_p^- - \alpha_s) P_s^+, \\[2mm]
\dfrac{dP_s^-}{dz} = -(g_R P_p^- - \alpha_s) P_s^- - \varepsilon P_s^+.
\end{cases}
\tag{24}
$$

If the fibre is short, one can neglect linear losses, $\alpha_s \approx \alpha_p \approx 0$, and find an analytical solution for the output power $P_s^+(L)$ versus pump power $P_p^-(L) = P_0$:

$$
P_s^+(L) = \frac{\lambda_p}{\lambda_s}(P_0 - P_{\text{th}}).
\tag{25}
$$

Here we used the condition, that the generation power $P_s^+(L)$ is zero at the generation threshold P_{th}.

Eq. (25) gives a remarkable result that the Stokes wave in the short backward-pumped random DFB fibre laser is generated with the maximal absolute efficiency, $\eta = \lambda_p/\lambda_s$, i.e. every pump photon above the generation threshold is converted to the Stokes photon. Note that 100% quantum conversion efficiency of the short backward-pumped random DFB fibre laser is a consequence of the stimulated Raman scattering process rather than of the specific nature of the feedback exploited in the laser. Results of numerical simulations using the full model, Eq. (17), i.e. taking into account optical losses, are close to a simple analytical expression, Eq. (25), not only for short lasers, but for any fibre length, Fig. 26b. Note that the output power dependence is linear in all ranges of pump power, this could be attractive in real applications.

Eq. (25) predicts rather well the output power, but not the generation threshold P_{th}. To find P_{th}, numerical simulation of the reduced equation set (24) with boundary conditions or numeric integration of gain/loss balance condition (21) is required.

In the case of a single-arm configuration, the output power can be calculated numerically from the full model, Eq. (17), that was investigated in details in [404]. Though slope efficiency in this case reaches almost ultimate quantum conversion value, the generation threshold is higher, and the overall conversion efficiency is lower than in the case of forward- and backward-pumped configuration, so long fibres are needed to achieve a generation at moderate pump power levels.

Note that in the single-arm configuration there are two non-equal laser outputs at the left and right fibre ends while in the forward- and backward-pumped schemes there is only one laser output, see Fig. 14. Here we stress one more time that we consider equivalent schemes of the laser shown in the right column of Fig. 14a, b; in a symmetrical configuration there are obviously two laser outputs which are identical because of the symmetry in the system, left column on Fig. 14a, b. We found from numerical simulations of Eq. (17) that in the single-arm scheme the output power of the forward propagating wave (i.e. propagating from $z = 0$ to $z = L$ and co-propagating with the pump wave) is always lower than the output power of the backward-propagating wave (i.e. propagating from $z = L$ to $z = 0$ and counter-propagating with the pump wave), Fig. 27a. The exact balance between forward- and backward-propagating waves powers depends on the fibre length with a larger difference in powers for longer systems. However well above the generation threshold, one can claim that the single-arm random DFB fibre laser always generates in the backward direction. The reason for that is connected with a specific power distribution along the fibre (see Section 5.4 for details): in brief, the backward-propagating generation wave arises in a small region close to the pump injection point, $z = 0$, so it is not attenuated by linear losses and is not affected by the gain depletion. As a result, the generation efficiency of the backward-propagating wave is close to the ultimate value determined
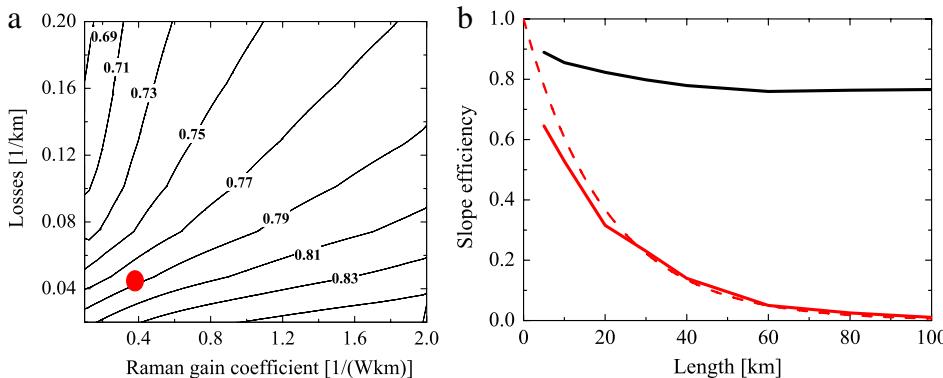
Fig. 28. (a) Generation efficiency dependence on fibre parameters for a single-arm random DFB fibre laser based on 40 km of fibre. The red dot corresponds to the SMF-28 fibre parameters. (b) Generation efficiency for backward (black) and forward (red) propagating generation waves at different fibre lengths. The dashed line is an exponential approximation, $\exp(-\alpha_s L)$.

by the energy of the pump and the laser quanta, Fig. 26c, similar to the case of the backward-pumped scheme. However, despite the same ultimate quantum efficiency, the single-arm configuration could be less attractive for applications, as the generation threshold in the single-arm configuration is two times higher than that in the backward-pumped laser.

It is important to point out that in real experiments additional parasitic reflections could easily be introduced into the system because of dirt/dust on fibre ends, fibre connectors etc. It was found that even tiny parasitic point-based reflections on fibre ends could change the power balance in random DFB fibre laser in a dramatic way, [404]. Namely, even additional parasitic reflection as small as 10^{-4} at the fibre ends leads to a sufficient decrease of the generation threshold and, what is more important, to different balance between backward- and forward-propagating generation waves, Fig. 27b. Note that the data presented on Fig. 27 corresponds to the laser generating at 1.2 μm spectral band. In a particular case, the power of forward-propagating wave becomes higher than the power of the backward-propagating wave despite the fact that the reverse balance should be observed in the ideal single-arm random DFB fibre laser, Fig. 27a. Note that the level of Fresnel reflection from the cleaved fibre end is 4%, so the values on the level of 10^{-4} can be achieved by just a small dust particle on the angled cleaved fibre end. Other consequence of the parasitic reflection is the reduced generation threshold of the second Stokes wave that limits the maximal achieved power of the first Stokes wave [321].

Finally, the power balance equation set Eq. (17) allows us to perform an optimization of the laser over the range of system parameters such as fibre length, Raman gain coefficient, linear losses etc. [404]. As an example, we performed the efficiency optimization for the single-arm configuration over the Raman gain and the linear loss values. Note that a variation of the Raman gain coefficient can be achieved by using different types of fibres as gain media, while a variation in linear losses corresponds to the change of the pump and generation wavelengths due to the strong dependence of the losses on the wavelength. We found that the slope efficiency for the backward-propagating wave is almost insensitive to the alteration of the system parameters, Fig. 28a. In addition, the generation efficiency is almost constant over the fibre length of the backward-propagating wave and reaches ∼90% in a short laser that is close to the quantum limit of 94%, Fig. 28b. For the forward-propagating generation wave, the efficiency decreases with the exponential law, $\eta \sim \exp(-\alpha_s L)$, similarly to the case of the output efficiency in the forward-pumped configuration.

Summarizing, the best power performance in terms of output power can be achieved for forward-pumped lasers based on short (less than 5 km) fibres. Moreover, despite the relatively high generation threshold in this case (more than 3 W), the output power is maximal among all the configurations, reaching almost 4 W of output power from 5 W of pump power. However, in terms of slope efficiency at high pump power, the best configuration is the backward-pumped or single-arm configuration.

5.4. Longitudinal power distribution in random DFB fibre lasers

5.4.1. Longitudinal distributions in forward- and backward-pumped lasers

The output power of the random DFB fibre laser is defined by the specific longitudinal distribution of the generated power along the fibre. The longitudinal distribution of the generated power could be calculated within the balance equation set (17) with high accuracy [31,404–406]. The numerically calculated profiles for the power distribution of the generation waves in the forward-pumped laser are shown on Fig. 29. The calculated profiles are in quantitative agreement with the experimental data, Fig. 29a. The longitudinal distribution of the generated wave is highly non-uniform having a maximum at the point $z = L_{RS}$ at which the optical gain is equal to the optical losses. The forward-propagating wave P_s^+ arises from the backscattered backward-propagating wave P_s^- and is gradually amplified while propagating from the left to the right within the amplification region $z < L_{RS}$. For $z > L_{RS}$, the forward-propagating wave P_s^+ is exponentially attenuated as the Raman gain is lower than optical losses in this region. It also produces weak seed signal at $z > L_{RS}$ for the backward wave
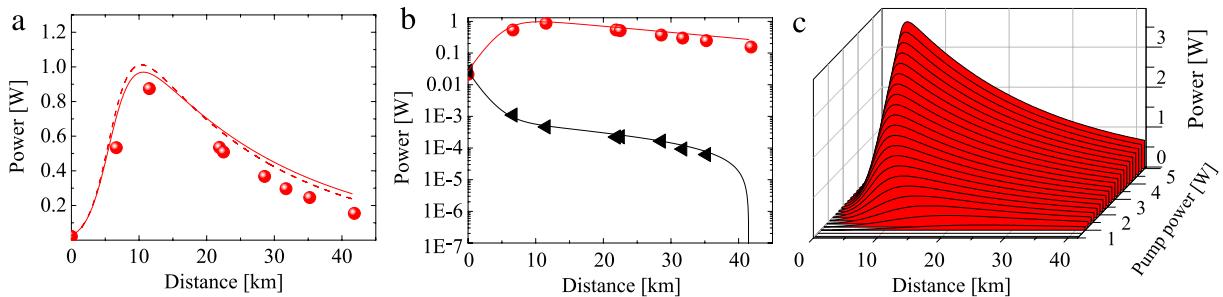
Fig. 29. Longitudinal distributions of the generated power in the forward-pumped random DFB fibre laser: (a) linear and (b) logarithmic scales. (c) Dependence on the pump power. Solid lines — numerical calculations within the power balance model (17), dashed line — analytical solution (30), circles and triangles — experimental data. Black colour corresponds to the backward-propagating generation wave, red colour is used for the forward-propagating generation wave. After Ref. [405].
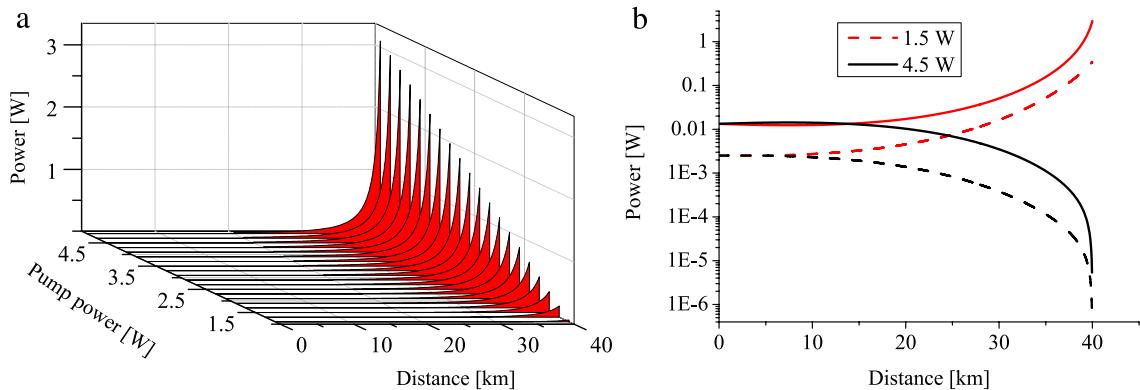

Fig. 30. Longitudinal distributions of the generated power in the backward-pumped random DFB fibre laser. (a) Dependence on the pump power. (b) Distribution of forward- and backward-propagating waves in a logarithmic scale. Data is numerically calculated from the power balance model (17). The black colour corresponds to the backward-propagating generation wave, the red colour — forward-propagating generation wave. Solid and dashed lines at (b) are data for 1.5 W and 4.5 W of pump power, respectively.

P_s^- due to the Rayleigh backscattering. Note that the power of the forward-propagating generation wave is higher than the power of the backward propagating generation wave, $P_s^+(z) \gg P_s^-(z)$, at every point along the fibre except for the small region $z \sim 0$ where $P_s^+(z) \sim P_s^-(z)$.

For real applications it is important that the generation power at point $z = 0$, $P_s^+(0)$, is much less than the maximal generation power at $z = L_{RS}$ or the output power $P_s^+(L)$. Indeed, at typical output power level of 1 W, $P_s^+(0)$ is 20–30 mW only, Fig. 29b. This allows one to manage the properties of the high-power generation in the random DFB fibre laser by using various low-power handling components placed at $z = 0$. In this way a tunable, multiwavelength and narrow-band generation is demonstrated, see Sections 4.6–4.8.

The higher the pump power, the narrower the longitudinal distribution of the generated wave intensity, Fig. 29c. At the same time, due to the pump power depletion via Stokes wave generation, the amplification length decreases, so the point L_{RS} moves towards $z = 0$.

In the backward-pumped scheme of the random DFB fibre laser, longitudinal distributions of the generated power are different from those in the forward-pumped configuration. The forward-propagating generation wave, $P_s^+(z)$, increases sufficiently in the region of the maximal gain which is located near the fibre end, Fig. 30a. The distribution has its maximum at the laser output, $z = L$, and becomes narrower while the pump power increases. The linear grows of the output power with increase of pump power is clearly seen. At the same time, the power of the backward-propagating wave, $P_s^-(z)$, is small in all points over the fibre, Fig. 30b, black curves. In the backward-pumped configuration, the generation power at the central point of the laser, $z = 0$, is low being less than 20 mW similar to the forward-pumped laser. Despite the small power at $z = 0$, the laser delivers up to 1.5 W of the output power, Fig. 30b, solid curves.

5.4.2. Longitudinal distributions of higher-order Stokes waves

It is known that at a higher pump power, the generation of the second Stokes wave could be achieved in the random DFB fibre laser, see Section 4.5. To model the cascaded generation, we modify the initial model by including the terms
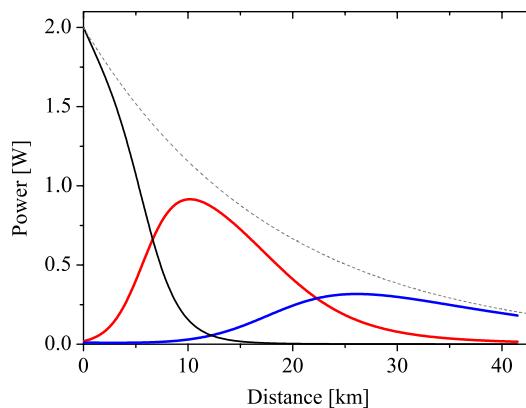
Fig. 31. Longitudinal distributions in the higher-order forward-pumped random DFB fibre laser: black curve — pump wave, red curve — first Stokes wave, blue curve — second Stokes wave. Pump power is 2 W. Grey dotted line — pump power distribution in the absence of the generation. Data is calculated from Eq. (26). After Ref. [405].

corresponding to the second Stokes wave:

$$\begin{cases} (\alpha_p \pm d/dz)P_p^\pm = -g_R P_p^\pm (P_s^+ + P_s^- + 4h\nu_s\Delta\nu)\dfrac{\nu_p}{\nu_s} \\ (\alpha_s \pm d/dz)P_s^\pm = g_R(P_p^+ + P_p^-)(P_s^\pm + 2h\nu_s\Delta\nu) + \varepsilon P_s^\mp - g_{2s}P_s^\pm(P_{2s}^+ + P_{2s}^- + 4h\nu_s\Delta\nu)\dfrac{\nu_s}{\nu_{2s}} \\ (\alpha_{2s} \pm d/dz)P_{2s}^\pm = g_{2s}(P_s^+ + P_s^-)(P_{2s}^\pm + 2h\nu_s\Delta\nu) + \varepsilon_{2s}P_{2s}^\mp. \end{cases} \qquad (26)$$

Here α_{2s}, g_{2s} and ε_{2s} are linear losses, Raman gain coefficient and backscattering strength, respectively, at the wavelength of the second Stokes. The equation set (26) must be accompanied with boundary conditions which are the same conditions as for the first Stokes wave, Eq. (18).

Using the model (26), generation thresholds, output powers and longitudinal distributions could be calculated in the cascaded random DFB fibre laser. As an example, we calculate the longitudinal distribution of the second Stokes wave in the forward-pumped laser. It is found that the second Stokes wave has a quite different longitudinal distribution. The position of the power maximum is shifted to longer distances, $z > L_{RS}$, compared to that for the first Stokes wave, Fig. 31. The second Stokes wave distribution is also more uniform compared to the first Stokes wave distribution at the same average generated power. Note that the distribution of the first Stokes wave, in turn, could be considered flatter than that of the pump wave, Fig. 31. So it is likely that the cascaded random DFB fibre laser could provide even flatter distribution that could be important for possible telecom applications such as quasi-lossless transmission, see Section 4.10. As the maximum of the second Stokes wave power distribution is shifted to longer lengths, the optimal fibre length needed for the efficient generation of the second Stokes wave is longer than the optimal length for the first Stokes wave.

5.4.3. Longitudinal distributions in the single-arm laser

Finally, we investigate longitudinal distributions of the generated waves in the single-arm configuration of the random DFB fibre laser. The longitudinal distribution of the forward-propagating (relative to the pump wave) wave is similar to the longitudinal distribution in the forward-pumped laser featuring by a power maximum at the point L_{RS}, Fig. 32, red. The effective amplification length becomes shorter with the pump power increase because the pump wave is depleted due to the power conversion into the Stokes waves. The distribution is flatter as compared to those in the forward-pumped configuration, however the generation power of the forward-propagating wave is low. At the same time, the distribution of the backward-propagating wave is similar to those observed for the forward-propagating wave in the backward-pumped laser, Fig. 32, grey. Indeed, the conditions for the backward-propagating wave are very similar in both configurations: The backward-propagating wave is sufficiently amplified in the small region only near $z \sim 0$, where the Raman gain is highest as the pump wave is almost undepleted. With the pump power increase, the longitudinal distribution of the backward-propagating wave becomes narrower because of the pump power depletion, while the distribution of the forward-propagating wave, vice versa, becomes flatter and wider. The linear increase of the output power of the backward-propagating wave with the pump power increase is clearly seen in Fig. 32.

An information about longitudinal distribution profiles can be used to derive fibre parameters. As an example, the Q-factor can be experimentally measured [406]. To do this, the single-arm laser based on 84 km long fibre was pumped at point $z = L/2$ instead of point $z = 0$. In this scheme, the part of the fibre at $z < L/2$ is completely unpumped thus acting only as a distributed mirror because of the Rayleigh backscattering. In this case, one can directly derive from the balance model (17) that

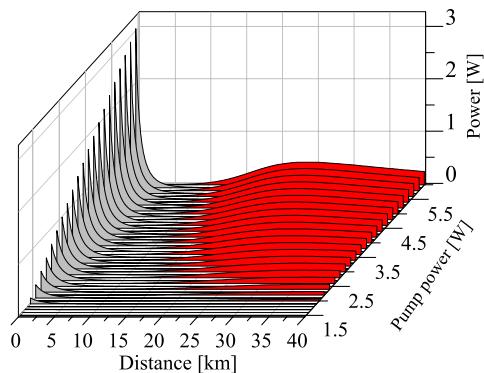$$P_s^+(z) = 0.5QP_s^-(z)\left[1 - e^{-2\alpha_s z}\right] \qquad (27)$$

Fig. 32. Longitudinal distributions in the single-arm configuration of the random DFB fibre laser: grey — backward-propagating wave, red — forward-propagating wave.
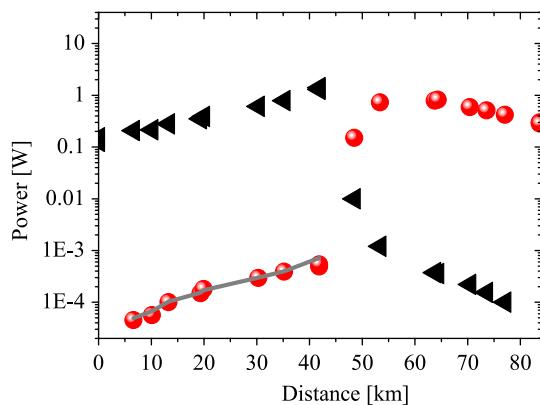

Fig. 33. Measurements of Q-factor value in the single-arm laser with the pump wave coupled at $z = L/2$: Experimentally measured (circles and triangles) and analytically calculated under Eq. (27) (grey curve) longitudinal distributions for the forward- (red circles) and backward- (black triangles) propagating Stokes waves. After Ref. [406].

for $0 < z < L/2$. Using this expression together with the experimentally measured longitudinal distributions $P_s^-(z)$ and $P_s^+(z)$, one can derive the Q-factor by fitting the experimental data with the Q-factor value as a fitting parameter, Fig. 33. The measured value of 10^{-3} is in good agreement with the specified data for the fibre under study [406].

5.4.4. Amplification length

Another important feature of the power distribution in the random DFB fibre laser is the position of the point at which the Raman gain is equal to the optical losses, L_{RS}, see Eq. (19). Amplification length value, L_{RS}, affects the output power in the system as the generation wave is exponentially attenuated at $z > L_{RS}$, see Section 5.4.1. Therefore, it is of practical interest to reveal the dependence of L_{RS} on the pump power.

Amplification length dependence can be obtained from experimentally measured longitudinal distributions of the generation power. We found that in the forward-pumped configuration of the random DFB fibre laser operating well above the threshold, L_{RS} decreases inversely proportional to the pump power [405], that is in a good agreement with numerical calculations within the power balance model, Fig. 34a. Note that L_{RS} value can be approximated by the analytic expression (38), see Section 5.4.5 for details.

In the single-arm configuration, L_{RS} shifts to the to $z = 0$ with increasing power similar to the behaviour in the forward-pumped laser. However, because of the different shape of the longitudinal distribution in single-arm laser, L_{RS} decreases more slowly compared to the forward-pumped scheme, obeying the law $1/\sqrt{P_p}$, Fig. 34b.

5.4.5. Analytical consideration of the longitudinal distributions in the forward-pumped laser

After an analysis of the main features of the longitudinal power distributions using the numerical simulations of the average power balance equations, we develop an analytical approximation in the case of the forward-pumped laser. In the forward-pumped scheme, the power of the forward-propagating Stokes wave, $P_s^+(z)$, is much higher than the power of the backward propagating wave, $P_s^-(z)$, almost for all points along the fibre, $P_s^+(z) \gg P_s^-(z)$, Fig. 29a. Therefore, one can neglect contribution of the backward-propagating wave, P_s^-, to the depletion of the pump power, P_p^+, as well as neglect its
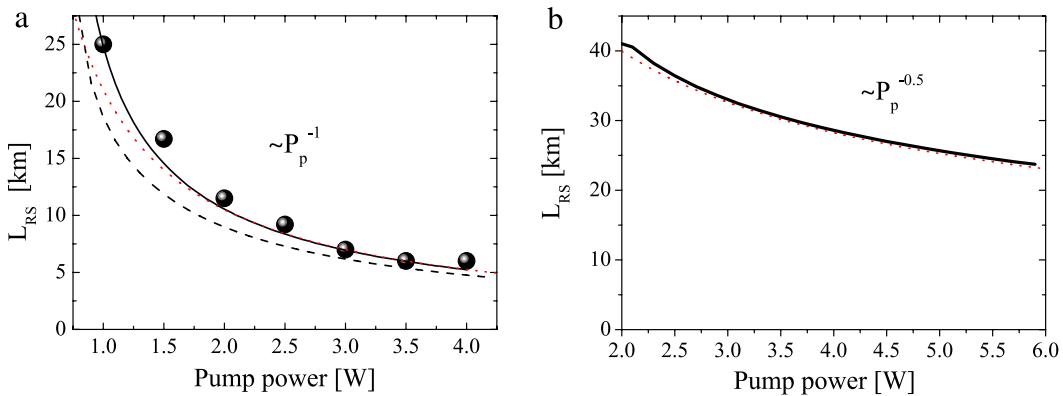
a

b

Fig. 34. Power scaling of the amplification lengths, L_{RS}, in (a) forward-pumped and (b) single-arm configurations of the random DFB fibre laser. Experimental values are shown by dots. Black solid and dashed curves are numerical simulations within Eq. (17) and analytical solution (38), respectively, red dotted curves − power law approximations. After Ref. [405].

contribution into the forward-propagating wave, P_s^+, via the Rayleigh backscattering. In 1.5 μm spectral domain, one can assume that $\alpha_s \approx \alpha_p \approx \alpha$. Under these assumptions, the equation set (17) can be simplified to the following form:

$$
\begin{cases}
\dfrac{dP_p^+}{dz} = -\alpha P_p^+ - g_P P_p^+ P_s^+, \\[2mm]
\dfrac{dP_s^+}{dz} = (g_R P_p^+ - \alpha)P_s^+, \\[2mm]
\dfrac{dP_s^-}{dz} = -(g_R P_p^+ - \alpha)P_s^- - \varepsilon P_s^+,
\end{cases}
\tag{28}
$$

here $g_p = g_R \lambda_s / \lambda_p$. The first and second equations in (28) are now independent of P_s^- and can be integrated. As a result, the longitudinal distribution of the pump wave, $P_p^+(z)$, can be found:

$$
P_p^+(z) = P_p^+(0)e^{-\alpha z} \frac{g_R P_p^+(0) + g_P P_s^+(0)}{g_P P_s^+(0) \exp\left[(g_R P_p^+(0) + g_P P_s^+(0))\frac{1-e^{-\alpha z}}{\alpha}\right] + g_R P_p^+(0)}.
\tag{29}
$$

The longitudinal distribution of the generated wave, $P_s^+(z)$, can be calculated as well:

$$
P_s^+(z) = P_s^+(0)e^{-\alpha z} \frac{g_R P_p^+(0) + g_P P_s^+(0)}{g_R P_p^+(0) \exp\left[-(g_R P_p^+(0) + g_P P_s^+(0))\frac{1-e^{-\alpha z}}{\alpha}\right] + g_P P_s^+(0)}.
\tag{30}
$$

Note that $P_s^+(L)$ is the output power of the random laser.

To plot the longitudinal distribution of the generated wave, $P_s^+(z)$, one needs to find the value of the generated power at $z = 0$, $P_s^+(0)$. This can be done analytically. Let us consider the second and third equations of set (28). After multiplying them on $P_s^-(z)$ and $P_s^+(z)$, respectively, summing up and using boundary conditions, one gets

$$
\frac{dP_s^+ P_s^-}{dz} = -\varepsilon P_s^{+2}
\tag{31}
$$

together with a relation

$$
P_s^{+2}(0) = P_s^+(0)P_s^-(0) = \varepsilon \int_0^L P_s^{+2}(z)dz.
\tag{32}
$$

After substitution of Eq. (32) to Eq. (30), one can find the following relation:

$$
1 = \varepsilon \int_0^L dz\, e^{-2\alpha z} \left(\frac{1 + g_P P_s^+(0)/g_R P_p^+(0)}{\exp\left[-g_R P_p^+(0)\frac{1-e^{-\alpha z}}{\alpha}(1 + g_P P_s^+(0)/g_R P_p^+(0))\right] + g_P P_s^+(0)/g_R P_p^+(0)} \right)^2.
\tag{33}
$$

We assume that the generation power at $z = 0$ is much lower than the pump power, $g_P P_s^+(0)/g_R P_p^+(0) \ll 1$, that is confirmed by the numerical simulations, Fig. 29a, that makes possible the following simplification:

$$
\frac{1}{\varepsilon} = \int_0^{L_{\text{eff}}} d\xi \frac{1 - \alpha\xi}{e^{-g_R P_p^+(0)\xi} + g_P P_s^+(0)/g_R P_p^+(0)},
\tag{34}
$$

where substitution $\xi = (1 - e^{-\alpha z})/\alpha$ is used. Note that the expression Eq. (34) is valid in the long length limit, $\alpha L \gg 1$; the effective length is defined by $L_{\text{eff}} = [1 - \exp(-\alpha L)]/\alpha \approx 1/\alpha$.

Well above the threshold, the Eq. (34) could be integrated (see details in [312]), that results in the following expression on the generation power at $z = 0$:

$$P_s^+(0) = \sqrt{\frac{\varepsilon}{2\alpha}} \frac{g_R}{g_P} \left(1 - \frac{P_{\text{th}}}{P_p^+(0)}\right) P_p^+(0). \tag{35}$$

The model is fully self-consistent, as the generation threshold P_{th} can be found from Eq. (34) by integrating it in the limit of zero generation power, $P_s^+(0) = 0$:

$$g_R P_{\text{th}} e^{-g_R P_{\text{th}}/\alpha} = \sqrt{\varepsilon \alpha/4}. \tag{36}$$

This analytical expression gives the generation threshold value of 0.76 W being remarkably close to the experimentally observed value of 0.8 W [31,405].

As a result, the longitudinal distribution of the generated power in the forward-pumped laser can be analytically calculated using Eq. (30) and Eq. (35). Analytical predictions coincides remarkably with the numerical calculations and the experimental data, Fig. 29.

There is a one more output of the developed analytical model: The analytical expression for the generation efficiency. Indeed, the efficiency $\eta_{total} = P_s^{out}/P_p^+(0)$ could be derived from the analytical solution of the generated power distribution, Eq. (30) and Eq. (35). In the case $g_P P_s(0) \ll g_R P_p^+(0)$ and well above the generation threshold, $P_p(0) \gg P_{\text{th}}$, the following expression for the generation efficiency η is valid:

$$\eta_{total} = \lambda_s/\lambda_p e^{-\alpha L} \left(1 - \exp\left[g_R(P_{\text{th}} - P_p^+(0))\frac{1 - \exp(-\alpha L)}{\alpha}\right]\right) \approx e^{-\alpha L}. \tag{37}$$

The calculated value of the generation efficiency is $\eta \approx 0.15$ being close to the experimental one in the 41 km-long laser, [405]. An important conclusion from the Eq. (37) is the generation efficiency in the forward-pumped laser decreases exponentially with the system length L high above the generation threshold. That means that the forward-pumped laser is more efficient if based on a shorter fibre in agreement with the numerical calculations, see Fig. 26a.

Finally, the analytical expression of the pump power longitudinal distribution, Eq. (29), makes possible to calculate analytically the dependence of the amplification length L_{RS} on the pump power:

$$L_{\text{RS}} = \frac{1}{g_R P_p^+(0)} \ln \left(g_R P_p^+(0)\sqrt{\frac{2}{\alpha \varepsilon}} \Big/ \left(1 - \frac{P_{\text{th}}}{P_p^+(0)}\right)\right). \tag{38}$$

The amplification lengths L_{RS} depends inversely proportional on the pump power being in a good agreement with the experimental data and the numerical calculations, Fig. 34a. Note that this result is valid for the forward-pumped laser under a number of assumptions, so the scaling law may be different in other configurations. As an example, in the single-arm configuration $L_{\text{RS}} \sim P_p^+(0)^{-0.5}$, Fig. 34b. It is a challenge to theory to derive an analytical expression for L_{RS} in this case.

5.5. RIN transfer

As Raman scattering is a fast process with typical time of less than a picosecond, any fluctuations of the pump wave power could be transferred into variations of the Raman gain and finally in fluctuations of the Stokes wave power. This effect, called the relative intensity noise (RIN) transfer is known to be a drawback in telecommunication distributed Raman amplifiers, as it results in additional noise arising at signal wavelength. For possible telecom applications of the random DFB fibre lasers, RIN transfer is an important question. In the paper [407], a numerical investigation of the RIN transfer function in a forward-pumped random DFB fibre laser configuration, Fig. 14a, was performed. To do this, the power balance model, Eq. (17), is expanded with equations for the spectral density of the noise intensity for the pump and the Stokes waves. The RIN transfer function was calculated for different pump powers and fibre lengths. It was shown that the noise transfer decreases while the random laser cavity length increases or the pump power increases. The authors compared RIN transfer properties of a 100 km random DFB fibre laser with those for the 100 km long Raman fibre laser with the conventional FBG-based cavity. The averaged level of the RIN transfer function was found to be similar in both lasers. However, in the case of the modeless random DFB fibre laser, there are no oscillations in the noise transfer function, see [407] for details. The dumping of the oscillations could play a positive role in applications of the random DFB fibre laser for distributed amplification schemes.

5.6. NLSE-based modelling of random fibre lasers

The average power balance model was applied in a number of very different fibre laser systems and has successfully proven its ability to depict the most important laser characteristics. However, despite the efficiency of the relatively simple average power balance equations (17), there is an important fibre laser feature that power average model fails to describe

— spectral properties and, in particular, a spectral broadening of the generated radiation. The spectral broadening is caused by the interplay of the nonlinear fibre Kerr effect and the group velocity dispersion. In other terms, one must take into account the optical phase of the radiation. A consideration of the optical phase is also important for an accurate description of temporal and statistical properties of the fibre laser generation. The generalized nonlinear Schrödinger equations (NLSEs) can be used to describe the evolution of both intensities and phases of the generated radiation in the fibre laser. This model requires more computational time and a nontrivial solution of the evolution and boundary problems, but it provides information about the phases evolution lacking in the average power model. The NLSE-based modelling adequately describes power, spectral, temporal and statistical properties of quasi-CW fibre lasers with conventional cavities made of point-based mirrors including Brillouin lasers [408], Ytterbium-doped fibre lasers [409,410] and Raman fibre lasers [411–414]. In the paper [415], an average Rayleigh scattering based feedback was taken into account in the context of the modelling of temporal, spectral and statistical properties of random DFB fibre lasers. We would like to stress that this model is still intermediate and phenomenological as it does not account for statistical variations of the Rayleigh scattering along the fibre span. However, it gives an important approximate (averaged over the spatial distribution of the scattering) information about the impact of the Rayleigh scattering on the temporal behaviour of the generated radiation. The following simplified amplitude equation model can be used for this purpose:

$$
\frac{\partial A_p}{\partial z} - \frac{1}{v_{gs}} \frac{\partial A_p}{\partial t} + \frac{i}{2} \beta_{2p} \frac{\partial^2 A_p}{\partial t^2} + \frac{\alpha_p}{2} A_p = i\gamma_p |A_p|^2 A_p - \frac{g_p(\omega)}{2} \left(\langle |A_s^{\pm}|^2 \rangle + \langle |A_s^{\mp}|^2 \rangle \right) A_p,
$$

$$
\frac{\partial A_s^{\pm}}{\partial z_{\pm}} + \frac{i}{2} \beta_{2s} \frac{\partial^2 A_s^{\pm}}{\partial t^2} + \frac{\alpha_s}{2} A_s^{\pm} = i\gamma_s |A_s^{\pm}|^2 A_s^{\pm} + \frac{g_s(\omega)}{2} \langle |A_p|^2 \rangle A_s^{\pm} + \frac{\Delta A_{Rayleigh}^{\pm}(\omega)}{\Delta z}. \tag{39}
$$

Here A is a complex field envelope, t is a time in a frame of references moving with the pump wave, v_{gs} is a difference between pump and generated Stokes waves inverse group velocities, ω is the frequency detuning from the centre of the gain profile, L is the laser total length. Indexes "+" and "-" denote generation waves co- and counter-propagating with the pump wave. Here we define the longitudinal coordinate for the generation wave $z_{\pm}$ as $z = 0$ at a starting point of the generation wave propagation (either A_s^+ or A_s^-) and $z = L$ at the final point of the propagation, i.e. "+" wave has a coordinate z_+ while propagating, and "-" wave has a coordinate z_-, and both waves propagates in the positive direction of z-axis. At the same time, the longitudinal coordinate value z_+ for the co-propagating Stokes wave A_s^+ corresponds to the value of the longitudinal coordinate $z_- = L - z_+$ for the counter-propagating Stokes wave A_s^- and vice versa. Eq. (39) are z-averaged over the dispersion walk-off length of the generation and pump waves, thus the phase in cross-modulation term is zero [414]. White noise as an initial condition is used to take into account the spontaneous Raman scattering [416]. Raman gain is approximated by the parabola, $g_i(\omega) = g_i - k\omega^2$, where $k = 0.0062$ ps^2 (W km)$^{-1}$, $i = s, p$. Eqs. (39) are integrated along z using an iterative approach with an integration step Δz, i.e. when integrating equations for A_s^+, values A_s obtained on previous iteration are used, and vice versa.

The Rayleigh backscattering feedback is taken into account via term $\Delta A_{Rayleigh}^{\pm}(\omega)$ defined as:

$$
\Delta A_{Rayleigh}^{\pm}(\omega) = \left(\varepsilon \Delta z \cdot \frac{\int_{-\infty}^{+\infty} d\omega |A_s^{\mp}(L - z, \omega)|^2}{\int_{-\infty}^{+\infty} d\omega |A_s^{\mp}(L - z_{prox}, \omega)|^2} \right)^{1/2} \cdot A_s^{\mp}(L - z_{prox}, \omega) \cdot e^{i\phi_0 + i\omega\tau_0}. \tag{40}
$$

Here only the energy income from the Rayleigh backscattering is taken into account in Eq. (39) via term $\Delta A_s^{\pm Rayleigh}$ similarly to the balance equation set, Eq. (17). At the same time, the generation wave depletion due to the Rayleigh backscattering is considered through the linear losses α_s. Rayleigh scattering induced energy income to the pump wave is neglected as it is not amplified. A random phase factor $\exp(i\phi_0 + i\omega\tau_0)$ with a random phase ϕ_0 and time τ_0 shifts is used. As the Rayleigh term includes the optical spectrum of the counter-propagating wave, $A_s^{\mp}(\omega)$, one needs to save optical spectra at each integration step, which is technically impossible. To deal with that, the optical spectra of the generation waves are saved only at very limited number of points along z coordinate at each iteration (at $N = 50$ z-points in the present case). That means $z_{prox}(z)$ is a staircase function which approximates z with a set of $N = 50$ steps along z, each of them is a z-coordinate of the closest point where the spectra of counter-propagating wave is saved at the previous iteration.

We use following values of fibre dispersion, nonlinearity and group velocity, namely: $\beta_{2s} = 20$ ps^2/km, $\beta_{2p} = 35$ ps^2/km, $\gamma_s = 1.09$ (km W)$^{-1}$, $\gamma_p = 1.31$ (km W)$^{-1}$, $1/v_{gs} = -2.3$ ns/km. A good agreement for the power characteristics of the random laser (i.e. for the generation threshold, the output power dependence on the pump power and the longitudinal distributions of the generated waves) is achieved between the NLSE-based numerical simulations, Eq. (39), and the power balance equations, Eq. (17). Even more important both models give results that agree well with the experimental data.

What is more interesting, the generation spectra of the random DFB fibre laser could be calculated, Fig. 35a. As in experiments, the calculated generation spectrum becomes narrower than the amplified spontaneous emission profile while the pump power increases over the generation threshold indicating that the real lasing is achieved. Note that at later stages of evolution, the spectrum becomes broader with the power, Fig. 35b. Similar nonlinear spectral broadening is observed in experiments too. In conventional fibre lasers, the spectral broadening is an interplay of Kerr nonlinearity and dispersion [377,410,411,417], similar processes could be important in random DFB fibre lasers.
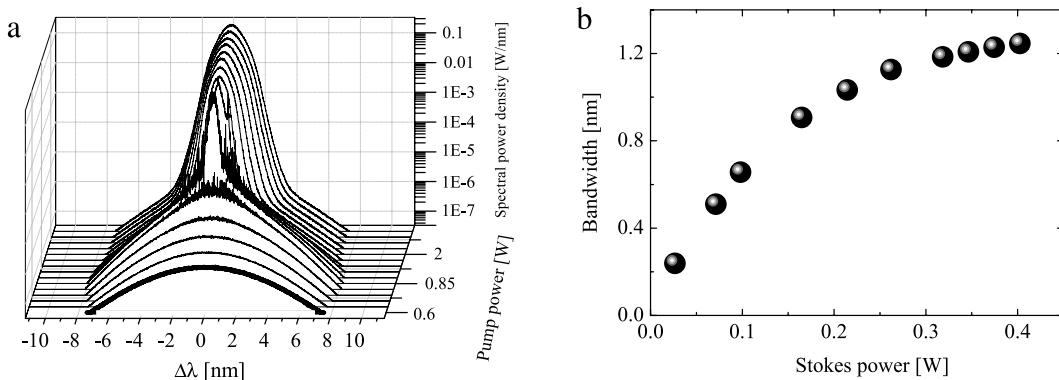
Fig. 35. Numerically calculated within the NLSE-based model (39) spectral properties of the random DFB fibre laser in the forward-pumped configuration. (a) The generation spectrum depending on the pump power. (b) The generation spectrum rms spectral width depending on the generation power. After Ref. [415].

Note that the spectral properties of the random DFB fibre lasers have not been yet studied systematically in experiments. There are only few attempts. As an example of some spectral studies, both power and spectral properties of the forward- and backward-pumped random DFB fibre lasers were measured depending on the ratio between the backward- and the forward-propagating pump wave powers in [418,419]. It was found that the spectral broadening was more pronounced in the forward-pumped configuration resulting in a 0.9 nm spectral width for 70 mW of the output power. The authors suggested a difference in the longitudinal power distributions as the origin of deviations in the random lasers behaviour.

Temporal and statistical properties of the random DFB fibre laser radiation could also be calculated within the NLSE-based model. Non-Gaussian intensity statistics of the radiation of some random DFB fibre laser was found in numerical calculations in [415]. Note that the non-Gaussian intensity statistics was previously reported in conventional fibre lasers of cavities based on point-based mirrors [411–413]. The non-Gaussian intensity statistics was connected with an existence of partial correlations between different longitudinal modes in the generation. Experimentally, intensity dynamics and statistical properties of the random DFB fibre lasers are under intensive studies world wide.

6. Conclusions and perspectives

The geometric properties of physical objects that affect photons propagation are very important in light science. Light propagation in a transparent material is affected by a variation of the refractive index n through the corresponding changes of the speed of light in a medium. The ground breaking insight, following the pioneering Bragg research on wave reflection in distributed periodic structures, is the design of structure-specific properties of spectral bands affecting particular Bloch modes in a pre-designed way. Periodic variations of the refractive index are nowadays routinely used in numerous scientific and industrial applications for manipulating light propagation. For instance, an important property of the periodic photonic structures is a possibility to alter the dispersion of electromagnetic waves to make a group velocity of light (in specific spectral regions) substantially smaller than the speed of light in a vacuum. The periodic optical structures are utilized in a number of functions: distributed feedback lasers, enhancement of nonlinear effects, optical memory, light delay lines, and other slow light based devices. In addition, purposely designed point defects allow tailoring of light propagation in periodic structures. For instance, in one-dimensional photonic structure the introduction of a defect state would act as a bandpass filter. Periodic and quasi-periodic optical structures already have become the integral part of the fabric of the modern photonic technology.

However, a refractive index can change in a number of various ways and this can be translated into new optical technologies. The next level of complexity of photonic structures includes dual periodicity and super-lattices that introduce more opportunities in terms of the dispersion curve control and manipulation. The design of new photonic devices with non-trivial geometric variations of the refractive index has become a captivating research area with luminous scientific and applied perspectives. The major step in this direction is to develop engineering design rules for photonic devices based on disorder that would offer rich new opportunities beyond the properties of periodic structures. It is nowadays well accepted that disorder (for example, random variations of the refractive index in a medium) can also be exploited to create useful photonic structures. Random variations of the refractive index can be both of a natural origin (for example, scattering on internal structure of a material as an sub-micron irregularities of a glass) or pre-designed artificially. A random laser is an important example of this new type of photonic device that can be created using the random properties of a transparent medium — disorder-based light source. The potential importance of such devices is linked to a wide range of applications of conventional lasers including material processing, manufacturing, communication systems, medical applications, metrology, imaging, and many others. The advantage of disorder-based light sources could be the potential low-cost and simplicity of fabrication, when the disorder is of natural origin and does not need to be pre-fabricated. Imaging without speckles is another promising application of random lasers where they can outperform traditional lasers. In any

case, the science of random lasers is a fascinating field of research attracting interest from very different areas — from the theory of disordered systems to optical communications.

The localization of waves propagating in random media has been a fascinating research topic over many years. The idea of the localization of photons in disordered transparent materials has initiated a considerable amount of work. The localization of waves in random lasers connects fundamental science research and photonic technology in which localized waves can generate exotic spectral emission and offer new methods of spatial manipulation through this light emission.

The random distributed feedback fibre lasers discussed in this work present an interesting family of random lasers. In this case disorder is an inherent part of any optical fibre that always has tiny scatterers leading to Rayleigh scattering of propagating light. The scale of the considered random fibre lasers can be from several metres to several hundred kilometres. The gain medium is created in a standard fibre medium via the distributed Raman effect that provides for additional degrees of spatial gain control. In random fibre lasers the uncontrollable nature of lasing becomes somewhat manageable. The fibre waveguide naturally provides for an excellent directionality of the generated laser beam. The emission spectrum is defined by the Raman gain curve. In schemes without any external spectral elements random Raman fibre lasers can be tunable over very broad spectral ranges holding a great promise for a number of applications.

Though the fibre disordered medium that determines much of the laser's characteristics consists of a random immobile distribution of scatterers, the properties of Raman pumping can potentially be engineered to achieve some control of emission through the longitudinal spatial profile of pumping waves. We anticipate that pumping waves can be pre-programmed through an optimization procedure based on a feedback loop between the pump source and the laser output. Note that in the standard fibre made of silica the scattering is weak, and the random laser modes are only weakly trapped by the medium leading to a high lasing threshold. In this case, the pump wave shaping might have a stronger impact on the random lasing modes.

Random fibre lasers are particularly attractive physical objects because of their inherent one-dimensional nature. It is well known that the properties of wave propagation in disordered media depend on the system dimensionality. The theoretical analysis of one-dimensional random fibre lasers is obviously easier compared to 2D and 3D laser configurations. At the same time the theory of one-dimensional random lasers is far from being simple. Therefore, we believe that random fibre laser systems will attract an interest from the theoreticians and mathematicians working in the field of disordered systems.

We hope that this review paper will attract new interest in the exciting research area of random fibre lasers from various research and engineering communities. The concept of an ultra-long random fibre laser may lead to new promising opportunities in telecommunications and distributed sensing. A disordered lasing medium of several hundred kilometres may be also very interesting for potential applications in secure communications, e.g. as a new type of classical key distribution system that might overcome the practical challenges faced by quantum key distribution systems. We expect that new applications and technologies will keep emerging from the study of the physics of random fibre lasers. While the concept can already be considered a breakthrough into new areas of lasers science, we believe it will also have a significant impact in areas of immediate practical importance in the nearest future.

Acknowledgements

References

[1] A. Siegman, Lasers, University Science Books, 1986.
[2] O. Svelto, D. Hanna, Principles of Lasers, Springer, 1998.
[3] A.C. Newell, Envelope equations, in: Lectures in Applied Mathematics, Nonlinear Wave Motion 15 (1974) 157–194.
[4] H.A. Haus, Theory of mode-locking with a fast saturable absorber, J. Appl. Phys. 46 (7) (1975) 3049–3058.
[5] K.P. Komarov, Theory of stationary ultrafast pulses in solid-state lasers with passive mode-locking, Opt. Spectrosc. 60 (1986) 231–234.
[6] E.P. Ippen, H.A. Haus, L.Y. Liu, Additive pulse mode locking, J. Opt. Soc. Amer. B 6 (1989) 1736–1745.
[7] H.A. Haus, J.G. Fujimoto, E.P. Ippen, Structures for additive pulse mode locking, J. Opt. Soc. Amer. B 8 (1991) 2068–2076.
[8] H.A. Haus, J.G. Fujimoto, E.P. Ippen, Analytic theory of additive pulse and Kerr mode locking, IEEE J. Quantum Electron. 28 (1992) 2086–2096.
[9] V.L. Ginzburg, L.D. Landau, On the theory of superconductivity, Zh. Eksp. Teor. Fiz. (Sov. JETP) 20 (1950) 1064–1082.
[10] A. Komarov, H. Leblond, F. Sanchez, Quintic complex ginzburg-landau model for ring fiber lasers, Phys. Rev. E 72 (2005) 025604.
[11] S.K. Turitsyn, B. Bale, M. Fedoruk, Dispersion-managed solitons in fibre systems and lasers, Phys. Rep. 521 (4) (2012) 135–203.
[12] J.N. Kutz, Mode-locked soliton lasers, SIAM Rev. 48 (2006) 629–678.
[13] B.G. Bale, S. Boscolo, J.N. Kutz, S.K. Turitsyn, Intracavity dynamics in high-power mode-locked fiber lasers, Phys. Rev. A 81 (2010) 033828.
[14] L.P. Shilnikov, A.L. Shilnikov, D.V. Turaev, L.O. Chua, Methods of Qualitative Theory in Nonlinear Dynamics. Part II, in: World Scientifc Series on Nonlinear Science, Series A, vol. 5, World Scientific Publishing, 2001.
[15] V. Gaisyonok, E. Grigorieva, S. Kashchenko, Poincaré mappings for targeting orbits in periodically driven lasers, Opt. Commun. 124 (1–4) (1996) 408–417.
[16] L.M. Sanchez, A.A. Hnilo, Description of kerr lens mode-locked lasers with poincaré maps in the complex plane, Opt. Commun. 199 (2001) 189–199.
[17] Y. Ma, X. Guo, X. Wu, L. Dai, L. Tong, Semiconductor nanowire lasers, Adv. Opt. Photon. 5 (3) (2013) 216–273.

[18] M.A. Noginov, G. Zhu, A.M. Belgrave, R. Bakker, V.M. Shalaev, E.E. Narimanov, S. Stout, E. Herz, T. Suteewong, U. Wiesner, Demonstration of a spaser-based nanolaser, Nat. Phys. 460 (2009) 1110–1112.

[19] S.K. Turitsyn, J.D. Ania-Castañón, S.A. Babin, V. Karalekas, P. Harper, D. Churkin, S.I. Kablukov, A.E. El-Taher, E.V. Podivilov, V.K. Mezentsev, 270-km ultralong Raman fiber laser, Phys. Rev. Lett. 103 (13) (2009) 133901.

[20] J.D. Ania-Castañón, V. Karalekas, P. Harper, S.K. Turitsyn, Simultaneous spatial and spectral transparency in ultralong fiber lasers, Phys. Rev. Lett. 101 (12) (2008) 123903.

[21] M.J. Feigenbaum, Quantitative universality for a class of non-linear transformations, J. Stat. Phys. 19 (1978) 25–52.

[22] P. Grelu, N. Akhmediev, Dissipative solitons for mode-locked lasers, Nature Photon. 6 (2012) 84–92.

[23] S. Kobtsev, S. Kukarin, S. Smirnov, S. Turitsyn, A. Latkin, Generation of double-scale femto/pico-second optical lumps in mode-locked fiber lasers, Opt. Express 17 (2009) 20707–20713.

[24] B.N. Nyushkov, V.I. Denisov, S.M. Kobtsev, V.S. Pivtsov, N.A. Kolyada, A.V. Ivanenko, S.K. Turitsyn, Generation of 1.7-μJ pulses at 1.55 μm by a self-modelocked all-fiber laser with a kilometers-long linear-ring cavity, Laser Phys. Lett. 7 (2010) 661–665.

[25] E.G. Turitsyna, S.V. Smirnov, S. Sugavanam, N. Tarasov, X. Shu, S.A. Babin, E.V. Podivilov, D.V. Churkin, G. Falkovich, S.K. Turitsyn, The laminar-turbulent transition in a fibre laser, Nature Photon. 7 (10) (2013) 783–786.

[26] H. Cao, Review on latest developments in random lasers with coherent feedback, J. Phys. - Math. Gen. 38 (49) (2005) 10497.

[27] D.S. Wiersma, The physics and applications of random lasers, Nat. Phys. 4 (5) (2008) 359–367.

[28] C.J.S. de Matos, L.d.S. Menezes, A.M. Brito-Silva, M.A.M. Gámez, A.S.L. Gomes, C.B. de Araújo, Random fiber laser, Phys. Rev. Lett. 99 (15) (2007) 153903.

[29] G.P. Agrawal, Fiber-Optic Communication Systems, John Wiley & Sons, 2010.

[30] M. Nakazawa, Rayleigh backscattering theory for single-mode optical fibers, J. Opt. Soc. Amer. 73 (9) (1983) 1175.

[31] S.K. Turitsyn, S.A. Babin, A.E. El-Taher, P. Harper, D.V. Churkin, S.I. Kablukov, J.D. Ania-Castanon, V. Karalekas, E.V. Podivilov, Random distributed feedback fibre laser, Nature Photon. 4 (4) (2010) 231–235.

[32] J. Herrmann, B. Wilhelmi, Mirrorless laser action by randomly distributed feedback in amplifying disordered media with scattering centers, Appl. Phys. B: Lasers Opt. 66 (3) (1998) 305–312.

[33] V. Letokhov, Stimulated emission of an ensemble of scattering particles with negative absorption, JETP Lett. 5 (1967) 212–215.

[34] V. Letokhov, Generation of light by a scattering medium with negative resonance absorption, Sov. Phys.—JETP 26 (1968) 835–840.

[35] D.S. Wiersma, M.P. van Albada, A. Lagendijk, Random laser? Nature 373 (1995) 203–204.

[36] M. Noginov, Solid-State Random Lasers, vol. 105, Springer, 2005.

[37] H. Cao, Lasing in random media, Waves in Random Media 13 (3) (2003) R1–R39.

[38] J. Andreasen, A. Asatryan, L. Botten, M. Byrne, H. Cao, L. Ge, L. Labonté, P. Sebbah, A. Stone, H. Türeci, C. Vanneste, Modes of random lasers, Advances in Optics and Photonics 3 (1) (2011) 88–127.

[39] B. Shivakiran Bhaktha, N. Bachelard, X. Noblin, P. Sebbah, Optofluidic random laser, Appl. Phys. Lett. 101 (15) (2012) 151101–151101.

[40] N. Bachelard, J. Andreasen, S. Gigan, P. Sebbah, Taming random lasers through active spatial control of the pump, Phys. Rev. Lett. 109 (3) (2012) 033903.

[41] X. Wu, W. Fang, A. Yamilov, A. Chabanov, A. Asatryan, L. Botten, H. Cao, Random lasing in weakly scattering systems, Phys. Rev. A 74 (5) (2006) 053812.

[42] V. Folli, A. Puglisi, L. Leuzzi, C. Conti, Shaken granular lasers, Phys. Rev. Lett. 108 (24) (2012) 248002.

[43] V. Folli, N. Ghofraniha, A. Puglisi, L. Leuzzi, C. Conti, Time-resolved dynamics of granular matter by random laser emission, Scientific Reports 3.

[44] B. Redding, M.A. Choma, H. Cao, Speckle-free laser imaging using random laser illumination, Nature Photon. 6 (6) (2012) 355–359.

[45] R. Ambartsumyan, N. Basov, P. Kryukov, V. Letokhov, Laser with nonresonant feedback, JETP Lett. 3 (1966) 167–169.

[46] R. Ambartsumyan, N. Basov, P. Kryukov, V. Letokhov, A laser with a non-resonant feedback, IEEE J. Quantum Electron. QE-2 (1966) 442–446.

[47] V. Markushev, V. Zolin, C.M. Briskina, Luminescence and stimulated emission of neodymium in sodium lanthanum molybdate powders, Sov. J. Quantum Electron. 16 (2) (1986) 281.

[48] C. Gouedard, D. Husson, C. Sauteret, F. Auzel, A. Migus, Generation of spatially incoherent short pulses in laser-pumped neodymium stoichiometric crystals and powders, J. Opt. Soc. Amer. B 10 (12) (1993) 2358–2363.

[49] M.A. Noginov, N.E. Noginova, H.J. Caulfield, P. Venkateswarlu, T. Thompson, M. Mahdi, V. Ostroumov, Short-pulsed stimulated emission in the powders of NdAl$_3$(BO$_3$)$_4$, NdSc$_3$(BO$_3$)$_4$, and Nd:Sr$_5$(PO$_4$)$_3$F laser crystals, J. Opt. Soc. Amer. B 13 (9) (1996) 2024–2033.

[50] N.M. Lawandy, R. Balachandran, A. Gomes, E. Sauvain, Laser action in strongly scattering media, Nature 368 (6470) (1994) 436–438.

[51] D.S. Wiersma, A. Lagendijk, Light diffusion with gain and random lasers, Phys. Rev. B 54 (4) (1996) 4256.

[52] H. Cao, Y. Zhao, H. Ong, S. Ho, J. Dai, J. Wu, R. Chang, Ultraviolet lasing in resonators formed by scattering in semiconductor polycrystalline films, Appl. Phys. Lett. 73 (25) (1998) 3656–3658.

[53] H. Cao, Y. Zhao, S. Ho, E. Seelig, Q. Wang, R. Chang, Random laser action in semiconductor powder, Phys. Rev. Lett. 82 (11) (1999) 2278.

[54] H. Cao, Y. Zhao, X. Liu, E. Seelig, R. Chang, Effect of external feedback on lasing in random media, Appl. Phys. Lett. 75 (9) (1999) 1213–1215.

[55] R. Thareja, A. Mitra, Random laser action in ZnO, Appl. Phys. B 71 (2) (2000) 181–184.

[56] H. Cao, J. Xu, D. Zhang, S. Chang, S. Ho, E. Seelig, X. Liu, R. Chang, et al., Spatial confinement of laser light in active random media, Phys. Rev. Lett. 84 (24) (2000) 5584–5587.

[57] H. Cao, Y. Ling, J. Xu, C. Cao, P. Kumar, Photon statistics of random lasers with resonant feedback, Phys. Rev. Lett. 86 (20) (2001) 4524.

[58] D. Anglos, A. Stassinopoulos, R.N. Das, G. Zacharakis, M. Psyllaki, R. Jakubiak, R.A. Vaia, E.P. Giannelis, S.H. Anastasiadis, Random laser action in organic–inorganic nanocomposites, J. Opt. Soc. Amer. B 21 (1) (2004) 208–213.

[59] M. Noginov, G. Zhu, I. Fowlkes, M. Bahoura, GaAs random laser, Laser Phys. Lett. 1 (6) (2004) 291.

[60] T. Nakamura, T. Takahashi, S. Adachi, Temperature dependence of GaAs random laser characteristics, Phys. Rev. B 81 (12) (2010) 125324.

[61] G. Zhu, C. Small, M. Noginov, Single-and two-photon excitation of a GaAs random laser, Opt. Lett. 33 (9) (2008) 920–922.

[62] T. Takahashi, T. Nakamura, S. Adachi, Blue-light-emitting ZnSe random laser, Opt. Lett. 34 (24) (2009) 3923–3925.

[63] I. Sorokina, E. Sorokin, V.G. Shcherbitsky, N.V. Kuleshov, G. Zhu, M. Noginov, Room-temperature lasing in nanocrystalline Cr^{2+}: ZnSe random laser, in: OSA Trends in Optics and Photonics, in: Advanced Solid-State Photonics, vol. 94, Optical Society of America, 2004, pp. 376–380.

[64] C. Kim, D. Martyshkin, V. Fedorov, S. Mirov, et al., Mid-infrared Cr^{2+}:ZnSe random powder lasers, Opt. Express 16 (7) (2008) 4952–4959.

[65] T. Nakamura, T. Hosaka, S. Adachi, Gold-nanoparticle-assisted random lasing from powdered gan, Opt. Express 19 (2) (2011) 467–475.

[66] U. Ozgur, Y.I. Alivov, C. Liu, A. Teke, M. Reshchikov, S. Dogan, V. Avrutin, S.-J. Cho, H. Morkoc, A comprehensive review of ZnO materials and devices, J. Appl. Phys. 98 (4) (2005) 041301–041301.

[67] H. Cao, Y. Zhao, H. Ong, R. Chang, Far-field characteristics of random lasers, Phys. Rev. B 59 (23) (1999) 15107.

[68] S. Yu, C. Yuen, S. Lau, H. Lee, Zinc oxide thin-film random lasers on silicon substrate, Appl. Phys. Lett. 84 (17) (2004) 3244–3246.

[69] E. Chelnokov, N. Bityurin, I. Ozerov, W. Marine, Two-photon pumped random laser in nanocrystalline ZnO, Appl. Phys. Lett. 89 (17) (2006) 171119–171119.

[70] X. Ma, P. Chen, D. Li, Y. Zhang, D. Yang, Electrically pumped ZnO film ultraviolet random lasers on silicon substrate, Appl. Phys. Lett. 91 (25) (2007) 251109–251109.

[71] H. Li, S. Yu, S. Lau, E.S. Leong, Simultaneous formation of visible and ultraviolet random lasings in ZnO films, Appl. Phys. Lett. 89 (2) (2006) 021110–021110.

[72] C. Yuen, S. Yu, E.S. Leong, H. Yang, S. Lau, N. Chen, H. Hng, Low-loss and directional output ZnO thin-film ridge waveguide random lasers with Mgo capped layer, Appl. Phys. Lett. 86 (3) (2005) 031112–031112.

[73] M. Chong, A. Abiyasa, K. Pita, S. Yu, Visible red random lasing in YO:Eu/ZnO polycrystalline thin films by energy transfer from ZnO films to Eu, Appl. Phys. Lett. 93 (2008) 151105.

[74] P. Chen, X. Ma, D. Li, Y. Zhang, D. Yang, Electric-field-induced random lasing from ZnO and $Mg_{0.1}Zn_{0.0}O$ films optically pumped with an extremely low intensity, Opt. Express 17 (21) (2009) 18513–18517.

[75] M.H. Huang, S. Mao, H. Feick, H. Yan, Y. Wu, H. Kind, E. Weber, R. Russo, P. Yang, Room-temperature ultraviolet nanowire nanolasers, Science 292 (5523) (2001) 1897–1899.

[76] S. Yu, C. Yuen, S. Lau, W.I. Park, G.-C. Yi, Random laser action in ZnO nanorod arrays embedded in ZnO epilayers, Appl. Phys. Lett. 84 (17) (2004) 3241–3243.

[77] S. Lau, H. Yang, S. Yu, H. Li, M. Tanemura, T. Okita, H. Hatano, H. Hng, Laser action in ZnO nanoneedles selectively grown on silicon and plastic substrates, Appl. Phys. Lett. 87 (1) (2005) 013104–013104.

[78] H. Yang, S. Lau, S. Yu, A. Abiyasa, M. Tanemura, T. Okita, H. Hatano, High-temperature random lasing in ZnO nanoneedles, Appl. Phys. Lett. 89 (1) (2006) 011103–011103.

[79] H.-C. Hsu, C.-Y. Wu, W.-F. Hsieh, Stimulated emission and lasing of random-growth oriented ZnO nanowires, J. Appl. Phys. 97 (6) (2005) 064315–064315.

[80] C. Wang, Y. Chen, H. Lin, Y. Chen, Y. Chen, Enhancement of random lasing through fluorescence resonance energy transfer and light scattering mediated by nanoparticles, Appl. Phys. Lett. 97 (19) (2010) 191104–191104.

[81] K. Firdaus, T. Nakamura, S. Adachi, Improved lasing characteristics of ZnO/organic-dye random laser, Appl. Phys. Lett. 100 (17) (2012) 171101–171101.

[82] M. Sakai, Y. Inose, K. Ema, T. Ohtsuki, H. Sekiguchi, A. Kikuchi, K. Kishino, Random laser action in gan nanocolumns, Appl. Phys. Lett. 97 (15) (2010) 151109–151109.

[83] S.-P. Chang, K.-P. Sou, C.-H. Chen, Y.-J. Cheng, J.-K. Huang, C.-H. Lin, H.-C. Kuo, C.-Y. Chang, W.-F. Hsieh, Lasing action in gallium nitride quasicrystal nanorod arrays, Opt. Express 20 (11) (2012) 12457–12462.

[84] H. Yang, S. Yu, S. Lau, S. Tsang, G. Xing, T. Wu, Ultraviolet coherent random lasing in randomly assembled SnO nanowires, Appl. Phys. Lett. 94 (24) (2009) 241121–241121.

[85] H. Yang, S. Yu, H. Liang, R.G. Mote, C. Cheng, H. Fan, T. Sun, H. Hng, High-temperature lasing characteristics of randomly assembled Sno backbone nanowires coated with ZnO nanofins, J. Appl. Phys. 106 (2009) 123105.

[86] H. Yang, S. Yu, J. Yan, L. Zhang, Random lasing action from randomly assembled ZnS nanosheets, Nanoscale Res. Lett. 5 (5) (2010) 809–812.

[87] M. Lu, H. Lin, T. Chen, Y. Chen, Random lasing in the composites consisting of photonic crystals and semiconductor nanowires, Appl. Phys. Lett. 99 (9) (2011) 091106–091106.

[88] C. Wang, H. Lin, T. Lin, Y. Chen, Enhancement of random lasing assisted by light scattering and resonance energy transfer based on ZnO/SnO nanocomposites, AIP Advances 2 (1) (2012) 012133–012133.

[89] W. Sha, C.-H. Liu, R. Alfano, Spectral and temporal measurements of laser action of Rhodamine 640 dye in strongly scattering media, Opt. Lett. 19 (23) (1994) 1922–1924.

[90] M. Noginov, H. Caulfield, N. Noginova, P. Venkateswarlu, Line narrowing in the dye solution with scattering centers, Opt. Commun. 118 (3) (1995) 430–437.

[91] M. Siddique, R. Alfano, G. Berger, M. Kempe, A. Genack, Time-resolved studies of stimulated emission from colloidal dye solutions, Opt. Lett. 21 (7) (1996) 450–452.

[92] J. Kitur, G. Zhu, M. Bahoura, M. Noginov, Dependence of the random laser behavior on the concentrations of dye and scatterers, J. Opt. 12 (2) (2010) 024009.

[93] L. Yang, G. Feng, J. Yi, K. Yao, G. Deng, S. Zhou, Effective random laser action in Rhodamine 6G solution with Al nanoparticles, Appl. Opt. 50 (13) (2011) 1816–1821.

[94] Z. Hu, Q. Zhang, B. Miao, Q. Fu, G. Zou, Y. Chen, Y. Luo, D. Zhang, P. Wang, H. Ming, et al., Coherent random fiber laser based on nanoparticles scattering in the extremely weakly scattering regime, Phys. Rev. Lett. 109 (25) (2012) 253901.

[95] B. Kumar, S. Patel, N. Gajbhiye, R.K. Thareja, Random laser action with nanostructures in a dye solution, J. Laser Appl. 25 (2013) 042012.

[96] G. Zacharakis, N.A. Papadogiannis, G. Filippidis, T.G. Papazoglou, Photon statistics of laserlike emission from polymeric scattering gain media, Opt. Lett. 25 (12) (2000) 923–925.

[97] R. Balachandran, D. Pacheco, N. Lawandy, Laser action in polymeric gain media containing scattering particles, Appl. Opt. 35 (4) (1996) 640–643.

[98] X. Meng, K. Fujita, Y. Zong, S. Murai, K. Tanaka, Random lasers with coherent feedback from highly transparent polymer films embedded with silver nanoparticles, Appl. Phys. Lett. 92 (20) (2008) 201112–201112.

[99] X. Meng, K. Fujita, S. Murai, K. Tanaka, Coherent random lasers in weakly scattering polymer films containing silver nanoparticles, Phys. Rev. A 79 (5) (2009) 053817.

[100] S. Frolov, M. Shkunov, A. Fujii, K. Yoshino, Z. Vardeny, Lasing and stimulated emission in π-conjugated polymers, IEEE J. Quantum Electron. 36 (1) (2000) 2–11.

[101] R. Polson, A. Chipouline, Z. Vardeny, Random lasing in π-conjugated films and infiltrated opals, Adv. Mater. 13 (10) (2001) 760–764.

[102] R.C. Polson, M.E. Raikh, Z.V. Vardeny, Universality in unintentional laser resonators in π-conjugated polymer films, C. R. Phys. 3 (4) (2002) 509–521.

[103] A. Tulek, Z. Vardeny, Studies of random laser action in π-conjugated polymers, J. Opt. 12 (2) (2010) 024008.

[104] R.C. Polson, M.E. Raikh, Z.V. Vardeny, Universal properties of random lasers, IEEE J. Sel. Top. Quant. Electron. 9 (1) (2003) 120–123.

[105] S. Frolov, W. Gellermann, M. Ozaki, K. Yoshino, Z. Vardeny, Cooperative emission in π-conjugated polymer thin films, Phys. Rev. Lett. 78 (4) (1997) 729.

[106] A. Tulek, R. Polson, Z. Vardeny, Naturally occurring resonators in random lasing of π-conjugated polymer films, Nat. Phys. 6 (4) (2010) 303–310.

[107] V. Apalkov, M. Raikh, B. Shapiro, Almost localized photon modes in continuous and discrete models of disordered media, J. Opt. Soc. Amer. B 21 (1) (2004) 132–140.

[108] R. Polson, Z. Vardeny, Organic random lasers in the weak-scattering regime, Phys. Rev. B 71 (4) (2005) 045205.

[109] S. Frolov, Z. Vardeny, K. Yoshino, A. Zakhidov, R. Baughman, Stimulated emission in high-gain organic media, Phys. Rev. B 59 (8) (1999) R5284.

[110] S. Kena-Cohen, P.N. Stavrinou, D.D. Bradley, S.A. Maier, Random lasing in low molecular weight organic thin films, Appl. Phys. Lett. 99 (4) (2011) 041114–041114.

[111] L. Cerdán, A. Costela, I. García-Moreno, Waveguided random lasing in red-emitting-dye-doped organic–inorganic hybrid polymer thin films, Org. Electron. 13 (8) (2012) 1463–1469.

[112] M. Anni, S. Lattante, R. Cingolani, G. Gigli, G. Barbarella, L. Favaretto, Far-field emission and feedback origin of random lasing in oligothiophene dioxide neat films, Appl. Phys. Lett. 83 (14) (2003) 2754–2756.

[113] M. Anni, S. Lattante, T. Stomeo, R. Cingolani, G. Gigli, G. Barbarella, L. Favaretto, Modes interaction and light transport in bidimensional organic random lasers in the weak scattering limit, Phys. Rev. B 70 (19) (2004) 195216.

[114] F. Quochi, F. Cordella, A. Mura, G. Bongiovanni, F. Balzer, H.-G. Rubahn, One-dimensional random lasing in a single organic nanofiber, J. Phys. Chem. B 109 (46) (2005) 21690–21693.

[115] A. Andreev, F. Quochi, F. Cordella, A. Mura, G. Bongiovanni, H. Sitter, G. Hlawacek, C. Teichert, N. Sariciftci, Coherent random lasing in the deep blue from self-assembled organic nanofibers, J. Appl. Phys. 99 (3) (2006) 034305–034305.

[116] F. Quochi, Random lasers based on organic epitaxial nanofibers, J. Opt. 12 (2) (2010) 024003.

[117] A. Costela, I. Garcia-Moreno, L. Cerdan, V. Martin, O. Garcia, R. Sastre, Dye-doped poss solutions: random nanomaterials for laser emission, Adv. Mater. 21 (41) (2009) 4163–4166.

[118] L. Cerdán, A. Costela, I. García-Moreno, O. García, R. Sastre, Laser emission from mirrorless waveguides based on photosensitized polymers incorporating poss, Opt. Express 18 (10) (2010) 10247–10256.

[119] X. Zhao, Z. Wu, S. Ning, S. Liang, D. Wang, X. Hou, Random lasing from granular surface of waveguide with blends of ps and pmma, Opt. Express 19 (17) (2011) 16126–16131.

[120] S.V. Frolov, Z.V. Vardeny, A.A. Zakhidov, R.H. Baughman, Laser-like emission in opal photonic crystals, Opt. Commun. 162 (4) (1999) 241–246.
[121] M. Shkunov, M. DeLong, M. Raikh, Z. Vardeny, A. Zakhidov, R. Baughman, Photonic versus random lasing in opal single crystals, Synth. Met. 116 (1) (2001) 485–491.
[122] S. García-Revilla, J. Fernández, M.A. Illarramendi, B. García-Ramiro, R. Balda, H. Cui, M. Zayat, D. Levy, et al., Ultrafast random laser emission in a dye-doped silica gel powder, Opt. Express 16 (16) (2008) 12251–12263.
[123] H.-W. Shin, S.Y. Cho, K.-H. Choi, S.-L. Oh, Y.-R. Kim, Directional random lasing in dye-tio doped polymer nanowire array embedded in porous alumina membrane, Appl. Phys. Lett. 88 (2006) 263112.
[124] D.S. Wiersma, S. Cavalieri, Light emission: a temperature-tunable random laser, Nature 414 (6865) (2001) 708–709.
[125] D.S. Wiersma, M. Colocci, R. Righini, F. Aliev, Temperature-controlled light diffusion in random media, Phys. Rev. B 64 (14) (2001) 144208.
[126] D.S. Wiersma, S. Cavalieri, Temperature-controlled random laser action in liquid crystal infiltrated systems, Phys. Rev. B 66 (5) (2002) 056612.
[127] G. Strangi, S. Ferjani, V. Barna, A. DeLuca, C. Versace, N. Scaramuzza, R. Bartolino, Random lasing and weak localization of light in dye-doped nematic liquid crystals, Opt. Express 14 (17) (2006) 7737–7744.
[128] S. Ferjani, V. Barna, A. DeLuca, C. Versace, N. Scaramuzza, R. Bartolino, G. Strangi, Thermal behavior of random lasing in dye doped nematic liquid crystals, Appl. Phys. Lett. 89 (12) (2006) 121109–121109.
[129] Q. Song, S. Xiao, X. Zhou, L. Liu, L. Xu, Y. Wu, Z. Wang, Liquid-crystal-based tunable high-Q directional random laser from a planar random microcavity, Opt. Lett. 32 (4) (2007) 373–375.
[130] S. Ferjani, L. Sorriso-Valvo, A. DeLuca, V. Barna, R. DeMarco, G. Strangi, Statistical analysis of random lasing emission properties in nematic liquid crystals, Phys. Rev. B 78 (1) (2008) 011707.
[131] S. Ferjani, V. Barna, A. De Luca, C. Versace, G. Strangi, Random lasing in freely suspended dye-doped nematic liquid crystals, Opt. Lett. 33 (6) (2008) 557–559.
[132] S. Ferjani, A. De Luca, V. Barna, C. Versace, G. Strangi, Thermo-recurrent nematic random laser, Opt. Express 17 (3) (2009) 2042–2047.
[133] Q. Song, L. Liu, L. Xu, Y. Wu, Z. Wang, Electrical tunable random laser emission from a liquid-crystal infiltrated disordered planar microcavity, Opt. Lett. 34 (3) (2009) 298–300.
[134] S. Gottardo, S. Cavalieri, O. Yaroshchuk, D.S. Wiersma, Quasi-two-dimensional diffusive random laser action, Phys. Rev. Lett. 93 (26) (2004) 263901.
[135] Y. Liu, X. Sun, H. Elim, W. Ji, Gain narrowing and random lasing from dye-doped polymer-dispersed liquid crystals with nanoscale liquid crystal droplets, Appl. Phys. Lett. 89 (1) (2006) 011111–011111.
[136] C.-W. Chen, H.-C. Jau, C.-T. Wang, C.-H. Lee, I.C. Khoo, T.-H. Lin, Random lasing in blue phase liquid crystals, Opt. Express 20 (21) (2012) 23978–23984.
[137] C.-R. Lee, J.-D. Lin, B.-Y. Huang, T.-S. Mo, S.-Y. Huang, All-optically controllable random laser based on a dye-doped liquid crystal added with a photoisomerizable dye, Opt. Express 18 (25) (2010) 25896–25905.
[138] C. Lee, S. Lin, C. Guo, S. Chang, T. Mo, S. Chu, All-optically controllable random laser based on a dye-doped polymer-dispersed liquid crystal with nano-sized droplets, Opt. Express 18 (3) (2010) 2406–2412.
[139] F. Yao, W. Zhou, H. Bian, Y. Zhang, Y. Pei, X. Sun, Z. Lv, Polarization and polarization control of random lasers from dye-doped nematic liquid crystals, Opt. Lett. 38 (9) (2013) 1557–1559.
[140] L. Li, L. Deng, Low threshold and coherent random lasing from dye-doped cholesteric liquid crystals using oriented cells, Laser Phys. 23 (8) (2013) 085001.
[141] S. Morris, A. Ford, M. Pivnenko, H. Coles, Electronic control of nonresonant random lasing from a dye-doped smectic a liquid crystal scattering device, Appl. Phys. Lett. 86 (2005) 141103.
[142] G. Dice, S. Mujumdar, A. Elezzabi, Plasmonically enhanced diffusive and subdiffusive metal nanoparticle-dye random laser, Appl. Phys. Lett. 86 (13) (2005) 131105–131105.
[143] O. Popov, A. Zilbershtein, D. Davidov, Random lasing from dye-gold nanoparticles in polymer films: enhanced gain at the surface-plasmon-resonance wavelength, Appl. Phys. Lett. 89 (19) (2006) 191116–191116.
[144] T. Zhai, X. Zhang, Z. Pang, X. Su, H. Liu, S. Feng, L. Wang, Random laser based on waveguided plasmonic gain channels, Nano Lett. 11 (10) (2011) 4295–4298.
[145] A. Kumar, S. Yu, X. Li, Random laser action in dielectric–metal–dielectric surface plasmon waveguides, Appl. Phys. Lett. 95 (23) (2009) 231114–231114.
[146] E. Heydari, R. Flehr, J. Stumpe, Influence of spacer layer on enhancement of nanoplasmon-assisted random lasing, Appl. Phys. Lett. 102 (13) (2013) 133110–133110.
[147] Y. Sun, Z. Wang, X. Shi, Y. Wang, X. Zhao, S. Chen, J. Shi, J. Zhou, D. Liu, Coherent plasmonic random laser pumped by nanosecond pulses far from the resonance peak of silver nanowires, J. Opt. Soc. Amer. B 30 (9) (2013) 2523–2528.
[148] J.U. Kang, Observation of random lasing in gold–silica nanoshell/water solution, Appl. Phys. Lett. 89 (22) (2006) 221112–221112.
[149] C.-S. Wang, H.-Y. Lin, J.-M. Lin, Y.-F. Chen, Surface-plasmon-enhanced ultraviolet random lasing from ZnO nanowires assisted by Pt nanoparticles, Appl. Phys. Express 5 (6) (2012) 062003.
[150] S.-H. Cheng, Y.-C. Yeh, M.-L. Lu, C.-W. Chen, Y.-F. Chen, Enhancement of laser action in ZnO nanorods assisted by surface plasmon resonance of reduced graphene oxide nanoflakes, Opt. Express 20 (106) (2012) A799–A805.
[151] B. Li, G. Williams, S. Rand, T. Hinklin, R. Laine, Continuous-wave ultraviolet laser action in strongly scattering Nd-doped alumina, Opt. Lett. 27 (6) (2002) 394–396.
[152] M. Noginov, I. Fowlkes, G. Zhu, J. Novak, Neodymium random lasers operating in different pumping regimes, J. Modern Opt. 51 (16–18) (2004) 2543–2553.
[153] M. Noginov, G. Zhu, C. Small, J. Novak, Neodymium random laser with external mirrors, Appl. Phys. B 84 (1–2) (2006) 269–273.
[154] M. Bahoura, K.J. Morris, G. Zhu, M. Noginov, Dependence of the neodymium random laser threshold on the diameter of the pumped spot, IEEE J. Quantum Electron. 41 (5) (2005) 677–685.
[155] R.J.R. Vieira, L. Gomes, J.R. Martinelli, N.U. Wetter, Upconversion luminescence and decay kinetics in a diode-pumped nanocrystalline Nd^{3+}:YVO$_4$ random laser, Opt. Express 20 (11) (2012) 12487–12497.
[156] G. Williams, S. Bayram, S. Rand, T. Hinklin, R. Laine, Laser action in strongly scattering rare-earth-metal-doped dielectric nanophosphors, Phys. Rev. A 65 (1) (2001) 013807.
[157] V. Markushev, N.É Ter-Gabriélyan, C.M. Briskina, V. Belan, V. Zolin, Stimulated emission kinetics of neodymium powder lasers, Sov. J. Quantum Electron. 20 (7) (1990) 773.
[158] M. Noginov, N. Noginova, S. Egarievwe, H. Caulfield, C. Cochrane, J. Wang, M. Kokta, J. Paitz, Study of the pumping regimes in Ti-sapphire and Nd$_{0.5}$La$_{0.5}$Al$_3$(BO$_3$)$_4$ powders, Opt. Mater. 10 (4) (1998) 297–303.
[159] M. Noginov, S. Egarievwe, N. Noginova, H. Caulfield, J. Wang, Interferometric studies of coherence in a powder laser, Opt. Mater. 12 (1) (1999) 127–134.
[160] M. Noginov, N. Noginova, S. Egarievwe, H. Caulfield, P. Venkateswarlu, A. Williams, S. Mirov, Color-center powder laser: the effect of pulverization on color-center characteristics, J. Opt. Soc. Amer. B 14 (8) (1997) 2153–2160.
[161] Y. Feng, S. Huang, G. Qin, M. Musha, K.-i. Ueda, Random microchip laser, Opt. Express 13 (1) (2005) 121–126.
[162] Y. Chen, J. Herrnsdorf, B. Guilhabert, Y. Zhang, I.M. Watson, E. Gu, N. Laurand, M.D. Dawson, Colloidal quantum dot random laser, Opt. Express 19 (4) (2011) 2996–3003.
[163] A.K. Tiwari, R. Uppu, S. Mujumdar, Aerosol-based coherent random laser, Opt. Lett. 37 (6) (2012) 1053–1055.
[164] N. Ghofraniha, I. Viola, F.D. Maria, G. Barbarella, G. Gigli, C. Conti, Random laser from engineered nanostructures obtained by surface tension driven lithography, Laser Photon. Rev. 7 (3) (2013) 432–438.
[165] I. Viola, N. Ghofraniha, A. Zacheo, V. Arima, C. Conti, G. Gigli, Random laser emission from a paper-based device, J. Mater. Chem. C 1 (48) (2013) 8128–8133.

[166] N. Ghofraniha, I. Viola, A. Zacheo, V. Arima, G. Gigli, C. Conti, Transition from nonresonant to resonant random lasers by the geometrical confinement of disorder, Opt. Lett. 38 (23) (2013) 5043–5046.
[167] R.C. Polson, Z.V. Vardeny, Random lasing in human tissues, Appl. Phys. Lett. 85 (7) (2004) 1289–1291.
[168] Q. Song, S. Xiao, Z. Xu, J. Liu, X. Sun, V. Drachev, V.M. Shalaev, O. Akkus, Y.L. Kim, Random lasing in bone tissue, Opt. Lett. 35 (9) (2010) 1425–1427.
[169] R. Polson, Z. Vardeny, Cancerous tissue mapping from random lasing emission spectra, J. Opt. 12 (2) (2010) 024010.
[170] L.S. Froufe-Pérez, W. Guerin, R. Carminati, R. Kaiser, Threshold of a random laser with cold atoms, Phys. Rev. Lett. 102 (17) (2009) 173903.
[171] Q. Baudouin, N. Mercadier, V. Guarrera, W. Guerin, R. Kaiser, A cold-atom random laser, Nat. Phys. 9 (6) (2013) 357–360.
[172] M.J. Mumma, D. Buhl, G. Chin, D. Deming, F. Espenak, T. Kostiuk, D. Zipoy, Discovery of natural gain amplification in the 10-micrometer carbon dioxide laser bands on mars: a natural laser, Science 212 (4490) (1981) 45–49.
[173] J. Yi, G. Feng, C. Yang, H. Zhang, K. Yao, S. Zhou, 2.18 μm random laser action based on Cr^{2+}:ZnSe nanocrystalline particles, Opt. Commun. 309 (2013) 170–174.
[174] D. Martyshkin, V. Fedorov, C. Kim, I. Moskalev, S. Mirov, Mid-IR random lasing of Cr-doped ZnS nanocrystals, J. Opt. 12 (2) (2010) 024005.
[175] M. Noginov, S. Egarievwe, N. Noginova, J. Wang, H. Caulfield, Demonstration of a second-harmonic powder laser, J. Opt. Soc. Amer. B 15 (12) (1998) 2854–2860.
[176] H. Fujiwara, K. Sasaki, Observation of upconversion lasing within a thulium-ion-doped glass powder film containing titanium dioxide particles, Japan. J. Appl. Phys. 43 (2004) 1337.
[177] F. Shi, X. Zhang, P. Wang, F. Xin, X. Yu, Q. Wu, J. Xu, Upconversion green-light-emitting macroporous Er: LN random laser, in: Lasers and Electro-Optics Europe (CLEO EUROPE/EQEC), 2011 Conference on and 12th European Quantum Electronics Conference, IEEE, 2011, pp. 1–1.
[178] M.A. deOliveira, C.B. de Araújo, Y. Messaddeq, Upconversion ultraviolet random lasing in Nd^{3+} doped fluoroindate glass powder, Opt. Express 19 (6) (2011) 5620–5626.
[179] E.S. Leong, S.F. Yu, UV random lasing action in p-SiC (4H)/i-ZnO–SiO_2 nanocomposite/n-ZnO: Al heterojunction diodes, Adv. Mater. 18 (13) (2006) 1685–1688.
[180] E.S. Leong, S. Yu, S. Lau, Directional edge-emitting UV random laser diodes, Appl. Phys. Lett. 89 (22) (2006) 221109–221109.
[181] S. Chu, M. Olmedo, Z. Yang, J. Kong, J. Liu, Electrically pumped ultraviolet ZnO diode lasers on si, Appl. Phys. Lett. 93 (18) (2008) 181106–181106.
[182] H.K. Liang, S.F. Yu, H.Y. Yang, ZnO random laser diode arrays for stable single-mode operation at high power, Appl. Phys. Lett. 97 (24) (2010) 241107.
[183] H. Liang, S. Yu, H. Yang, Directional and controllable edge-emitting ZnO ultraviolet random laser diodes, Appl. Phys. Lett. 96 (10) (2010) 101116–101116.
[184] H. Zhu, C.-X. Shan, J.-Y. Zhang, Z.-Z. Zhang, B.-H. Li, D.-X. Zhao, B. Yao, D.-Z. Shen, X.-W. Fan, Z.-K. Tang, X. Hou, K.-L. Choy, Low-threshold electrically pumped random lasers, Adv. Mater. 22 (16) (2010) 1877–1881.
[185] Y. Tian, X. Ma, P. Chen, Y. Zhang, D. Yang, Electrically pumped wavelength-tunable ultraviolet random lasing from $Mg_xZn_{1−x}$O films on Si, Opt. Express 18 (10) (2010) 10668–10673.
[186] X. Ma, J. Pan, P. Chen, D. Li, H. Zhang, Y. Yang, D. Yang, Room temperature electrically pumped ultraviolet random lasing from ZnO nanorod arrays on Si, Opt. Express 17 (16) (2009) 14426–14433.
[187] K. Wu, P. Ding, Y. Lu, X. Pan, H. He, J. Huang, B. Zhao, C. Chen, L. Chen, Z. Ye, Electrically pumped ultraviolet lasing from ZnO in metal–insulator-semi devices, Appl. Phys. A (2013) 1–6.
[188] Q. Qiao, C.-X. Shan, J. Zheng, H. Zhu, S.-F. Yu, B.-H. Li, Y. Jia, D.-Z. Shen, Surface plasmon enhanced electrically pumped random lasers, Nanoscale 5 (2) (2013) 513–517.
[189] G. Zhu, C. Small, M. Noginov, Control of gain and amplification in random lasers, J. Opt. Soc. Amer. B 24 (9) (2007) 2129–2135.
[190] M. Noginov, Random lasers: resonance control, Nature Photon. 2 (7) (2008) 397–398.
[191] C.-R. Lee, J.-D. Lin, B.-Y. Huang, S.-H. Lin, T.-S. Mo, S.-Y. Huang, C.-T. Kuo, H.-C. Yeh, Electrically controllable liquid crystal random lasers below the Fréedericksz transition threshold, Opt. Express 19 (3) (2011) 2391–2400.
[192] S. Mujumdar, S. Cavalieri, D.S. Wiersma, Temperature-tunable random lasing: numerical calculations and experiments, J. Opt. Soc. Amer. B 21 (1) (2004) 201–207.
[193] H. Fujiwara, Y. Hamabata, K. Sasaki, Numerical analysis of resonant and lasing properties at a defect region within a random structure, Opt. Express 17 (5) (2009) 3970–3977.
[194] H. Fujiwara, Y. Hamabata, K. Sasaki, Numerical analysis of resonant properties of a waveguide structure within a random medium, Opt. Express 17 (13) (2009) 10522–10528.
[195] H. Fujiwara, T. Ikeda, K. Sasaki, Numerical analysis of random lasing properties of a waveguide defect within a random structure, Japan. J. Appl. Phys. 49 (11) (2010) 2002.
[196] H. Fujiwara, R. Niyuki, Y. Ishikawa, N. Koshizaki, T. Tsuji, K. Sasaki, Low-threshold and quasi-single-mode random laser within a submicrometer-sized ZnO spherical particle film, Appl. Phys. Lett. 102 (6) (2013) 061110–061110.
[197] Y. Chen, J. Herrnsdorf, B. Guilhabert, Y. Zhang, A.L. Kanibolotsky, P.J. Skabara, E. Gu, N. Laurand, M.D. Dawson, Modification of emission wavelength in organic random lasers based on photonic glass, Org. Electron. 13 (7) (2012) 1129–1135.
[198] G. Van Soest, M. Tomita, A. Lagendijk, Amplifying volume in scattering media, Opt. Lett. 24 (5) (1999) 306–308.
[199] C. Vanneste, P. Sebbah, Selective excitation of localized modes in active random media, Phys. Rev. Lett. 87 (18) (2001) 183903.
[200] P. Sebbah, C. Vanneste, Random laser in the localized regime, Phys. Rev. B 66 (14) (2002) 144202.
[201] M. Leonetti, C. López, Active subnanometer spectral control of a random laser, Appl. Phys. Lett. 102 (7) (2013) 071105–071105.
[202] M. Leonetti, C. Conti, C. López, The mode-locking transition of random lasers, Nature Photon. 5 (10) (2011) 615–617.
[203] T. Hisch, M. Liertzer, D. Pogany, F. Mintert, S. Rotter, Pump-controlled directional light emission from random lasers, Phys. Rev. Lett. 111 (2013) 023902.
[204] S. Gottardo, R. Sapienza, P.D. Garcia, A. Blanco, D.S. Wiersma, C. López, Resonance-driven random lasing, Nature Photon. 2 (7) (2008) 429–432.
[205] P. Garcia, M. Ibisate, R. Sapienza, D. Wiersma, C. López, Mie resonances to tailor random lasers, Phys. Rev. A 80 (1) (2009) 013833.
[206] R.G. El-Dardiry, A. Lagendijk, Tuning random lasers by engineered absorption, Appl. Phys. Lett. 98 (16) (2011) 161106–161106.
[207] M. Leonetti, C. Conti, C. López, Random laser tailored by directional stimulated emission, Phys. Rev. A 85 (4) (2012) 043841.
[208] A. Burin, M.A. Ratner, H. Cao, S. Chang, Random laser in one dimension, Phys. Rev. Lett. 88 (9) (2002) 093904.
[209] V. Milner, A.Z. Genack, Photon localization laser: low-threshold lasing in a random amplifying layered medium via wave localization, Phys. Rev. Lett. 94 (7) (2005) 073901.
[210] A. Monguzzi, F. Scotognella, F. Meinardi, R. Tubino, Lasing in one dimensional dye-doped random multilayer, Phys. Chem. Chem. Phys. 12 (40) (2010) 12947–12950.
[211] Z. Hu, H. Zheng, L. Wang, X. Tian, T. Wang, Q. Zhang, G. Zou, Y. Chen, Q. Zhang, Random fiber laser of POSS solution-filled hollow optical fiber by end pumping, Opt. Commun. 285 (19) (2012) 3967–3970.
[212] Z. Hu, B. Miao, T. Wang, Q. Fu, D. Zhang, H. Ming, Q. Zhang, Disordered microstructure polymer optical fiber for stabilized coherent random fiber laser, Opt. Lett. 38 (22) (2013) 4644–4647.
[213] N. Lizárraga, N. Puente, E. Chaikina, T. Leskova, E. Méndez, Single-mode Er-doped fiber random laser with distributed Bragg grating feedback, Opt. Express 17 (2) (2009) 395–404.
[214] Y. Bliokh, E.I. Chaikina, N. Lizárraga, E.R. Méndez, V. Freilikher, F. Nori, Disorder-induced cavities, resonances, and lasing in randomly layered media, Phys. Rev. B 86 (5) (2012) 054204.
[215] A.G. Ardakani, M.G.G. Ali, S.M. Mahdavi, A.R. Bahrampour, Mode analysis of fiber Bragg grating random lasers in the presence of mode competition, Opt. Laser Technol. 44 (4) (2012) 969–975.
[216] M. Gagné, R. Kashyap, Demonstration of a 3 mW threshold Er-doped random fiber laser based on a unique fiber Bragg grating, Opt. Express 17 (21) (2009) 19067–19074.

[217] N.P. Puente, E.I. Chaikina, S. Herath, A. Yamilov, Fabrication, characterization, and theoretical analysis of controlled disorder in the core of optical fibers, Appl. Opt. 50 (6) (2011) 802.

[218] S. Derevyanko, Design of a flat-top fiber Bragg filter via quasi-random modulation of the refractive index, Opt. Lett. 33 (20) (2008) 2404–2406.

[219] H. Kogelnik, c.V. Shank, Stimulated emission in a periodic structure, Appl. Phys. Lett. 18 (4) (1971) 152–154.

[220] C.V. Shank, J.E. Bjorkholm, H. Kogelnik, Tunable distributed-feedback dye laser, Appl. Phys. Lett. 18 (9) (1971) 395–396.

[221] j.T. Kringlebotn, J.-L. Archambault, L. Reekie, D.N. Payne, Er^{3+}:Yb^{3+}-codoped fiber distributed-feedback laser, Opt. Lett. 19 (24) (1994) 2101–2103.

[222] F. Leo, S. Coen, S.-P.G. PascalKockaert, P. Emplit, M. Haelterman, Temporal cavity solitons in one-dimensional Kerr media as bits in an all-optical buffer, Nature Photon. 4 (2010) 471–476.

[223] K. Predehl, G. Grosche, S.M.F. Raupach, S. Droste, O. Terra, J. Alnis, T. Legero, T.W. Hänsch, T. Udem, R. Holzwarth, H. Schnatz, A 920-kilometer optical fiber link for frequency metrology at the 19th decimal place, Science 336 (6080) (2012) 441–444.

[224] P.J. Wisoff, M.W. Bowers, G.V. Erbert, D.F. Browning, D.R. Jedlovec, NIF injection laser system, Proc. SPIE 5341 (2004) 146–155.

[225] M. Bowers, S. Burkhart, S. Cohen, G. Erbert, J. Heebner, M. Hermann, D. Jedlovec, The injection laser system on the National Ignition Facility, Proc. SPIE 6451 (2007) 64511M.

[226] H. Kogelnik, C.V. Shank, Coupled-wave theory of distributed feedback lasers, J. Appl. Phys. 43 (5) (1972) 2327–2335.

[227] M. Nakamura, A. Yariv, H.W. Yen, S. Somekh, H.L. Garvin, Optically pumped GaAs surface laser with corrugation feedback, Appl. Phys. Lett. 22 (10) (1973) 515–516.

[228] H.W. Yen, M. Nakamura, E. Garmire, S. Somekh, A. Yariv, H.L. Garvin, Optically pumped GaAs waveguide lasers with a fundamental $0.11\,\mu$ corrugation feedback, Opt. Commun. 9 (1) (1973) 35–37.

[229] D.R. Scifres, R.D. Burnham, W. Streifer, Distributed-feedback single heterojunction GaAs diode laser, Appl. Phys. Lett. 25 (4) (1974) 203–206.

[230] H.A. Haus, C.V. Shank, Antisymmetric taper of distributed feedback lasers, IEEE J. Quantum Electron. 12 (9) (1976) 532–539.

[231] K. Utaka, S. Akiba, K. Sakai, Y. Matsushima, $\lambda/4$-shifted InGaAsP/InP lasers, IEEE J. Quantum Electron. 22 (7) (1986) 1042–1051.

[232] J.C. Fletcher, C. Elachi, G.A. Evans, C. Yeh, Fiber distributed feedback laser, US Patent 3 958 188 (May 18 1976).

[233] W.H. Loh, R.I. Laming, 1.55 μm phase-shifted distributed feedback fibre laser, Electron. Lett. 31 (17) (1995) 1440–1442.

[234] M. Sejka, P. Varming, J. Hubner, M. Kristensen, Distributed feedback Er^{3+}-doped fibre laser, Electron. Lett. 31 (17) (1995) 1445–1446.

[235] A. Asseh, H. Storoy, J.T. Kringlebotn, W. Margulis, B. Sahlgren, S. Sandgren, R. Stubbe, G. Edwall, 10 cm Yb^{3+} DFB fibre laser with permanent phase shifted grating, Electron. Lett. 31 (12) (1995) 969–970.

[236] S. Agger, J.H. Povlsen, P. Varming, Single-frequency thulium-doped distributed-feedback fiber laser, Opt. Lett. 29 (13) (2004) 1503–1505.

[237] P.S. Westbrook, K.S. Abedin, J.W. Nicholson, T. Kremp, J. Porque, Raman fiber distributed feedback lasers, Opt. Lett. 36 (15) (2011) 2895–2897.

[238] K.S. Abedin, P.S. Westbrook, J.W. Nicholson, J. Porque, T. Kremp, X. Liu, Single-frequency Brillouin distributed feedback fiber laser, Opt. Lett. 37 (4) (2012) 605–607.

[239] H. Coles, S. Morris, Liquid-crystal lasers, Nature Photon. 4 (2010) 676–685.

[240] M.J. Marell, B. Smalbrugge, E.J. Geluk, P.J. van Veldhoven, B. Barcones, B. Koopmans, R. Nötzel, M.K. Smit, M.T. Hill, Plasmonic distributed feedback lasers at telecommunications wavelengths, Opt. Express 19 (16) (2011) 15109–15118.

[241] A. Schilke, C. Zimmermann, P.W. Courteille, W. Guerin, Optical parametric oscillation with distributed feedback in cold atoms, Nature Photon. 6 (2) (2012) 101–104.

[242] C.W. Wilmsen, H. Temkin, L.A. Coldren, Vertical-Cavity Surface-Emitting Lasers: Design, Fabrication, Characterization, and Applications, in: Cambridge Studies in Modern Optics, vol. 24, Cambridge University Press, 2001.

[243] K.I. HerbertLi (Ed.), Vertical-Cavity Surface-Emitting Laser Devices, in: Springer Series in Photonics, vol. 6, Springer, 2010.

[244] R. Michalzik (Ed.), VCSELs, in: Springer Series in Optical Sciences, vol. 166, Springer, Berlin, Heidelberg, 2013.

[245] H. Ghafouri-Shiraz, Distributed Feedback Laser Diodes and Optical Tunable Filters, Wiley, 2004.

[246] S. Akiba, Distributed feedback lasers, in: K. Iga, Y. Kokubun (Eds.), Encyclopedic Handbook of Integrated Optics, CRC Press, 2010, pp. 41–53.

[247] G.A. Cranch, G.M.H. Flockhart, C.K. Kirkendall, Distributed feedback fiber laser strain sensors, IEEE Sens. J. 8 (7–8) (2008) 1161–1172.

[248] S. Foster, Fundamental limits on $1/f$ frequency noise in rare-earth-metal-doped fiber lasers due to spontaneous emission, Phys. Rev. A 78 (1) (2008) 013820.

[249] E. Rønnekleiv, S.W. Løvseth, J.T. Kringlebotn, Er-doped fiber distributed feedback lasers: properties, applications and design considerations, in: V. Pruneri, R.P. Dahlgren, G.M. Sanger (Eds.), Fiber-Based Component Fabrication, Testing, and Connectorization, 29 October 2002, Brugge, Belgium, in: Proc. SPIE, vol. 4943, SPIE, 2003, pp. 69–80.

[250] G.P. Agrawal, Applications of Nonlinear Fiber Optics, second ed., Academic Press, 2010.

[251] M.N. Zervas, Advances in fiber distributed-feedback lasers, in: I. Kaminow, T. Li, A.E. Willner (Eds.), Optical Fiber Telecommunications, sixth ed., Academic Press, Boston, 2013, pp. 1–24.

[252] H. Kogelnik, Coupled wave theory for thick hologram gratings, Bell Syst. Tech. J. 48 (9) (1969) 2909–2947.

[253] T. Erdogan, Fiber grating spectra, J. Lightwave Technol. 15 (8) (1997) 1277–1294.

[254] R. Kashyap, Fiber Bragg Gratings, second ed., Academic Press, 2009.

[255] A. Othonos, K. Kalli, Fiber Bragg Gratings: Fundamentals and Applications in Telecommunications and Sensing, Artech House, 1999.

[256] M. Yamada, K. Sakuda, Analysis of almost-periodic distributed feedback slab waveguides via a fundamental matrix approach, Appl. Opt. 26 (16) (1987) 3474–3478.

[257] T. Qiu, S. Suzuki, A. Schülzgen, L. Li, A. Polynkin, V. Temyanko, J.V. Moloney, N. Peyghambarian, Generation of watt-level single-longitudinal-mode output from cladding-pumped short fiber lasers, Opt. Lett. 30 (20) (2005) 2748–2750.

[258] A. Tikhomirov, S. Foster, DFB FL sensor cross-coupling reduction, J. Lightwave Technol. 25 (2) (2007) 533–538.

[259] Haifeng Qi, Zhiqiang Song, Shujuan Li, Jian Guo, Chang Wang, Gang-Ding Peng, Apodized distributed feedback fiber laser with asymmetrical outputs for multiplexed sensing applications, Opt. Express 21 (9) (2013) 11309–11314.

[260] V.C. Lauridsen, J.H. Povlsen, P. Varming, Design of DFB fibre lasers, Electron. Lett. 34 (21) (1998) 2028–2030.

[261] Y. Lai, A. Martinez, I. Khrushchev, I. Bennion, Distributed Bragg reflector fiber laser fabricated by femtosecond laser inscription, Opt. Lett. 31 (11) (2006) 1672–1674.

[262] B. Jaskorzynska, E.V. Vanin, S. Helmfrid, A. Asseh, Gain saturation and pump depletion in high-efficiency distributed-feedback rare-earth-doped lasers, Opt. Lett. 21 (17) (1996) 1366–1368.

[263] V.C. Lauridsen, J.H. Povlsen, P. Varming, Optimising erbium-doped DFB fibre laser length with respect to maximum output power, Electron. Lett. 35 (4) (1999) 300–302.

[264] W.H. Loh, M.J. Cole, M.N. Zervas, S. Barcelos, R.I. Laming, Complex grating structures with uniform phase masks based on the moving fiber–scanning beam technique, Opt. Lett. 20 (20) (1995) 2051–2053.

[265] A. Asseh, H. Storoy, B. Sahlgren, S. Sandgren, R.A.H. Stubbe, A writing technique for long fiber Bragg gratings with complex reflectivity profiles, J. Lightwave Technol. 15 (8) (1997) 1419–1423.

[266] K. Yelen, L.M.B. Hickey, M.N. Zervas, A new design approach for fiber DFB lasers with improved efficiency, IEEE J. Quantum Electron. 40 (6) (2004) 711–720.

[267] K. Yelen, L.M.B. Hickey, M.N. Zervas, Experimentally verified modeling of erbium–ytterbium co-doped DFB fiber lasers, J. Lightwave Technol. 23 (3) (2005) 1380–1392.

[268] K. Yelen, M.N. Zervas, L.M.B. Hickey, Fiber DFB lasers with ultimate efficiency, J. Lightwave Technol. 23 (1) (2005) 32–43.

[269] S. Foster, Dynamical noise in single-mode distributed feedback fiber lasers, IEEE J. Quantum Electron. 40 (9) (2004) 1283–1293.

[270] S. Foster, Spatial mode structure of the distributed feedback fiber laser, IEEE J. Quantum Electron. 40 (7) (2004) 884–892.

[271] S. Foster, A new derivation of the fundamental mode equations for low gain distributed feedback lasers, IEEE J. Quantum Electron. 43 (1) (2007) 4–5.

[272] S.D. Agger, J.H. Povlsen, Comments on "dynamical noise in single-mode distributed feedback fiber lasers", IEEE J. Quantum Electron. 42 (7) (2006) 733–734.
[273] S.D. Agger, Thulium distributed-feedback fiber lasers, Ph.D. Thesis, Technical University of Denmark, 2006.
[274] M.A. Nikulin, D.E. Churin, A.A. Vlasov, E.V. Podivilov, Distributed feedback ytterbium fiber laser: experiment and analytical model, J. Opt. Soc. Amer. B 27 (7) (2010) 1414–1420.
[275] C. Barnard, P. Myslinski, J. Chrostowski, M. Kavehrad, Analytical model for rare-earth-doped fiber amplifiers and lasers, IEEE J. Quantum Electron. 30 (8) (1994) 1817–1830.
[276] Y. Qian, P. Varming, J.H. Povlsen, V.C. Lauridsen, Dynamic noise response of DFB fibre lasers in presence of pump fluctuation, Electron. Lett. 35 (4) (1999) 299–300.
[277] E. Rønnekleiv, Frequency and intensity noise of single frequency fiber Bragg grating lasers, Opt. Fiber Technol. 7 (3) (2001) 206–235.
[278] S. Foster, A. Tikhomirov, M. Milnes, Fundamental thermal noise in distributed feedback fiber lasers, IEEE J. Quantum Electron. 43 (5) (2007) 378–384.
[279] T. Okoshi, K. Kikuchi, A. Nakayama, Novel method for high resolution measurement of laser output spectrum, Electron. Lett. 16 (16) (1980) 630–631. http://dx.doi.org/10.1049/el:19800437.
[280] A.L. Schawlow, C.H. Townes, Infrared and optical masers, Phys. Rev. 112 (1958) 1940–1949.
[281] C.H. Henry, Theory of the linewidth of semiconductor lasers, IEEE J. Quantum Electron. 18 (2) (1982) 259–264.
[282] C.H. Henry, Theory of the phase noise and power spectrum of a single mode injection laser, IEEE J. Quantum Electron. 19 (9) (1983) 1391–1397.
[283] S. Foster, Complex susceptibility of saturated erbium-doped fiber lasers and amplifiers, IEEE Photon. Technol. Lett. 19 (12) (2007) 895–897.
[284] A. Yariv, P. Yeh, Photonics: Optical Electronics in Modern Communications, sixth ed., in: The Oxford Series in Electrical and Computer Engineering, Oxford University Press, 2006.
[285] M. Lax, Classical noise. v. noise in self-sustained oscillators, Phys. Rev. 160 (1967) 290–307.
[286] G.A. Ball, C.G. Hull-Allen, J. Livas, Frequency noise of a Bragg grating fibre laser, Electron. Lett. 30 (15) (1994) 1229–1230.
[287] S.W. Løvseth, J.T. Kringlebotn, E. Rønnekleiv, K. Bløtekjær, Fiber distributed-feedback lasers used as acoustic sensors in air, Appl. Opt. 38 (22) (1999) 4821–4830.
[288] N.Y. Voo, P. Horak, M. Ibsen, W.H. Loh, Anomalous linewidth behavior in short-cavity single-frequency fiber lasers, IEEE Photon. Technol. Lett. 17 (3) (2005) 546–548.
[289] P. Horak, N.Y. Voo, M. Ibsen, W.H. Loh, Pump-noise-induced linewidth contributions in distributed feedback fiber lasers, IEEE Photon. Technol. Lett. 18 (9) (2006) 998–1000.
[290] S.B. Foster, A.E. Tikhomirov, Pump-noise contribution to frequency noise and linewidth of distributed-feedback fiber lasers, IEEE J. Quantum Electron. 46 (5) (2010) 734–741.
[291] F.W.J. Olver, D.W. Lozier, R.F. Boisvert, C.W. Clark (Eds.), NIST Handbook of Mathematical Functions, Cambridge University Press, New York, NY, 2010. Print companion to [292].
[292] Nist digital library of mathematical functions, http://dlmf.nist.gov/, Release 1.0.6 of 2013-05-06, online companion to [291], 2013.
[293] K.H. Wanser, Theory of thermal phase noise in Michelson and Sagnac fiber interferometers, in: B. Culshaw, J.D.C. Jones (Eds.), 10th Int. Conf. Optical Fibre Sensors, 11 Oct. 1994, Glasgow, UK, in: Proc. SPIE, vol. 2360, 1994, p. 584.
[294] S. Foster, G.A. Cranch, A. Tikhomirov, Experimental evidence for the thermal origin of $1/f$ frequency noise in erbium-doped fiber lasers, Phys. Rev. A 79 (5) (2009) 053802.
[295] R. Dicke, Coherence in spontaneous radiation processes, Phys. Rev. 93 (1) (1954) 99.
[296] L. Duan, General treatment of the thermal noises in optical fibers, Phys. Rev. A 86 (2012) 023817.
[297] S.P. Smith, F. Zarinetchi, S. Ezekiel, Narrow-linewidth stimulated Brillouin fiber laser and applications, Opt. Lett. 16 (6) (1991) 393–395.
[298] V.E. Perlin, H.G. Winful, Distributed feedback fiber Raman laser, IEEE J. Quantum Electron. 37 (1) (2001) 38–47.
[299] V.E. Perlin, H.G. Winful, Stimulated raman scattering in nonlinear periodic structures, Phys. Rev. A 64 (4) (2001) 043804.
[300] Y. Hu, N.G. Broderick, Improved design of a DFB Raman fibre laser, Opt. Commun. 282 (16) (2009) 3356–3359.
[301] J. Shi, S. ul Alam, M. Ibsen, Highly efficient Raman distributed feedback fiber lasers, Opt. Express 20 (5) (2012) 5082–5091.
[302] J. Shi, S. ul Alam, M. Ibsen, Sub-watt threshold, kilohertz-linewidth Raman distributed-feedback fiber laser, Opt. Lett. 37 (9) (2012) 1544–1546.
[303] J. Shi, S. ul Alam, M. Ibsen, Ultrawide-range four-wave mixing in Raman distributed-feedback fiber lasers, Opt. Lett. 38 (6) (2013) 944–946.
[304] M. Ibsen, M.K. Durkin, M.J. Cole, R. Laming, Sinc-sampled fiber Bragg gratings for identical multiple wavelength operation, IEEE Photon. Technol. Lett. 10 (6) (1998) 842–844.
[305] M. Ibsen, E. Rønnekleiv, G.J. Cowle, M.N. Zervas, R.I. Laming, Multiple wavelength all-fibre DFB lasers, Electron. Lett. 36 (2) (2000) 143–144.
[306] W.H. Loh, J.P. de Sandro, G.J. Cowle, B.N. Samson, A.D. Ellis, 40 GHz optical-millimetre wave generation with a dual polarisation distributed feedback fibre laser, Electron. Lett. 33 (7) (1997) 594–595.
[307] D. Jiang, X. Chen, Y. Dai, H. Liu, S. Xie, A novel distributed feedback fiber laser based on equivalent phase shift, IEEE Photon. Technol. Lett. 16 (12) (2004) 2598–2600.
[308] Q. Lin, G.P. Agrawal, Raman response function for silica fibers, Opt. Lett. 31 (21) (2006) 3086–3088.
[309] M. Barnoski, M. Rourke, S. Jensen, R. Melville, Optical time domain reflectometer, Appl. Opt. 16 (9) (1977) 2375–2379.
[310] A.A. Fotiadi, R.V. Kiyan, Cooperative stimulated Brillouin and Rayleigh backscattering process in optical fiber, Opt. Lett. 23 (23) (1998) 1805–1807.
[311] C.-J. Chen, H.K. Lee, Y.-J. Cheng, Instability in Raman amplifiers caused by distributed Rayleigh reflection, in: Optical Fiber Communications Conference, vol. 1, Optical Society of America, 2003, p. 157.
[312] D.V. Churkin, S.A. Babin, A.E. El-Taher, P. Harper, S.I. Kablukov, V. Karalekas, J.D. Ania-Castanon, E.V. Podivilov, S.K. Turitsyn, Raman fiber lasers with a random distributed feedback based on Rayleigh scattering, Phys. Rev. A 82 (3) (2010) 033828.
[313] S.A. Babin, V. Karalekas, E.V. Podivilov, V. Mezentsev, P. Harper, J.D. Ania-Castañón, S.K. Turitsyn, Turbulent broadening of optical spectra in ultralong Raman fiber lasers, Phys. Rev. A 77 (3) (2008) 033803.
[314] A.A. Fotiadi, Random lasers: an incoherent fibre laser, Nature Photon. 4 (4) (2010) 204–205.
[315] S.A. Babin, V. Karalekas, P. Harper, E.V. Podivilov, V.K. Mezentsev, J.D. Ania-Castañón, S.K. Turitsyn, Experimental demonstration of mode structure in ultralong Raman fiber lasers, Opt. Lett. 32 (9) (2007) 1135–1137.
[316] S. Babin, D. Churkin, A. Fotiadi, S. Kablukov, O. Medvedkov, E. Podivilov, Relative intensity noise in cascaded Raman fiber lasers, IEEE Photon. Technol. Lett. 17 (12) (2005) 2553.
[317] S.A. Babin, A.E. El-Taher, P. Harper, E.V. Podivilov, S.K. Turitsyn, Tunable random fiber laser, Phys. Rev. A 84 (2) (2011) 021805.
[318] Y.J. Rao, L.W. Zhang, J.M. Zhu, Z.X. Yang, Z.N. Wang, X.H. Jia, Hybrid lasing in an ultra-long ring fiber laser, Opt. Express 20 (20) (2012) 22563.
[319] D.V. Churkin, I.D. Vatnik, S.K. Turitsyn, S.A. Babin, Random distributed feedback Raman fiber laser operating in a 1.2 μm wavelength range, Laser Phys. 21 (8) (2011) 1525–1529.
[320] R. Teng, Y. Ding, L. Chen, Random fiber laser operating at 1,115 nm, Appl. Phys. B 111 (2) (2013) 169–172.
[321] I.D. Vatnik, D.V. Churkin, S.A. Babin, S.K. Turitsyn, Cascaded random distributed feedback Raman fiber laser operating at 1.2 μm, Opt. Express 19 (19) (2011) 18486–18494.
[322] E. Dianov, I. Bufetov, M. Bubnov, M. Grekov, S. Vasiliev, O. Medvedkov, Three-cascaded 1407-nm Raman laser based on phosphorus-doped silica fiber, Opt. Lett. 25 (6) (2000) 402–404.
[323] W.L. Zhang, Y.J. Rao, J.M. Zhu, Z.X.Y. Wang, Zi Nan, X.H. Jia, Low threshold 2nd-order random lasing of a fiber laser with a half-opened cavity, Opt. Express 20 (13) (2012) 14400.
[324] W.L. Zhang, Y.Y. Zhu, Y.J. Rao, Z.N. Wang, X.H. Jia, H. Wu, Random fiber laser formed by mixing dispersion compensated fiber and single mode fiber, Opt. Express 21 (7) (2013) 8544–8549.
[325] Z. Wang, H. Wu, M. Fan, Y. Rao, X. Jia, W. Zhang, Third-order random lasing via Raman gain and Rayleigh feedback within a half-open cavity, Opt. Express 21 (17) (2013) 20090.

[326] A.E. El-Taher, P. Harper, S.A. Babin, D.V. Churkin, E.V. Podivilov, J.D. Ania-Castanon, S.K. Turitsyn, Effect of Rayleigh-scattering distributed feedback on multiwavelength Raman fiber laser generation, Opt. Lett. 36 (2) (2011) 130–132.

[327] S. Sugavanam, Z. Yan, V. Kamynin, A.S. Kurkov, L. Zhang, D.V. Churkin, Multiwavelength generation in a random distributed feedback fiber laser using an all fiber Lyot filter, Opt. Express 22 (2014) 2839–2844.

[328] Z. Yan, C. Mou, H. Wang, K. Zhou, Y. Wang, W. Zhao, L. Zhang, All-fiber polarization interference filters based on 45-tilted fiber gratings, Opt. Lett. 37 (3) (2012) 353–355.

[329] Z. Yan, K. Zhou, L. Zhang, In-fiber linear polarizer based on UV-inscribed 45 tilted grating in polarization maintaining fiber, Opt. Lett. 37 (18) (2012) 3819–3821.

[330] C.-S. Kim, J.U. Kang, Multiwavelength switching of Raman fiber ring laser incorporating composite polarization-maintaining fiber Lyot-Sagnac filter, Appl. Opt. 43 (15) (2004) 3151–3157.

[331] K. Özgören, F. Ilday, All-fiber all-normal dispersion laser with a fiber-based Lyot filter, Opt. Lett. 35 (8) (2010) 1296–1298.

[332] A. Pinto, O. Frazão, J. Santos, M. Lopez-Amo, Multiwavelength fiber laser based on a photonic crystal fiber loop mirror with cooperative Rayleigh scattering, Appl. Phys. B 99 (3) (2010) 391–395.

[333] A. Pinto, O. Frazão, J. Santos, M. Lopez-Amo, Multiwavelength Raman fiber lasers using Hi-Bi photonic crystal fiber loop mirrors combined with random cavities, J. Lightwave Technol. 29 (10) (2011) 1482–1488.

[334] A. Pinto, M. Bravo, M. Fernandez-Vallejo, M. Lopez-Amo, J. Kobelke, K. Schuster, Suspended-core fiber Sagnac combined dual-random mirror Raman fiber laser, Opt. Express 19 (12) (2011) 11906–11915.

[335] A. Pinto, M. Lopez-Amo, Double random mirror Hi–Bi photonic crystal fiber Sagnac based multiwavelength fiber laser, Appl. Phys. B 103 (4) (2011) 771–775.

[336] S.A. Babin, D.V. Churkin, S.I. Kablukov, M.A. Rybakov, A.A. Vlasov, All-fiber widely tunable Raman fiber laser with controlled output spectrum, Opt. Express 15 (13) (2007) 8438–8443.

[337] E. Bélanger, M. Bernier, D. Faucher, D. Côté, R. Vallée, High-power and widely tunable all-fiber raman laser, J. Lightwave Technol. 26 (12) (2008) 1696–1701.

[338] Y.-E. Im, S. Hann, H. Kim, D.-H. Kim, C.-S. Park, An all-fibre robust and tunable raman fibre laser with reconfigurable asymmetric cavities, Meas. Sci. Technol. 20 (3) (2009) 034022.

[339] F. Anquez, E. Courtade, A. SivÚry, P. Suret, S. Randoux, A high-power tunable raman fiber ring laser for the investigation of singlet oxygen production from direct laser excitation around 1270 nm, Opt. Express 18 (22) (2010) 22928–22936.

[340] P. Reeves-Hall, J. Taylor, Wavelength tunable CW Raman fibre ring laser operating at 1486-1551 nm, Electron. Lett. 37 (8) (2001) 491–492.

[341] K. Yeo, M. Mahdi, H. Mohamad, S. Hitam, M. Mokhtar, Widely tunable Raman ring laser using highly nonlinear fiber, Laser Phys. 19 (12) (2009) 2200–2203.

[342] A.R. Sarmani, R. Zamiri, M.H.A. Bakar, B.Z. Azmi, A.W. Zaidan, M.A. Mahdi, Tunable Raman fiber laser induced by Rayleigh back-scattering in an ultra-long cavity, J. Eur. Opt. Soc, Rapid Publ. 6 (2011) 11043.

[343] S. Sugavanam, N. Tarasov, X. Shu, D.V. Churkin, Narrow-band generation in random distributed feedback fiber laser, Opt. Express 21 (14) (2013) 16466–16472.

[344] Y.Y. Zhu, W.L. Zhang, Y. Jiang, Tunable multi-wavelength fiber laser based on random Rayleigh back-scattering, IEEE Photon. Technol. Lett. 25 (16) (2013) 1559–1561.

[345] G. Yin, B. Saxena, X. Bao, Tunable Er-doped fiber ring laser with single longitudinal mode operation based on Rayleigh backscattering in single mode fiber, Opt. Express 19 (27) (2011) 25981.

[346] S.A. Babin, E.I. Dontsova, S.I. Kablukov, Random fiber laser directly pumped by a high-power laser diode, Opt. Lett. 38 (17) (2013) 3301–3303.

[347] S.H. Baek, W.B. Roh, Single-mode Raman fiber laser based on a multimode fiber, Opt. Lett. 29 (2) (2004) 153.

[348] S.I. Kablukov, E.I. Dontsova, E.A. Zlobina, I.N. Nemov, A.A. Vlasov, S.A. Babin, An LD-pumped raman fiber laser operating below 1 μm, Laser Phys. Lett. 10 (8) (2013) 085103.

[349] J.D. Ania-Castañón, Quasi-lossless transmission using second-order Raman amplification and fibre Bragg gratings, Opt. Express 12 (19) (2004) 4372–4377.

[350] J.D. Ania-Castañón, T.J. Ellingham, R. Ibbotson, X. Chen, L. Zhang, S.K. Turitsyn, Ultralong Raman fiber lasers as virtually lossless optical media, Phys. Rev. Lett. 96 (2) (2006) 023902.

[351] X.-H. Jia, Y.-J. Rao, Z.-N. Wang, W.-L. Zhang, Z.-L. Ran, K. Deng, Z.-X. Yang, Detailed theoretical investigation on improved quasi-lossless transmission using third-order Raman amplification based on ultralong fiber lasers, J. Opt. Soc. Amer. B 29 (4) (2012) 847–854.

[352] A. Bednyakova, M. Fedoruk, Spatially cascaded cavities for power saving distributed Raman amplification, Opt. Commun. 291 (2013) 274–278.

[353] X.-H. Jia, Y.-J. Rao, Z.-N. Wang, W.-L. Zhang, Y. Jiang, J.-M. Zhu, Z.-X. Yang, Towards fully distributed amplification and high-performance long-range distributed sensing based on random fiber laser, in: Proc. SPIE, vol. 8421, 2012, p. 842127-1.

[354] X.-H. Jia, Y.-J. Rao, F. Peng, Z.-N. Wang, W.-L. Zhang, H.-J. Wu, Y. Jiang, Random-lasing-based distributed fiber-optic amplification, Opt. Express 21 (5) (2013) 6572.

[355] X.-H. Jia, Y.-J. Rao, C.-X. Yuan, J. Li, X.-D. Yan, Z.-N. Wang, W.-L. Zhang, H. Wu, Y.-Y. Zhu, F. Peng, Hybrid distributed Raman amplification combining random fiber laser based 2nd-order and low-noise ld based 1st-order pumping, Opt. Express 21 (21) (2013) 24611–24619.

[356] X.-H. Jia, Y.-J. Rao, Z.-N. Wang, W.-L. Zhang, C.-X. Yuan, X.-D. Yan, J. Li, H. Wu, Y.-Y. Zhu, F. Peng, Distributed Raman amplification using ultra-long fiber laser with a ring cavity: characteristics and sensing application, Opt. Express 21 (18) (2013) 21208–21217.

[357] M.H. Abu Bakar, F.R. Mahamd Adikan, M.A. Mahdi, Rayleigh-based Raman fiber laser with passive erbium-doped fiber for secondary pumping effect in remote L-band erbium-doped fiber amplifier, IEEE Photon. J. 4 (3) (2012) 1042–1050.

[358] X. Bao, L. Chen, Recent progress in distributed fiber optic sensors, Sensors 12 (7) (2012) 8601–8639.

[359] M. Fernandez-Vallejo, M. Bravo, M. Lopez-AmoMartins, Ultra-long laser systems for remote fiber Bragg gratings arrays interrogation, IEEE Photon. Technol. Lett. 25 (14) (2013) 1362–1364.

[360] H. Martins, M. Marques, O.O Frazo, Intensity vibration sensor based on raman fiber laser using a distributed mirror combined with Bragg grating structures, Appl. Phys. B 114 (1) (2014) 6–7.

[361] Z.N. Wang, Y.J. Rao, H. Wu, P.Y. Li, Y. Jiang, X.H. Jia, W.L. Zhang, Long-distance fiber-optic point-sensing systems based on random fiber lasers, Opt. Express 20 (16) (2012) 17695.

[362] Z. Wang, X. Jia, Y. Rao, Y. Jiang, W. Zhang, Novel long-distance fiber-optic sensing systems based on random fiber lasers, in: Proc. SPIE, Vol. 8351, 2012, p. 835142.

[363] A.M.R. Pinto, O. Frazão, J.L. Santos, M. Lopez-Amo, J. Kobelke, K. Schuster, Interrogation of a suspended-core Fabry–Perot temperature sensor through a dual wavelength Raman fiber laser, J. Lightwave Technol. 28 (21) (2010) 3149–3155.

[364] A.M.R. Pinto, M. Lopez-Amo, J. Kobelke, K. Schuster, Temperature fiber laser sensor based on a hybrid cavity and a random mirror, J. Lightwave Technol. 30 (8) (2012) 1168–1172.

[365] H. Martins, M.B. Marques, O. Frazão, 300 km-ultralong Raman fiber lasers using a distributed mirror for sensing applications, Opt. Express 19 (19) (2011) 18149.

[366] H.F. Martins, M.B. Marques, O. Frazão, Temperature-insensitive strain sensor based on four-wave mixing using Raman fiber Bragg grating laser sensor with cooperative Rayleigh scattering, Appl. Phys. B 104 (4) (2011) 957–960.

[367] M. Bravo, M. Fernandez-Vallejo, M. Lopez-Amo, Internal modulation of a random fiber laser, Opt. Lett. 38 (9) (2013) 1542–1544.

[368] G.P. Agrawal, Nonlinear Fiber Optics, Springer, 2000.

[369] S.V. Chernikov, Y. Zhu, J.R. Taylor, V.P. Gapontsev, Supercontinuum self-Q-switched ytterbium fiber laser, Opt. Lett. 22 (5) (1997) 298.

[370] A.A. Fotiadi, R. Kiyan, O. Deparis, P. Mégret, M. Blondel, Statistical properties of stimulated Brillouin scattering in single-mode optical fibers above threshold, Opt. Lett. 27 (2) (2002) 83–85.

ARTICLE IN PRESS

[371] A.A. Fotiadi, E. Preda, P. Mégret, Brillouin fiber laser with incoherent feedback, in: Lasers and Electro-Optics (CLEO), 2011 Conference on, IEEE, 2011, pp. 1–2.
[372] A.A. Fotiadi, I. Lobach, P. Mégret, Dynamics of ultra-long Brillouin fiber laser, in: Proc. SPIE, Vol. 8601, 2013, pp. 86011K–86011K-9.
[373] E.G. Turitsyna, G. Falkovich, V.K. Mezentsev, S.K. Turitsyn, Optical turbulence and spectral condensate in long-fiber lasers, Phys. Rev. A 80 (3) (2009) 031804.
[374] E. Turitsyna, G. Falkovich, A. El-Taher, X. Shu, P. Harper, S.K. Turitsyn, Optical turbulence and spectral condensate in long fibre lasers, Proc. R. Soc. A 468 (2145) (2012) 2496–2508.
[375] S. Turitsyn, S. Babin, E. Turitsyna, G. Falkovich, E. Podivilov, D. Churkin, Optical wave turbulence, in: V. Shrira, S. Nazarenko (Eds.), Advances in Wave Turbulence, World Scientific Publishing, 2013, pp. 113–164.
[376] S.A. Babin, D.V. Churkin, A.E. Ismagulov, S.I. Kablukov, E.V. Podivilov, Spectral broadening in Raman fiber lasers, Opt. Lett. 31 (20) (2006) 3007–3009.
[377] S.A. Babin, D.V. Churkin, A.E. Ismagulov, S.I. Kablukov, E.V. Podivilov, Four-wave-mixing-induced turbulent spectral broadening in a long Raman fiber laser, J. Opt. Soc. Amer. B 24 (8) (2007) 1729–1738.
[378] S.A. Babin, D.V. Churkin, A.E. Ismagulov, S.I. Kablukov, E.V. Podivilov, Turbulence-induced square-root broadening of the Raman fiber laser output spectrum, Opt. Lett. 33 (6) (2008) 633–635.
[379] B. Barviau, B. Kibler, A. Picozzi, Wave-turbulence approach of supercontinuum generation: influence of self-steepening and higher-order dispersion, Phys. Rev. A 79 (6) (2009) 063840.
[380] U. Bortolozzo, J. Laurie, S. Nazarenko, S. Residori, Optical wave turbulence and the condensation of light, J. Opt. Soc. Amer. B 26 (12) (2009) 2280–2284.
[381] K. Hammani, B. Kibler, C. Finot, A. Picozzi, Emergence of rogue waves from optical turbulence, Phys. Lett. A 374 (34) (2010) 3585–3589.
[382] B. Kibler, K. Hammani, C. Michel, C. Finot, A. Picozzi, Rogue waves, rational solitons and wave turbulence theory, Phys. Lett. A 375 (35) (2011) 3149–3155.
[383] J. Laurie, U. Bortolozzo, S. Nazarenko, S. Residori, One-dimensional optical wave turbulence: experiment and theory, Phys. Rep. 514 (4) (2012) 121–175.
[384] M. Pang, S. Xie, X. Bao, D.-P. Zhou, Y. Lu, L. Chen, Rayleigh scattering-assisted narrow linewidth Brillouin lasing in cascaded fiber, Opt. Lett. 37 (15) (2012) 3129.
[385] M. Pang, X. Bao, L. Chen, Observation of narrow linewidth spikes in the coherent Brillouin random fiber laser, Opt. Lett. 38 (11) (2013) 1866–1868.
[386] M. Pang, X. Bao, L. Chen, Z. Qin, Y. Lu, P. Lu, Frequency stabilized coherent Brillouin random fiber laser: theory and experiments, Opt. Express 21 (22) (2013) 27155–27168.
[387] H. Winful, I.V. Kabakova, B.J. Eggleton, Model for distributed feedback brillouin lasers, Opt. Express 21 (13) (2013) 16191–16199.
[388] K.-D. Park, B. Min, P. Kim, N. Park, J.-H. Lee, J.-S. Chang, Dynamics of cascaded Brillouin–Rayleigh scattering in a distributed fiber Raman amplifier, Opt. Lett. 27 (3) (2002) 155.
[389] A.K. Zamzuri, M.H. Al-Mansoori, N.M. Samsuri, M.A. Mahdi, Contribution of Rayleigh scattering on Brillouin comb line generation in Raman fiber laser, Appl. Opt. 49 (18) (2010) 3506–3510.
[390] H. Wu, Z. Wang, X. Jia, P. Li, M. Fan, Y. Li, Y. Zhu, Flat amplitude multiwavelength Brillouin–Raman random fiber laser with a half-open cavity, Appl. Phys. B (2013) 1–5.
[391] Z. Wang, H. Wu, M. Fan, Y. Li, Y. Gong, Y. Rao, Broadband flat-amplitude multiwavelength Brillouin-Raman fiber laser with spectral reshaping by Rayleigh scattering, Opt. Express 21 (24) (2013) 29358–29363.
[392] H. Ahmad, M. Zulkifli, M. Jemangin, S. Harun, Distributed feedback multimode Brillouin–Raman random fiber laser in the S-band, Laser Phys. Lett. 10 (5) (2013) 055102.
[393] T. Zhu, X. Bao, L. Chen, A self-gain random distributed feedback fiber laser based on stimulated Rayleigh scattering, Opt. Commun. 285 (6) (2012) 1371–1374.
[394] M. Rini, I. Cristiani, V. Degiorgio, Numerical modeling and optimization of cascaded CW Raman fiber lasers, IEEE J. Quantum Electron. 36 (10) (2000) 1117–1122.
[395] S.A. Babin, D.V. Churkin, E.V. Podivilov, Intensity interactions in cascades of a two-stage Raman fiber laser, Opt. Commun. 226 (1) (2003) 329–335.
[396] P. Suret, S. Randoux, Influence of spectral broadening on steady characteristics of Raman fiber lasers: from experiments to questions about validity of usual models, Opt. Commun. 237 (1) (2004) 201–212.
[397] C. Headley, M. Mermelstein, J.-C. Bouteiller, Raman fiber lasers, in: M. Islam (Ed.), Raman Amplifiers for Telecommunications 2, in: Springer Series in Optical Sciences, vol. 90/2, Springer, New York, 2004, pp. 353–382.
[398] Q. Zujun, Z. Xiaojun, L. Qing, W. Haocheng, Z. Zili, An improved theoretical model of n th-order cascaded Raman fiber lasers, J. Lightwave Technol. 25 (6) (2007) 1555–1560.
[399] S. Namiki, Y. Emori, Ultrabroad-band Raman amplifiers pumped and gain-equalized by wavelength-division-multiplexed high-power laser diodes, IEEE J. Sel. Top. Quant. Electron. 7 (1) (2001) 3–16.
[400] E. Brinkmeyer, Analysis of the backscattering method for single-mode optical fibers, J. Opt. Soc. Amer. 70 (8) (1980) 1010.
[401] M.N. Zervas, R.I. Laming, Rayleigh scattering effect on the gain efficiency and noise of erbium-doped fiber amplifiers, IEEE J. Quantum Electron. 31 (3) (1995) 468–471.
[402] S.A. Babin, A.S. Kurkov, V.V. Potapov, D.V. Churkin, Dependence of the spectral parameters of a Raman fibre laser on the Bragg grating temperature, Quant. Electron. 33 (12) (2003) 1096–1100.
[403] S.A. Babin, D.V. Churkin, A.E. Ismagulov, S.I. Kablukov, E.V. Podivilov, Broadening of the intracavity and output spectra of a Raman fiber laser with low-Q cavity, Laser Phys. 17 (11) (2007) 1279–1285.
[404] I.D. Vatnik, D.V. Churkin, S.A. Babin, Power optimization of random distributed feedback fiber lasers, Opt. Express 20 (27) (2012) 28033.
[405] D.V. Churkin, A.E. El-Taher, I.D. Vatnik, J.D. Ania-Castanon, P. Harper, E.V. Podivilov, S.A. Babin, S.K. Turitsyn, Experimental and theoretical study of longitudinal power distribution in a random DFB fiber laser, Opt. Express 20 (10) (2012) 11178–11188.
[406] D.V. Churkin, A.E. El-Taher, I.D. Vatnik, S.A. Babin, Study of the longitudinal distribution of power generated in a random distributed feedback Raman fibre laser with unidirectional pumping, Quant. Electron. 42 (9) (2012) 774–777.
[407] J. Nuño, M. Alcon-Camas, J.D. Ania-Castañón, RIN transfer in random distributed feedback fiber lasers, Opt. Express 20 (24) (2012) 27376–27381.
[408] C.E. Preda, G. Ravet, A.A. Fotiadi, P. Mégret, Iterative method for Brillouin fiber ring resonator, in: Lasers and Electro-Optics Europe (CLEO EUROPE/EQEC), 2011 Conference on and 12th European Quantum Electronics Conference, IEEE, 2011, pp. 1–1.
[409] S.K. Turitsyn, A.E. Bednyakova, M.P. Fedoruk, A.I. Latkin, A.A. Fotiadi, A.S. Kurkov, E. Sholokhov, Modeling of CW Yb-doped fiber lasers with highly nonlinear cavity dynamics, Opt. Express 19 (9) (2011) 8394–8405.
[410] A.E. Bednyakova, O.A. Gorbunov, M.O. Politko, S.I. Kablukov, S.V. Smirnov, D.V. Churkin, M.P. Fedoruk, S.A. Babin, Generation dynamics of the narrowband Yb-doped fiber laser, Opt. Express 21 (7) (2013) 8177–8182.
[411] D.V. Churkin, S.V. Smirnov, E.V. Podivilov, Statistical properties of partially coherent CW fiber lasers, Opt. Lett. 35 (19) (2010) 3288–3290.
[412] D.V. Churkin, O.A. Gorbunov, S.V. Smirnov, Extreme value statistics in Raman fiber lasers, Opt. Lett. 36 (18) (2011) 3617–3619.
[413] S. Randoux, N. Dalloz, P. Suret, Intracavity changes in the field statistics of Raman fiber lasers, Opt. Lett. 36 (6) (2011) 790–792.
[414] D.V. Churkin, S.V. Smirnov, Numerical modelling of spectral, temporal and statistical properties of Raman fiber lasers, Opt. Commun. 285 (8) (2012) 2154–2160.
[415] S.V. Smirnov, D.V. Churkin, Modeling of spectral and statistical properties of a random distributed feedback fiber laser, Opt. Express 21 (18) (2013) 21236–21241.
[416] R.G. Smith, Optical power handling capacity of low loss optical fibers as determined by stimulated Raman and Brillouin scattering, Appl. Opt. 11 (11) (1972) 2489–2494.

[417] P. Suret, P. Walczak, S. Randoux, Transient buildup of the optical power spectrum in Raman fiber lasers, Opt. Express 21 (2) (2013) 2331–2336.
[418] A.R. Sarmani, M.H. Abu Bakar, A.A.A. Bakar, F.R.M. Adikan, M.A. Mahdi, Spectral variations of the output spectrum in a random distributed feedback Raman fiber laser, Opt. Express 19 (15) (2011) 14152.
[419] M.H. Abu Bakar, F.R. Mahamd Adikan, M.A. Mahdi, A.R. Sarmani, Laser parameter variations in a Rayleigh scattering-based Raman fiber laser with single fiber Bragg grating reflector, IEEE Photon. J. 4 (2) (2012) 461–466.